Inverse optimal control for redundant systems of biological motion

Adina Panchea

UNIVERSITÉ D'ORLÉANS

ECOLE DOCTORALE
MATHEMATIQUES, INFORMATIQUE, PHYSIQUE THEORIQUE ET INGENIERIE DES SYSTEMES

LABORATOIRE PRISME

THÈSE présentée par :

Adina M. PANCHEA

soutenue le : **10 décembre 2015 à 10 heures**
Salle Sigaud de Lafond, IUT de Bourges

pour obtenir le grade de : **Docteur de l'université d'Orléans**
Discipline : SCIENCES ET TECHNOLOGIES INDUSTRIELLES

Inverse optimal control for redundant systems of biological motion.

THÈSE dirigée par :
Nacim RAMDANI Professeur des universités, Université d'Orléans, Bourges

RAPPORTEURS :
Philippe SOUERES Directeur de recherche CNRS, LAAS, Toulouse
Frédéric JEAN Professeur des universités, ENSTA ParisTech Université Paris-Saclay

---

JURY :

Philippe SOUERES	Directeur de recherche CNRS, LAAS, Toulouse
Frédéric JEAN	Professeur des universités, ENSTA ParisTech Université Paris-Saclay
Philippe FRAISSE	Professeur des universités, Université Montpellier 2, Montpellier
David DANEY	Chargé de recherche, INRIA Bordeaux
Francesco NORI	Team Leader, Istituto Italiano di Tecnologia, Italie
Olivier BUTTELLI	Maître de conférences- HDR, Université d'Orléans, Orléans
Nacim RAMDANI	Professeur des universités, Université d'Orléans, Bourges

"If we knew what it was we were doing, it would not be called research, would it?"

Albert EINSTEIN

Dedicated to Gauthier, Anita and Maya

Acknowledgements

This doctoral thesis could not have been possible without the Region Centre fellowship and the support of some special people. First, I would like to thank my supervisor, Prof.Dr.Nacim RAMDANI for giving me the opportunity to analyze such a challenging and ambitious research topic. His ideas and his critical remarks were of immense value in finding the solution strategies, and in teaching me how to be a good and professional researcher. Thank you for your great support, for all the times you showed me how important it is to be a leader of a team and not just a director. Second, I would like to thank my thesis committee. Firstly, many thanks to my two reviewers Dr.Philippe SOUERES and Prof.Dr.Frederic JEAN for their comments and constructive criticisms. Secondly, all my appreciation goes to my thesis jury: Dr.Francesco NORI (the president of the jury), Prof.Dr.Philippe FRAISSE, Dr.David DANEY, Dr.Olivier BUTTELLI and my two reviewers for accepting to be part of it and for the fruitful and interesting scientific discussion that we had on December 10th, 2015, during my PhD defense. I am also truly grateful to Prof.Dr.Sukyung PARK and her team for their help and support during the time spent with them at KAIST laboratory in Daejeon, South Korea. Many thanks to Prof.Dr.Philippe FRAISSE, Dr.Vincent BONNET and Dr.Nahema SYLLA for the nice collaboration that we had, which I hope it will continue in the future, and for sharing their interesting application scenarios along with data recording and processing.

I would like to thank the permanent stuff from my research group (Laure, Matthieu, Sylvain, Pierre, Didier, Yasmina, Selma, Natalie), but also many thank to my PhD and postdoc fellow colleagues: Myriam, Alexandre, Pietro, Ludovic, Lucio, Juan, Sonia, Louniss, Nabil, Hamid, Dorra and Mohamed (thank you for sharing the oriental delicacy with me: *miam miam*). Many thank also for all the colleagues that I have crossed in the different departments where I had the opportunity to teach young students different courses. All my thoughts go to Guillaume SPECKENS (thank you very much for being so kind with e when I mostly needed!!!) Special thanks to a particular person, Dr. Moussa MAIGA, once a colleague, now a brother. Nabil AMARI and Julien VAUDOLON, thanks to both of you for all your support. Thank you, Severus OLTEANU, for being the best friend ever, I couldn't ask for more.

Finally, I want to thank my French and Romanian family for their understanding and support over the years, when research consumed most of my time, and it was difficult for us to get together,especially to my twin nieces Anita and Maya (hopefully a new generation of researchers) and my beloved sister, Ana-Maria. Last but not least, I thank Gauthier LASSALLE for his constant support, understanding and love.

Contents

List of Figures

List of Tables

Chapter 1

Introduction

The human body is known to have many Degree Of Freedoms or DOFs: it has redundant anatomical DOFs (at muscles and joints), redundant kinematic DOFs (the same task can be achieved with different trajectories, velocities, and accelerations), and redundant neurophysiological DOFs (multiple motoneurons synapsing on the same muscle, and vice versa). One well-known difficulty in understanding human motor control is the way the central nervous system (CNS) "chooses" a subset of these near-infinite DOFs. Numerous experimental studies suggested that the CNS overcomes the redundancy of human movement accomplishment by following some rules and principles. These principles were investigated by many researchers in the framework of the optimal control theory and it is assumed that the human movements possess motion invariants that are the results of an optimization process [4] involving one or more objective functions (or cost functions or criteria). Several of such cost functions have been proposed and can be found in literature, but the actual/true objective functions remain unknown.

If the main point is to identify the human movements to be optimal with respect to one of these proposed cost functions, a dynamical model of the human system is required. This means that the value that can be controlled i.e the controls need to be related to the values corresponding to the current state of the system, i.e. the states, through a differential equation. Combining a chosen cost functions with the dynamical model of the human being and with the constraints stating the motor task, a mathematical optimal control problem can be identified. Under the hypothesis that the proposed human model captures well the dynamical aspects and that the cost function is the actual/real one, the optimal control problem should estimate well the observed human motion. Even so, this optimal control problem is only a modeling tool with a range of assumptions that need to be specified, and it should not be confused or identified with the real biological system. Nevertheless, this modeling tool can only exist if we have an

idea about the actual cost function minimized during a motor task. If we accept the idea that the human motor control can be considered to be an optimal process, the following question arises: Which cost function does the human motor control minimize when doing a certain motor control task? We attempt to answer this question, by solving the inverse optimal control or the inverse optimization problem, that consists in imputing the cost function that can explain the observations of the optimal expert trajectories. In literature, there are found multiple ways of solving this kind of problem, and the next section presents a detailed literature review on this matter.

The idea of having a cost function that can explain daily human tasks arises in the need of having humans and robots collaborate intuitively in an industrial, medical or daily life environment. Because the environment is a non-static one and also due to the changes of human decisions when performing a task, an adaptive control in online applications is required in order to control the robot. Consequently, if we understand some of the principles on which the human motor control works, the robots can be controlled accordingly and thus increasing their motion anticipation when collaborating with humans.

1.1 Related works

In 1964, Kalman first formulated the inverse optimal control for the linear quadratic regulator, which has triggered ever since the research efforts in that direction, with applications in a variety of domains spanning from economics to control and robotics. Recently, this issue regained further interest, especially in the humanoid robotics. Interestingly, [5] used an inverse optimization approach to model piecewise affine (PWA) dynamical systems as the outcome of an optimization process, with nice perspectives for model predictive control (MPC) implementation with PWA or nonlinear systems. In the robotics field, the inverse optimal control and the inverse optimization techniques were used, for instance, to address the stabilization design for a rigid spacecraft [6], to develop autonomous outdoor robots [7], or robots capable of navigating through crowds [8], and also to make drones capable of deciding by themselves as an expert human pilot [9],[10].

The researchers also used the inverse optimal control to study the human locomotion data by defining the objective cost functions that can explain the given observations [11, 12, 13, 14]. The latter imputed cost functions were then implemented on actual robots that could walk or move in an autonomous way. [15] proposed new solution techniques to address the inverse optimal control for the time-invariant linear quadratic

regulator (LQR) and returned results that may provide a useful insight on the goals of the human motor control goal. [16] proposed an approximate local inverse optimal control algorithm, where the reward function was learned from motion-captured demonstrations of human running, then reconstructed in simulation the locomotion behavior of a humanoid robot in new environments including running on flat ground, rough terrain and under strong lateral perturbation.

Very recently, the inverse optimal control problem has been addressed in the framework of human-robot collaboration. Co-robotics requires robots to act in anticipation of future human behavior and to realize the desired levels of seamless interaction. [17] imputed from the actual data, the objective cost functions underlying a human-human collaborative task, which were then used within a direct motion planning algorithm to predict the motion of a human avatar in the presence of a moving collaborator. [18] proposed a complementary approach to linearization and quadratic approximation for learning the human acceptable manipulation trajectories. [19] extended the maximum entropy inverse optimal control linear quadratic regulator model to the task of predicting target intentions and inferring continuous hand motion trajectories using depth camera data. Other works also focused on tight human-robot cognitive interaction [20, 21, 22].

Inverse problems were also addressed for stochastic optimal control problems. [23] used the inverse optimization approach to the stabilization in probability of the discrete-time stochastic nonlinear systems. [24] considered statistical machine learning techniques to solve an inverse optimal control problem to predict probabilistic pointing-at-target tasks in graphic user interfaces. [25] solved inverse optimal control using the maximum entropy principle within the Markov Decision Process to model route preferences for taxi drivers using hundreds of thousands of miles of collected GPS data. [26] addressed inverse optimal control with partially observable Markov decision processes. [27], [28] and [29] used inverse reinforcement learning for Markov decision processes. [30] proposed an approach for unsupervised Inverse Reinforcement Learning with noisy data using a hidden variable of the Markov Decision Processes representation, to address the agent's behavior during surveillance scenarios. [31] combined the behavioral cloning and the inverse optimal control to address the imitation learning, with application to the turn-prediction for taxi drivers, and the pedestrian's prediction within an office environment. [32] synthesized a nonlinear optimal control law for a class of nonlinear time delay systems by making use of inverse optimality based on combining the Control Lyapunov Function (CLF) framework with the complete type of the Lyapunov-Krasovskii functionals. The feasibility of their method was demonstrated by considering two processes with transport delay. [33] proposed a new inverse optimality design method based on the Hamilton-Jacobi-Bellman equations, where the cost function is built with a linear

function, mainly the Gaussian Radial Basic one and [34] focused on finding the cost function, consisting on graph edges, by solving the shortest inverse path problem while given sets of observations of the shortest path. [35] employed a class of games with utilities that are linear functions of features defined over the outcome space and they extended the inverse optimal control problem to multi-agent settings by combining the principle of maximum entropy with the game-theoretic notion of regret. They showed how their formulation led to a simple gradient-based optimization procedure. [36] studied the inverse optimal control in an apprenticeship learning algorithms framework, that is not specific for the helicopters, and was able to create the first autonomous helicopter capable of flying as an human expert pilot. [37] solves the inverse optimal control by using the max-margin inverse reinforcement learning method, where the cost function that produces realistic trajectories needs to be recovered.

The inverse optimal control is solved with the inverse optimization idea in a polynomial framework, where a proper solution is to search the right Lagrangian candidate, while the Hamilton-Jacobi-Bellman optimality equation is an appropriate tool for analyzing and solving the problem [38, 39] and another one is to impute the proper polynomial cost function while given observations, while making use of the Putnar's positivstellensatz theorem benefits [40]. [38] and [39] solve the inverse optimal control problem by searching the proper lagrangian candidate. In their study, they claim that the Hamilton-Jacobi-Bellman optimality equation is an appropriate tool for analyzing and solving the inverse optimal control problems. They proposed a method, by using HJB optimality condition or its relaxation (translated into a positivity condition for certain function or some set), based on polynomial optimization, semi-definite programs (SDPs) or linear matrix inequalities (LMIs). [40] considers the inverse optimization problems in order to impute the proper polynomial cost function for the given observations in a polynomial optimization framework. This includes a large class of optimization problems i.e. nonconvex, discrete and nonlinear ones. This framework benefits from Putnar's positivstellensatz theorem that can adapt to the actual computational capabilities for a given problem size. They also describe how a practical inverse optimization is reduced to solving a semidefinite program and exhibit the canonical form of the optimal solution for the $l1$-norm.

In this thesis, we will focus on the methods available for deterministic systems. For such systems, some solving methods use the Hamilton-Jacobi-Bellman optimality equation ([39, 33]) or the Pontryagin maximum principle ([13]), whereas most techniques use the parametrized Lagrangians to obtain finite-dimensional problems. In the latter form, available methods work under two different perspectives: the bi-level approach and the *approximately optimal* approach.

[11] presented the bi-level approach, where the observations are regarded as the outcome of a perfect human motor control decision process while all imperfections reside in the observations. The method implements two optimization loops. The inner loop (or lower level loop) solves a direct optimal control problem for a given composite objective cost, written as a weighted sum of base objective functions. The outer loop (or upper level loop) then chooses the optimal values for the weights in order to minimize the least square error between the actual motion trajectory observations and the ones reconstructed by the direct optimal control problem. This method was used for instance by [41] and [42] for finding the weighted sum of objective functions that can explain an arm-pointing-to-a-bar paradigm. In [42] is proved that this paradigm is better explained when minimizing a composite objective cost. Moreover, the results from [41] support the previous idea and also show that even though we humans don't have prior knowledge of the bar end-target we are restricting ourselves in the same region on the bar. [43] and [44] used the same method in order to explain and to better understand the human arm motion in an industrial screwing task. In these papers, it was concluded that the criteria that needs to be minimized, in this kind of human motion planning, is a combination of known criteria, mainly energy and geodesic expenditure. This approach can also be applied on hybrid systems [5], where the goal is to find proper classes of criteria suitable to use when trying to explain and analyze this kind of systems.

[45] proposed a strategy that transformed the bilevel problem to a standard (one-level) optimization problem, by using the Karush-Kuhn-Tucker (KKT) conditions of optimality. In order to do that, they applied the KKT conditions to the lower level loop and then coupled them to the upper level loop, transforming the bilevel problem into a standard constrained optimization one. The latter, minimizes the squared difference error between the actual motion trajectory observations and the reconstructed ones, while satisfying the KKT conditions associated to the lower level loop. This approach was used to analyze the human arm movements [45], the rest-to-rest arm movements for different external dynamics [46] and the human navigation problems including the case of crossing interferer [47]. Also, in [48] they used this approach to infer the criteria minimized during the human reaching task in a kitchen environment, in order to use them on a 53 DoF iCub humanoid robot, so that the robot has a human-like behavior.

Contrariwise to the bi-level approach, [49] considers imperfections in the motor control decision process hence introducing the idea of *approximately optimal* decisions that may explain measured observations. Using parametrized Lagrangians, they interestingly showed that solving the inverse problem boils down to linear least square optimization, hence with explicit solution derived far more quickly than with the bi-level approach. In fact, they applied the residual techniques for inverse parametric optimization to the

KKT optimality conditions of the nonlinear program underlying a direct optimal control or an optimal planning problem. The method was then used, further emphasizing her nice computational performance with either continuous nonlinear systems ([50, 51]) and hybrid dynamical systems [52]. Recently, the inverse approximately optimal approach was used by [14] to analyze human locomotion paths data; they imputed a composite criterion involving energy expenditure and distance to target.

Nevertheless, when it is used with actual noisy data, the least square problem underlying the inverse approximately optimal approach needs to be handled with care because in such cases, the regressor may contain noise correlated to the noise acting on the right-hand side, then the outcome will be biased [53]. To prevent this issue, one has to apply filtering on the actual data or to use the instrumental variable method [54]. [55] shows how spline fitting and output filtering can be applied to the inverse optimal control problem in order to obtain better solutions in the presence of sampled and noisy data and proposed a recursive version of the inverse optimal control solution for differentially flat systems. They used this approach to obtain a model for the human stair ascent with application to learning controllers for lower limb prosthetic devices.

Finally, in our previous study [53], we proposed a new way of solving the inverse optimal control problem, when dealing with errors or uncertainties acting on the observations. We only assume that the errors are bounded with known bounds, otherwise unknown and we are interested in finding the outer set of feasible criteria solutions, while satisfying the KKT conditions.

1.2 Problem statement

The inverse optimal control problem can briefly be formulated as follows.
Given system dynamics:

$$\dot{x}(t) = f(x(t), u(t)), \tag{1.1}$$

with possible state and/or control constraints:

$$x(t) \in X \ , \ u(t) \in U \ , \ t \in [t_0, t_f] \tag{1.2}$$

and a set of trajectories

$$(x(t) \ , \ u(t))_{t \in [t_0, t_f], x_0 \in X} \tag{1.3}$$

parametrized by time and initial states.

The goal of the inverse optimal control is to impute the unknown parameter vector (c) associated to the preselected basis of criteria functions ($\Phi : X \times U \to \Re$) with respect to which all state and control trajectories are optimal trajectories for the direct optimal control problem with integral cost:

$$\begin{aligned} \underset{x,u}{\text{minimize}} \quad & \int_{t_0}^{t_f} c\Phi(t, x(t), u(t))dt \\ \text{subject to} \quad & h_j(t, x(t), u(t)) = 0, \quad j = 1, \ldots, m_1. \\ & g_j(t, x(t), u(t)) \leq 0, \quad j = 1, \ldots, m_2. \end{aligned} \tag{1.4}$$

with fixed or free terminal time t_f. Where c is an unknown parameter vector associated to the preselected basis of criteria, $x(t) \in X \subset \Re^n$ is the state, $u(t) \in U \subset \Re^m$ is the input, $\Phi : X \times U \to \Re$ are the preselected basis of criteria, while $h(t, x(t), u(t)) : \Re^k \longrightarrow \Re^{m_2}$ and $g(t, x(t), u(t)) : \Re^k \longrightarrow \Re^{m_1}$ are the possible equality and inequality constraints.

In practical settings, one rarely has access to complete trajectories. Typical experiments produce discrete samples from trajectories and possibly with additional experimental noise. The time samples consists of a set of $n \in N$ points $(t_i, x(t_i), u(t_i))_{i=1\ldots n}$. In our study we replace the integral from problem (1.4) by a discrete sum:

$$\begin{aligned} \underset{x_i,u_i}{\text{minimize}} \quad & \frac{1}{n}\sum_{i=1}^{n} c\Phi(t_i, x(t_i), u(t_i)) \\ \text{subject to} \quad & h_j(t_i, x(t_i), u(t_i)) = 0, \quad j = 1, \ldots, m_1. \\ & g_j(t_i, x(t_i), u(t_i)) \leq 0, \quad j = 1, \ldots, m_2. \end{aligned} \tag{1.5}$$

In this thesis, when analyzing experimental data by the means of an inverse optimal control problem, we assume that we have perfect observations of the system evolution while the imperfections are considered in the motor control decision process.

1.3 Outline of the thesis and contributions

In the followings, the organization of the thesis is discussed.

This thesis consists of a methodological part and an application on experimental data one. Chapter 2 and Chapter 6 correspond to the methodological part, while the other three (Chapter 3 to Chapter 5) illustrate Chapter's 2 methodology on human observed trajectories for three different human motor control tasks: the human arm trajectories

during an industrial screwing task, the postural coordination in a visual tracking task and the walking gait initialization task.

In Chapter 2, the approximately inverse optimal control approach is discussed. This chapter starts (see section 2.1) by presenting the KKT optimality conditions for a constrained optimization problem, and showing how these ones, combined with the residual techniques can reduce the inverse optimal control problem to a least square optimization one. The latter is known to be subjected to bias when dealing with noisy and sampled data and we illustrate this fact by imputing 3 criteria from simulated uniform distributed noisy data, with different noise variances. The simulated data is generated by using the unicycle robot type model and by solving an optimal control problem. This analysis is done to acknowledge the fact that before using the method on measured data, filtering or interpolation techniques need to be applied to them. We use this approach to infer criteria for experimental paradigms, in chapters 3 - 5, as it can be found stated below.

The above mentioned chapters are dealing with three different human motor tasks. For each of the three examples we impute the criteria that can explain the collected experimental data. All these tasks have in common the fact that they describe human tasks where humans select characteristic controls, but the tasks differ in the complexity of dynamics, constraints and criteria. Consequently, for each task we address the aspects of modeling problems. For all of these three tasks we assume that the human motor control, considered to be an optimal 'expert' process, is imperfect while the observed trajectories are perfect, considering the approximately inverse optimal control framework. Also the observations are the ones planned by the human motor control. Moreover, for each of the three applications an open loop analysis is performed. We will now briefly describe each task and the structure of the according chapter.

In chapter 3, the human arm trajectories during an industrial screwing task is analyzed, by addressing the approximately optimal control problem on the collected human arm trajectories. Section 3.1 introduces the state of the art of various related disciplines. In literature, this task is analyzed by the mean of a bi-level inverse optimal control problem with the price of a prolonged computational time and thus, the necessity of proposing the approximately optimal approach in order to reduce the computational time. The proposed task, the collected experimental data, the dynamical and geometrical human arm model are described in section 3.2. In section 3.3 is presented the direct optimal control problem with the equality and inequality constraints stating the human arm motion. The choice of the pre-selected basis of criteria needed to formulate the inverse optimal control problem is also discussed. The proposed criteria are the one found in the literature when analyzing the human arm motions. Certainly, each of these criteria have

certain limitations and the actual one used by the human motor control is unknown. Consequently, we propose our Inverse Approximately Optimal Control (IAOC) algorithm that will be firstly applied to the artificial data in section 4.5. In the next section (see section 3.5), we apply our algorithm to actual arm trajectories and we analyze the results. The used experimental data and the dynamical and geometrical models are provided by Prof. Dr. Philippe Fraisse, Dr. Vincent Bonnet and Dr. Nahema Sylla that they used in [44].

The second example of the application of our IAOC algorithm (from section 4.5 of chapter 3), consists of the postural coordination in a visual tracking task and is the subject of discussion in chapter 4. For this application, as for the previous one, we start with a literature review in section 4.1. The measurements, dynamical modeling and the conditions stating this human task are discussed in section 4.3 and section 4.3. This particular human motor control task has a bistable postural response, namely an in-phase mode and an anti-phase one. In this chapter, we will apply our algorithm to both in-phase and anti-phase modes, for which the problem is convex. The IAOC algorithm is applied in section 4.6, to the artificial data and in section 4.5 to the experimental ones. In both cases the numerical results of our algorithm are discussed. A further aspect related to this task consists in operating it in a closed loop. This aspect, along with a gain synthesis method are proposed for artificial data in section 4.7. The used experimental data is provided by Prof. Dr. Philippe Fraisse and Dr. Vincent Bonnet.

The third example of the IAOC algorithm application is discussed in chapter 5. Here, a pilot study for the human walking gait initialization task for non-parkinsonian and parkinsonian subjects is proposed. This chapter, starts with a literature review on the topic. We choose to model this paradigm by using a model predictive control (MPC) scheme, as it was done in [56]. The selected criteria are already proposed in literature and they can be found in section 5.2. The task consists of asking non-parkinsonian and parkinsonian subjects to start a normal and a quick walk on a force platform. After collecting the observations, i.e. the center of pressure returned by the force platform, we apply a pattern generator schema, proposed in [57], to reconstruct the center of mass trajectories (see section 5.3). Section 5.4 presents, on the one hand, the optimal control problem that is planning the walking gait initialization task. On the other hand, we apply the IAOC algorithm on artificial data and a first study is done for 6 non parkinsonian and 5 parkinsonian subjects, one trial per subject. The used experimental data is provided by EcoTech ANR project consortium.

Chapter 6 represents a methodological contribution of this thesis, in which we propose another approach to solve the inverse optimal control in a bounded error framework.

Solving the inverse optimal control problem in a bounded error framework arises because usually the errors and uncertainties action on the system and the observations may have a barely known nature. We formulated the problem in section 6.1, where it is discussed that this approach will find the convex hull of the set of feasible cost function solutions that can explain the optimal trajectories. Moreover, we have the certainty that the actual criteria is within the found convex hull set. Our method is capable of finding a set of feasible cost functions and not only one criterion or a combination of criteria. We validate it, in section 6.2, on the simulated uniform distributed noisy data described in Chapter 2. In subsection 6.2.3, we propose a way of numerically guaranteeing our method by using the IBEX tool, usually used for interval arithmetic and contractor programming. Our proposed approach will satisfy the KKT optimality constraints and therefore we assume that the imperfection are in the observations while the human motor control is a perfect optimal process.

Finally, conclusions on the presented results are stated in Chapter 7. Future work research ideas completes this thesis.

Chapter 2

Approximately inverse optimal control

The main objective of this chapter is to formally describe the approximately inverse optimal control approach in order to solve the inverse optimal control. We use the discretized unicycle robot type model, usually used when validating this approach [50], to generate noise free and uniform distributed noisy data in simulation to validate the approach.

2.1 Problem formulation

We consider an optimization problem with constraints, in which a decision x is made based on the optimization of a criterion subject to constraints:

$$\begin{aligned} \underset{x}{\text{minimize}} \quad & f(x) \\ \text{subject to} \quad & h_i(x) = 0, \quad i = 1, \ldots, m_1. \\ & g_i(x) \leq 0, \quad i = 1, \ldots, m_2. \end{aligned} \tag{2.1}$$

where $x \in \Re^n$ is the optimization variable, $f(x)$ is the known criterion also known as objective function or cost function to be minimized, h is the set of m_1 equality constraints such as $h(x) : \Re^k \longrightarrow \Re^{m_1}$, while g is the set of m_2 inequality constraints like $g(x) : \Re^k \longrightarrow \Re^{m_2}$.

We define the Lagrangian $L \in \Re^n \times \Re^{m_1} \times \Re^{m_2} \to \Re$ associated to the problem (2.1) as:

$$L(x, \nu, \lambda) = f(x) + \sum_{i=1}^{m_1} \nu_i h_i(x) + \sum_{i=1}^{m_2} \lambda_i g_i(x), \tag{2.2}$$

where ν_i and λ_i are known as the Lagrange multiplier associated with the ith equality constraint $h_i(x) = 0$ and inequality $g_i(x) = 0$, respectively. The Lagrange multipliers ν_i and λ_i are called the dual variables or Lagrange multiplier vector associated with the problem (2.1).

2.1.1 Karush-Kuhn-Tucker optimality conditions

If the given objective function, the equality and inequality constraints functions are differentiable functions, any pair of primal and dual variables must satisfy the KKT conditions [58].

We consider x^* and (ν, λ) to be the primal and dual optimal points with zero duality gap (meaning one can think of (ν, λ) as a certificate that proves x^* is optimal and similarly, we think of x^* as the assurance that proves (ν, λ) is dual optimal).

Since the primal optimal x^* minimizes the Lagrange associated to problem (2.1) over x, it implies that the Lagrangian gradient must be equal to zero at x^* :

$$\nabla_x L(x^*, \nu, \lambda) = \nabla_x f(x^*) + \sum_{i=1}^{m_1} \nu_i \nabla_x h_i(x^*) + \sum_{i=1}^{m_2} \lambda_i \nabla_x g_i(x^*) = 0. \tag{2.3}$$

We can now introduce the Karush-Kuhn-Tucker (KKT) conditions

$$g_i(x^*) \leq 0, \quad i = 1, \ldots, m_2 \tag{2.4}$$

$$h_i(x^*) = 0, \quad i = 1, \ldots, m_1 \tag{2.5}$$

$$\lambda_i g_i(x^*) = 0, \quad i = 1, \ldots, m_2 \tag{2.6}$$

$$\lambda_i \geq 0, \quad i = 1, \ldots, m_2 \tag{2.7}$$

$$\nabla_x f(x^*) + \sum_{i=1}^{m_2} \lambda_i \nabla_x g_i(x^*) + \sum_{i=1}^{m_1} \nu_i \nabla_x h_i(x^*) = 0, \tag{2.8}$$

where the first two conditions (2.4)-(2.5) are known as the primal feasibility conditions, Eqs. (2.6)-(2.7) are known as the complementary slackness conditions and the condition (2.8) is known as the stationarity condition. The latter condition is also known as Lagrange duality which takes into account the constraints by augmenting the criteria with

a weighted sum of the equality and inequality constraint functions. The complementary slackness condition implies:

$$\lambda_i > 0 \Longrightarrow g_i(x^*) = 0 \quad \text{and} \quad g_i(x^*) < 0 \Longrightarrow \lambda_i = 0 \tag{2.9}$$

When the problem (2.1) is convex, the KKT conditions are necessary and sufficient for the x^* and (ν, λ) points to be primal and dual optimal, with zero duality gap.

The formulation above is a *direct* optimization problem and it is used when one questions the optimal decision x^* when optimizing a known criteria f.

The purpose of this thesis is to solve the *inverse* problem of (2.1), which enables to impute the unknown criteria f and the dual optimal variables (ν, λ) while the constraints functions g and h and the primal optimal variables x^* are assumed known, as given by a set of observations.

To make the problem tractable, the focus of this thesis will be on the class of optimal control problems where the sought criterion is written as a weighted sum, hence a linear combination of known criteria base functions.

The criterion in (2.1) is now written as

$$f(x^*) = \sum_{i=1}^{k} c_i f_i(x^*), \quad c_i \geq 0, \tag{2.10}$$

where k is the number of pre-selected base functions and $c = \{c_i\} \in \Re_+^k$ is the unknown vector of weight values associated to each base function $f_i(x)$.

Here the choice $c_i \geq 0$, $i = 1, \ldots, k$ ensures that the composite criterion f is also convex when the basis functions f_i are convex.

Thanks to this parametrization, the stationarity and complementarity slackness KKT conditions (2.6)-(2.8) can be rewritten in compact form introducing also the *residuals* [49]

$$r_{c,i}(\lambda, x^*) \equiv \lambda_i g_i(x^*), \quad i = 1, \ldots, m_2 \tag{2.11}$$

and

$$r_s(c, \lambda, \nu, x^*) \equiv \sum_{i=1}^{k} c_i \nabla_x f_i(x^*) + \sum_{i=1}^{m_2} \lambda_i \nabla_x g_i(x^*) + \sum_{i=1}^{m_1} \nu_i \nabla_x h_i(x^*), \tag{2.12}$$

while the primal feasibility KKT conditions are satisfied, i.e. $g_i(x^*) \leq 0,\ i = 1, \ldots, m_2$ and $h_i(x^*) = 0,\ i = 1, \ldots, m_1$.

Then, solving the inverse optimal problem boils down to finding the weight vector $c \in \Re_+^k$ and the dual optimal variables $\lambda \in \Re_+^{m_2}$, $\nu \in \Re^{m_1}$ such as:

$$(r_s(c, \lambda, \nu, x^*) = 0) \wedge (\forall i \in \{1, \ldots, m_2\}\, r_{c,i}(\lambda, x^*) = 0) \tag{2.13}$$

2.1.2 Approximately inverse optimal control approach

The idea underlying the *approximately optimal* solution resides in the relaxation of constraints (2.13), i.e. the latter conditions are only held approximately, hence the residuals should be close to zero or merely minimized [49]. In the latter case, the magnitude of the residuals norm and of the dual variables may be used to assess the validity of the results: a large residuals norm and large values for the dual variables should indicate that the imputed composite criterion is not a good solution for the inverse optimization problem.

Observations x^* are now only approximately optimal, hence solving the inverse optimization problem boils down to :

$$\begin{aligned} \underset{c,\,\lambda,\,\nu}{\text{minimize}} \quad & \|r_s(c, \lambda, \nu, x^*)\|^2 + \sum_{i=1}^{m_2} \|r_{c,i}(\lambda, x^*)\|^2 \\ \text{subject to} \quad & \lambda_i \geq 0, \quad i = 1, \ldots, m_2, \\ & c_i \geq 0, \quad i = 1, \ldots, k. \end{aligned} \tag{2.14}$$

Note that the solution is obtained from the stationarity and complementarity residuals, while the equality and inequality residuals are only used to check the feasibility of solution x^*.

Interestingly, the residuals are linear with respect to the unknown variables c, λ and ν, it is easy to see that the problem (2.14) is a convex one and it should simplify to a least-square estimation. Gathering the gradients as column vectors of the following matrix A_0 as follows, where x^* dependence is omitted,

$$A_0 = [\nabla_x f_1,\ \ldots\ , \nabla_x f_k,\ g_1 + \nabla_x g_1,\ \ldots,\ g_{m_2} + \nabla_x g_{m_2},\ \nabla_x h_1,\ \ldots,\ \nabla_x h_{m_1}], \tag{2.15}$$

and defining

$$z_0 = [c\ \lambda\ \nu]\,, \tag{2.16}$$

Eq. (2.14) becomes

$$\begin{aligned} \underset{z_0=[c\ \lambda\ \nu]}{\text{minimize}} \quad & \|A_0(x^*)z_0\|^2 \\ \text{subject to} \quad & \lambda_i \geq 0, \quad i = 1, \ldots, m_2, \\ & c_i \geq 0, \quad i = 1, \ldots, k. \end{aligned} \tag{2.17}$$

The formulation (2.17) emphasizes well that the inverse optimal control problems are ill-posed problems. Firstly, when matrix A_0 is not singular, trivial solutions arise. For instance, $z_0 = 0$ is clearly a solution. Furthermore, if a given composite criterion f is a solution, so do $G \circ f$ or $f + \kappa$, where G is any convex increasing function and κ any constant. This issue is classically handled by using some prior knowledge on the sought objective function, hence one of the weights is arbitrary fixed to 1 [11]. In the sequel, we will denote this particular basis function as a *pivot* and denote the index by i^*,

$$\text{pivot} \equiv i^* \Rightarrow c_{i^*} = 1. \tag{2.18}$$

Remark 1. Given the experimental paradigms we will analyze in this thesis, we do not have access to such prior information. Therefore, we will have to consider all the basis functions as a potential pivot.

Using (2.18), we can build sub-matrix A from A_0 by removing $\nabla_x f_{i^*}$,

$$\begin{aligned} A = [\nabla_x f_1, \ \ldots \ , \nabla_x f_{i^*-1}, \ \nabla_x f_{i^*+1}, \ \ldots \ , \nabla_x f_k, \\ g_1 + \nabla_x g_1, \ \ldots, \ g_{m_2} + \nabla_x g_{m_2}, \ \nabla_x h_1, \ \ldots, \ \nabla_x h_{m_1}] \in \Re^{m \times n}, \end{aligned} \tag{2.19}$$

and define vector

$$b = -\nabla_x f_{i^*} \in \Re^m. \tag{2.20}$$

Defining the sub-vector

$$c_* = \{c_1, \ldots, \ c_{i^*-1}, \ c_{i^*+1}, \ldots, c_k\}, \tag{2.21}$$

If we have more equations than variables, i.e A is a 'tall' matrix (more rows than columns $m \geq n$) with linearly independent columns, Eq. (2.17) is an overdetermined least square one and can be rewritten as

$$\begin{aligned} \underset{z=[c_*\ \lambda\ \nu]}{\text{minimize}} \quad & \|A(x^*)z - b(x^*)\|^2 \\ \text{subject to} \quad & \lambda_i \geq 0, \quad i = 1, \ldots, m_2, \\ & c_i \geq 0, \quad i = 1, \ldots, i^* - 1, \ i^* + 1, \ldots, k. \end{aligned} \tag{2.22}$$

where $A(x^*) \in \Re^{m \times n}$ and $b(x^*) \in \Re^m$ are problem's data and $z \in \Re^n$ is the variable composed of the criteria weights c_*, inequality λ and equality ν Lagrange multipliers.

To the contrary, if there are more variables than equations, i.e A is a 'wide' matrix (more columns than rows $m \prec n$) with linearly independent rows, Eq.(2.17) is an underdetermined least square one and can be solved by using l_1 norm regularization techniques:

$$\begin{aligned} \underset{z=[c_* \ \lambda \ \nu]}{\text{minimize}} \quad & \|A(x^*)z - b(x^*)\|^2 + \eta \, |z|_1 \\ \text{subject to} \quad & \lambda_i \geq 0, \quad i = 1, \ldots, m_2, \\ & c_i \geq 0, \quad i = 1, \ldots, i^* - 1, \, i^* + 1, \ldots, k. \end{aligned} \tag{2.23}$$

where η is a small positive value.

To ensure an unique solution, for both underdetermined and overdetermined least square problems, the A matrix needs to be not singular i.e. its rows for the underdetermined case and columns for the overdetermined one are linearly independent.

Remark 2. In the case of each experimental task analyzed in this thesis, if the A matrix is found singular, it means that the chosen basis of criteria is redundant. In order to prevent this, a closer study will be done for each experimental paradigm. The study will consist in analyzing the form correlation between each criteria gradient's vectors.
The correlation between two vectors X and Y is calculated with the following mathematical expression:

$$Corr(X, Y) = \frac{\sum_{i=1}^{n}(x_i - \overline{x})(y_i - \overline{y})}{\sqrt{\sum_{i=1}^{n}(x_i - \overline{x})^2 \sum_{i=1}^{n}(y_i - \overline{y})^2}} \tag{2.24}$$

where $\overline{x}$ and $\overline{y}$ are the sample means of X and Y vectors.
If, for example, two criteria gradient's vectors (∇f_1 and ∇f_2) are found correlated:

$$|Corr(X, Y)| \geq \xi, \tag{2.25}$$

where ξ's value is equal to 0.95 for each application, we will conclude that this 2 gradient vectors cannot be used together. This can be explained by geometrical interpretation means, as follows: if the $Corr(X, Y)$ value is close to $\pm$ 1, the two vectors are collinear. So, they cannot be separated at the minimum value and it will be sufficient to keep only one in the A matrix.

2.2 Application to simulated data

2.2.1 Artificial optimal trajectories generation

We consider the discrete model of the unicycle robot type where the start and the end points are supposed known:

$$\begin{cases} x_{i+1} = x_i + \tau u_{1,i} \cos\theta_i \\ y_{i+1} = y_i + \tau u_{1,i} \sin\theta_i \\ \theta_{i+1} = \theta_i + \tau u_{2,i} \\ \zeta_0 = \zeta_{start} \\ \zeta_{N-1} = \zeta_{target} \end{cases} \tag{2.26}$$

Where τ is the sampling rate and $i = 0 : N-1$ is the time step, (x, y) the position, θ the orientation and u_1, u_2 the forward (linear) speed and angular speed respectively and $\zeta = \begin{bmatrix} x & y & \theta & u_1 & u_2 \end{bmatrix}^T$.

Then the artificial data is generated by solving an equality constrained optimization problem:

$$\begin{aligned} \underset{\zeta}{\text{minimize}} \quad & \frac{1}{2}\tau \sum_{i=0}^{N-1} \|u_{2,i}\|^2 + c_1 \|u_{1,i}\|^2 + c_2 \|\theta_i\|^2 + c_3 \|\varphi(\zeta, \zeta_{target})_i\|^2 \\ \text{subject to} \quad & \text{eq.(2.26)} \\ & c_i \geq 0 \;\; i = 1:3 \end{aligned} \tag{2.27}$$

with $\varphi(\zeta, \zeta_{target})$ the error between orientation and direction to the goal:

$$\varphi(\zeta_i, \zeta_{targeti}) = arctan(\frac{y_{targeti} - y_i}{x_{targeti} - x_i}) - \theta_i, \; i = 0 : N-1$$

2.2.2 The defining of the residual functions

Based on the equations formulated in Section 2.1, we apply the approximately optimal control approach to the (2.27) in order to recover the unknown weights $c = \{c_i\} \in \Re^{3\times 1}$ associated to the linear velocity, orientation and squared error between orientation and direction to the goal. The residual functions, presented in (2.11)-(2.12), associated to

the optimization problem (2.27) are:

$$\begin{aligned} &r_{eq} = h_j(\zeta),\ j = 1, \ldots, 3N \\ &r_s(c, \nu) = \nabla_\zeta \left\|u_2\right\|^2 + c_1 \nabla_\zeta \left\|u_1\right\|^2 + c_2 \nabla_\zeta \left\|\theta\right\|^2 + c_3 \nabla_\zeta \left\|\varphi\right\|^2 + \\ &+ \textstyle\sum_{j=1}^{3N} \nu_j \nabla_\zeta h_j(\zeta) \end{aligned} \tag{2.28}$$

Where $h_j(\zeta)$ represents the first three equality constraints presented in eq.(2.27). In this approach the measurements are supposed optimal, therefore r_{eq} needs to be satisfied, whereas the stationarity residuals, r_s vector, have the following form:

$$r_s(c, \nu^j) = \begin{bmatrix} c_3(\nabla_{x_1} \left\|\varphi\right\|^2) + \sum_{j=1}^{3N} \nu_j \nabla_{x_1} h_j(\zeta) \\ c_3(\nabla_{x_2} \left\|\varphi\right\|^2) + \sum_{j=1}^{3N} \nu_j \nabla_{x_2} h_j(\zeta) \\ c_2(\nabla_\theta \left\|\theta\right\|^2) + c_3(\nabla_\theta \left\|\varphi\right\|^2) + \sum_{j=1}^{3N} \nu_j \nabla_\theta h_j(\zeta) \\ c_1(\nabla_{u_1} \left\|u_1\right\|^2) + \sum_{j=1}^{3N} \nu_j \nabla_{u_1} h_j(\zeta) \\ \nabla_{u_2} \left\|u_2\right\|^2 + \sum_{j=1}^{3N} \nu_j \nabla_{u_2} h_j(\zeta) \end{bmatrix} \tag{2.29}$$

Finally, the solution is given by an unconstrained least square problem, easier than the first one (see (2.27)):

$$\begin{aligned} \underset{c,\nu_j}{\text{minimize}} \quad & \left\|r_s(c, \nu_j, \nu_{j+1})\right\|^2 \\ & c_i \geq 0 \ \ i = 1:3 \end{aligned} \tag{2.30}$$

The dimension of the residual, r_s, is of $(5N, 1)$, where N is the number of time sample and $\zeta \in \Re^5$. This problem is solved using algorithms for unconstrained least-squares problems presented in [58].

2.2.3 The criteria weights recovery

By testing the approach on the noise free data, we concluded that it is capable of finding the exact true criteria's weight.

First, we generate a trajectory using the optimization problem described in (2.27) with $\{c_1, c_2, c_3\}$ chosen randomly to be equal to $\{1.8508, 42.0533, 0.6590\}$. The observations on position, orientation, linear and angular velocities are used to solve the unconstrained least square optimization problem (2.30). Furthermore, uniform distributed noise with zero mean and three different values for the p variance is added to the observations and 100 trajectories for each of the three different variance values are generated.

We start by adding :

- σ_1 case: 0.5% of error to the positions and linear velocities, 1% error to the orientation and angular velocities.
- σ_2 case: 1.5% of error to the positions and linear velocities, 3% error to the orientation and angular velocities.
- σ_3 case: 2% of error to the positions and linear velocities, 4% error to the orientation and angular velocities

and we generated 100 trajectories for each of the three cases as presented in Fig. 2.1.

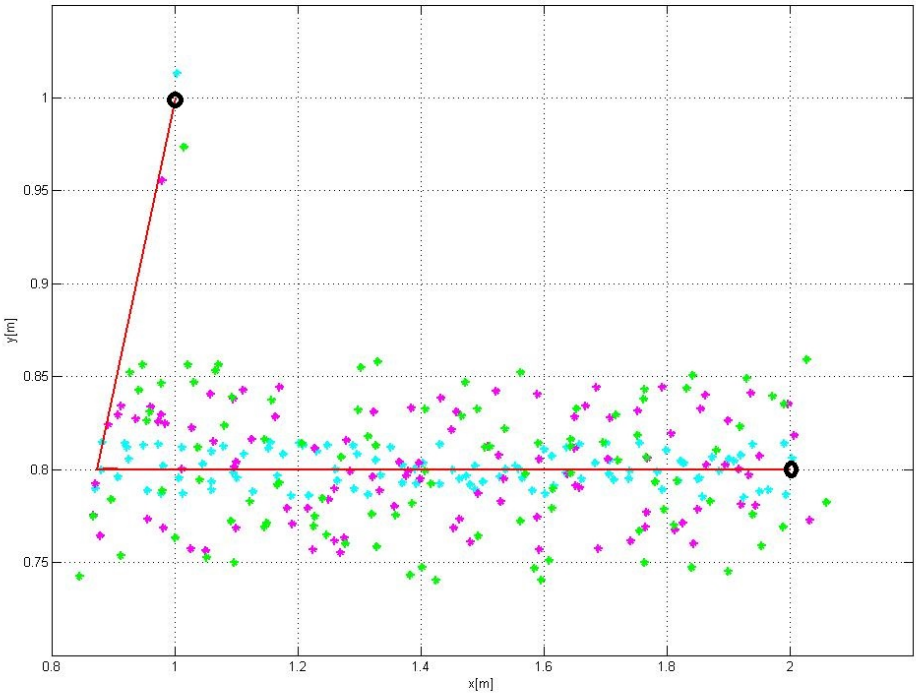

FIGURE 2.1: The trajectory obtained for $\{c_1, c_2, c_3\}$ equal to $\{1.8508, 42.0533, 0.6590\}$, using the unicycle model (red trajectory) with three different noisy trajectories. Uniformly distributed noise is added to the obtained trajectory as follows: 0.005 of error to the positions and the linear velocities, 0.01 error to the orientation and the angular velocities (cyan trajectories), 0.015 of error to the positions and the linear velocities, 0.03 error to the orientation and the angular velocities (magenta trajectories), 0.02 of error to the positions and the linear velocities, 0.04 error to the orientation and the angular velocities (green trajectories)

An unconstrained least square optimization problem is used to recover the $\{c_1, c_2, c_3\}$ weight values for each generated trajectory. The results illustrates a well known fact, that is least square with noisy regressor yields biased results [54].

Fig.2.2 shows that when noise variance is increased, the method exhibits bias in finding the criteria weights that can explain the observations.

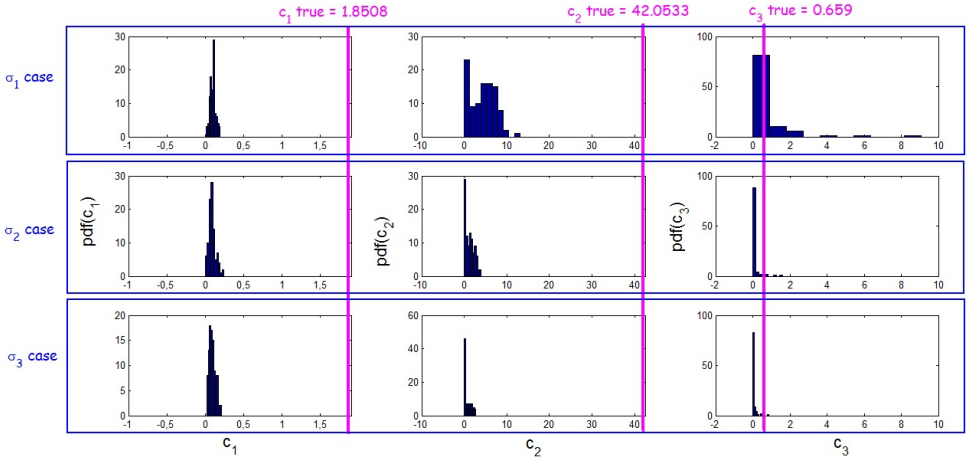

FIGURE 2.2: $\{c_1, c_2, c_3\}$ values obtained via the inverse approximately optimal control approach with 300 trials, 100 for each $\sigma_i, i = \{1, 2, 3\}$ case, where the correct value is represented by the pink dash line ($\{c_1, c_2, c_3\} = \{1.8508, 42.0533, 0.6590\}$)

These results clearly show that the approximately inverse optimal approach is very sensitive to the presence of noise in the measurement. In order to reduce bias, one should add minima filter data, use more advanced estimation methods [54] or use spline interpolation on measurements [55].

2.3 Summary

The use of the approximately optimal control approach to solve the inverse optimal control problem was presented in this chapter. Direct benefits of this approach is the computational time efficiency (it recovers the unknown criteria weight in 2 seconds) and reduces the initial constrained optimization problem to a least square one (eq.(2.22) or eq.(2.23)) in order to estimate criteria weights that can explain optimal trajectories.

When using this approach on noise free optimal observations, it is capable of finding the true value of the criteria weights. The fact that solving least square problems with noisy regressor can encounter bias problems is well known. The study of the noisy artificial data was done to acknowledge the fact that before using this method on measured data (usually noisy with unknown type of noise) one should use existing methods of filtering the regressor.

In this thesis, different experimental data will be analyzed by using the approximately optimal approach in order to impute the criteria that can explain them. Before applying it to measured data, we interpolate the experimental data with cubic splines (see Chapter 3 and Chapter 5) or with Fourier coefficients (see Chapter 4).

While analyzing the approximately optimal approach we had the idea about how solving the inverse optimal control in a bounded error framework. This is because usually the errors and uncertainties acting on the system and observations may have a barely known nature. This new approach will be the subject of discussion in Chapter 6.

Chapter 3

The human arm movement analysis during an industrial screwing task

In this chapter, we analyze the human arm movement during an industrial screwing task by the means of the approximately inverse optimization, in order to impute criteria that can explain this kind of task.

3.1 The analysis of human arm movements

During the years, efforts were made to explain the observed trajectories from human arm movements as a solution to the optimization problems. Hence, different optimal models have been proposed in literature and grouped [41] into five models: kinematics models, dynamic models, geodesic models, energetic models and neural or effort models. The term optimal models is understood as the criteria minimized in an optimization problem.

The kinematics models help us to obtain maximum smoothness in Cartesian or joint spaces and includes the minimization of hand jerk [59], the minimization of the angle jerk [60] and the constraint minimization of the angle acceleration [61]. The dynamic models are taken into account to avoid inverse dynamics and/or kinematics computations and to obtain the motor commands. These models plan the minimization of the torque [62] and of the torque change [63]. The geodesic model was proposed to predict human arm

movements in 3D dimensions [64, 65] and it is based upon the hypothesis that the spatial-temporal characteristics of the movements are evaluated separately. The temporal aspect suggests that the arm trajectories are obtained while minimizing the minimum jerk criteria, while the spatial aspect is described in the Riemannian manifold. Hence, the geodesic model selects the shortest path in the configuration space by using the kinetic energy metric and it presents the connection between the dynamic and kinematic models [65]. The energetic model was widely used in literature [66, 67, 68, 69] to predict human arm movements. This model involves the peak of work's minimization of torques [70], the positive work of torques [67] and the total absolute work of torques [68, 69] minimization. The latter corresponds to the mechanical energy spent to move the arm. Also, it has been considered that the total absolute work of torques or of muscular forces minimization can explain the inactivation principle. Meaning that both agonistic and antagonistic muscles acting on a joint during fast movements inactivates simultaneously [68, 69]. The neural models were often used to minimize the motor neural activity during a movement [71, 72]. Moreover, [41] assumed that the motor neurons give the motor command composed of efforts taken as torques accelerations as neural input to muscles.

All the optimal models presented above were used as a pre-selected base of objective functions for the inverse optimal control analysis of human arm movements, e.g. for the arm pointing to a bar paradigm [41, 42]. In these studies the bi-level approach was used and it was attain that this paradigm is better explained when minimizing not only one, but a combination of energy expenditure and joint-level smoothness [42], with further evidence presented in [41]. This shows that even though we, humans, do not have prior knowledge of bar end-target position we restrict it to the same region on the bar.

More recently, [43] and [44] investigated the motor task consisting in human arm motion during an industrial screwing task using inverse optimal control. They used the bi-level approach to impute the criteria with experimental data collected in human arm motion with and without exoskeleton assistance. The pre-selected basis of the objective functions they used were composed of seven objective functions related to the four optimal models, i.e. the kinematics, the dynamics, the geodesic and the energetic models. They showed that the human arm motion could be planned by optimizing a combination of energetic expenditure and geodesic criterion.

However, the outcomes of the bi-level approach were reached at the price of a prolonged computation time (around 30h as reported in [44]), significantly hampering its use for online applications. In this chapter, we will show that our method built upon the inverse approximately optimal control approach is capable of giving more thorough results in a very small computation time, in less than 1min.

3.2 The industrial screwing task

3.2.1 The task description

Eight right handed subjects (height: 1.70 m ± 0.5 m; weight: 63 kg ± 11 kg; age: 24 ± 7 years old), not familiar with the task to reproduce a typical screwing task. The task procedure can be summarized as follows: starting from an initial position with both hands across the body, they were asked to reach a target located 2 m above the ground, holding on a 0.95 kg screw gun in their right hand (seen fig. 3.1(a)). They maintained the target position for about 3 seconds, until they heard a sonar signal that indicated to return to the initial position. No instruction was given to the subjects about how to perform the movement. The subjects therefore performed the task in a natural way and at a preferred velocity.

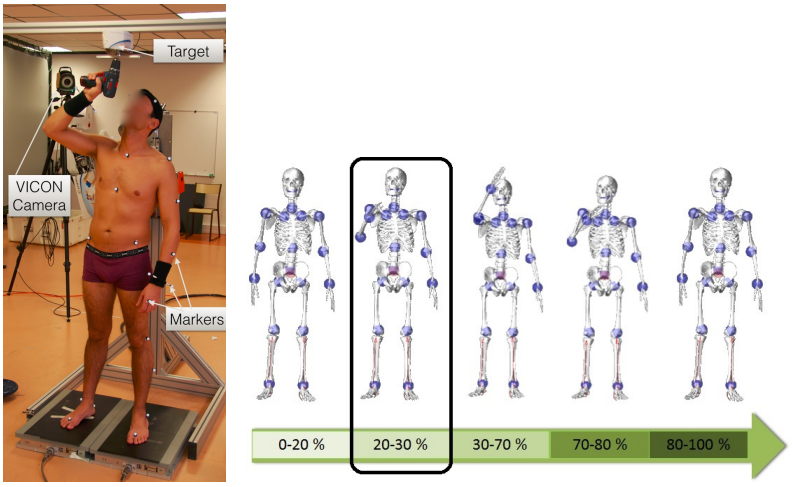

(a) (b)

FIGURE 3.1: The investigated motor task fig. 3.1(a); The different phases of the screwing task fig. 3.1(b)

The screwing task is composed of five operations, as presented in Fig. 3.1(b) :

- Phase 1. (0% to 20%) The subjects are in the initial position.
- Phase 2. (20% to 30%) The subjects raise their right arm to reach the target.
- Phase 3. (30% to 70%) The screw position is maintained and the right hand is above the heart.
- Phase 4. (70% to 80%) The subjects return to their initial position.
- Phase 5. (80% to 100%) The initial position is maintained.

In this thesis, we are only interested in analyzing phase 2 between 20% and 30% from the screw task cycle, during which subjects rise their arm.

3.2.2 The experimental measurements

A motion caption system of type VICON composed of 6 MX cameras that operate at 100 Hz, in combination with a set of 38 retro-reflective markers placed on anatomical landmarks in accordance with the Plug-in-Gait, the whole body marker template (Vicon Motion Systems) was used to record 3D kinematic quantities.

Subjects' joint angles averages and standard deviation were normalized to 100 points as it can be seen in fig. 3.3(c). One can see in this figure the relative low standard deviation of joint angles, showing that subjects perform similar and consistent movements to accomplish the screwing task. As it can be observed the wrist joints range of motion are very small (see θ_5 and θ_6). In consequence, the wrist joints will be neglected from the human arm model due to the small values exhibited when the shoulder is rotated, flexioned or extended and when the wrist is inclined. The human arm model used in this study contains only 4 DOF as represented in fig. 3.3(a).

3.2.3 The geometrical model

The used articular variables θ_1, θ_2, θ_3 and θ_4 are properly redefined in table 3.1. The

Angular position	Degree of freedom (DoF)
θ_1	flexion/extension of the shoulder
θ_2	abduction/adduction of the shoulder
θ_3	pronation/supination of the forearm
θ_4	flexion/extension of the elbow

TABLE 3.1: The articular variables used in human arm modeling definition

kinematic equations are given by the Denavit-Hartenberg parameters and the articular frames in the base reference frame can be seen in fig. 3.3(b). The direct geometric model (DGM) is used in order to calculate the orientation matrices and the hand Cartesian positions $(x(t), y(t), z(t))$ in the base frame with respect to angular position variables (θ_1, θ_2, θ_3, θ_4).

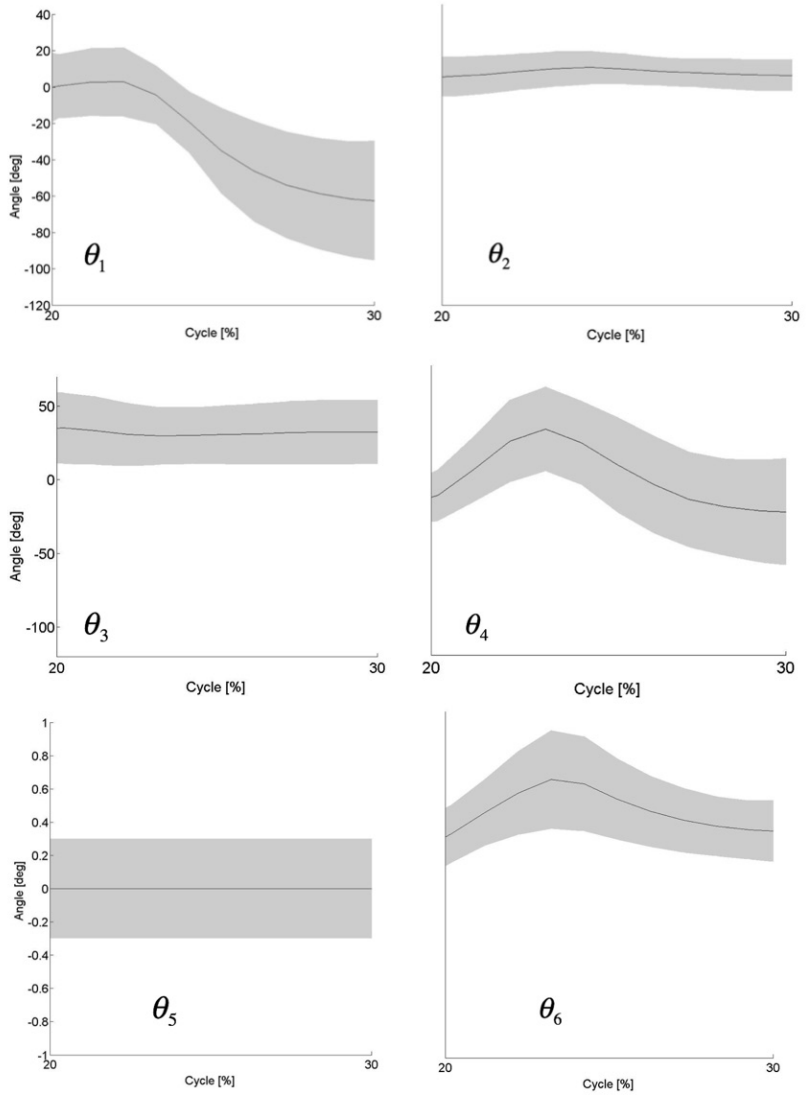

FIGURE 3.2: The average and the standard deviation of measured shoulder flexion/extension (θ_1), shoulder abduction/adduction (θ_2), forearm pronation/supination (θ_3), elbow flexion/extension (θ_4), wrist flexion/extension (θ_5) and wrist abduction adduction (θ_6), during phase 2 (20%-30% of the cycle) where the subjects raise their right arm to reach the target.

3.2.4 The dynamical model

The vector of joint torques are computed via the inverse dynamical model, derived from Lagrange formulation:

$$\Gamma = M(\theta)\ddot{\theta} + C(\theta, \dot{\theta})\dot{\theta} + G(\theta) \tag{3.1}$$

where $\theta = [\ \theta_1 \quad \theta_2 \quad \theta_3 \quad \theta_4\ ]^T$ corresponds to the vector of joint angles, $\Gamma = [\ \Gamma_1 \quad \Gamma_2 \quad \Gamma_3 \quad \Gamma_4\ ]^T$ is the vector of joint torques, $M(\theta) \in \Re^{4\times4}$ is the inertial matrix, $C(\theta, \dot{\theta}) \in \Re^{4\times4}$ is the Coriolis and Centrifugal effect matrix and $G(\theta) \in \Re^{4\times1}$ is the gravity vector. One can

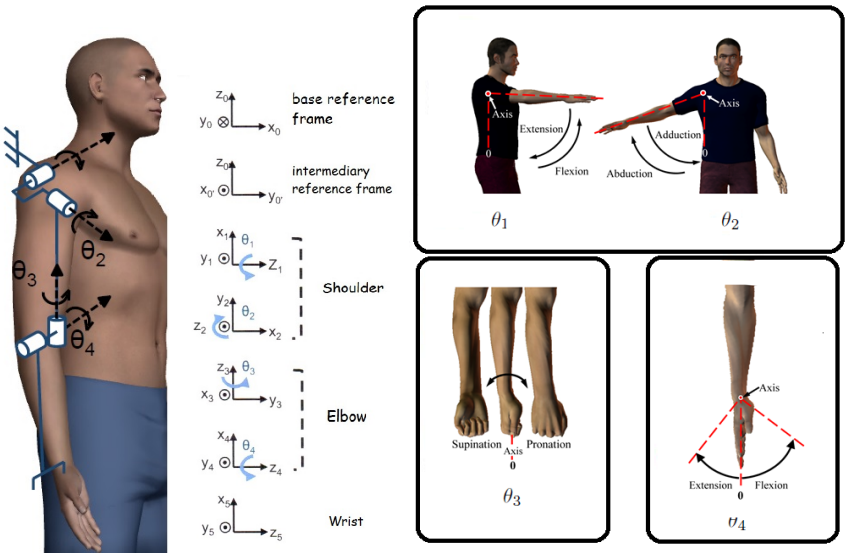

(a) (b) (c)

FIGURE 3.3: The human arm kinematic model used [1].

find presented in more details the calculation of this matrices in [73], where the inertial parameters are estimated from the anthropomorphic table presented in [74].

3.3 The inverse optimal control problem solution

We will now analyze the arm movement joint trajectories collected during the screwing task by means of the inverse approximately optimal approach. To do this, we need to formulate first the direct optimal control (DOC) problem and the underlying KKT optimality conditions.

3.3.1 The direct optimal control problem

The direct problem is formulated as a planning problem where joint angle trajectories are sought, which minimize a given composite criterion and satisfy the constraints. To curb the planning problem complexity, we will use parameterized joint trajectories with B-spline interpolation as it is classically done in robotics motion planning, but also in the framework of inverse optimal control (a.o. [55, 44]). As a consequence, the actual joint trajectories will also be interpolated by applying spline-fitting on the observed data as in [55]. Finally, the optimal planning problem will be solved with respect to the B-spline *knots* vectors w.

Interestingly, spline interpolation will act as a filtering procedure and should prevent any distortion in the estimation that can be due to the presence of correlated noise in the regressor of the least square problem (2.22). In addition, the angular positions and their derivatives are afterwards deduced from the knots by using a spline interpolation with the degree dependent on the number of derivatives desired to be found. Generally a spline of r^{th} order can be differentiated $(r-2)^{th}$ times. Since we need the 3^{rd} derivative of the angular position, a 5^{th} order spline should be enough in order to obtain good interpolation. Here, we will use then a spline polynomials of the 5^{th} order with $n' = 13$ knots per joint angular position trajectory. Finally, in the direct optimization problem, we assume that the initial and final joint positions are known by the subjects, then the direction optimal planning problem formulates as follows:

The direct optimal control problem: "Find the $n \equiv 4(n'-2)$ knots vector w, between a prior known initial and final positions, such as this spline-interpolated joint trajectories passing through the knots can achieve the industrial screwing task while satisfying given bounds on joint angle positions and minimizing a given composite criteria".

3.3.1.1 The inequality constraints

In order to obtain realistic human arm movements, the optimal trajectories need to satisfy the joint angular limitation values, as defined in the literature [75, 76]. The inequality constraints are gathered below:

$$\begin{aligned} g_1(\theta_j) &= \theta_{j_{min}} - \theta_j, \quad k = 1:4. \\ g_2(\theta_j) &= \theta_j - \theta_{j_{max}}, \quad k = 1:4. \end{aligned} \tag{3.2}$$

where $\theta_{j_{min}}$ and $\theta_{j_{max}}$ are the minimal and maximal angular values for each joint position presented in table 3.2.

TABLE 3.2: The angular limitation values for the 4 joints

	θ_{min} [deg]	θ_{max} [deg]
θ_1	-180	50
θ_2	-150	30
θ_3	-90	85
θ_4	-160	0

3.3.1.2 The choice of the objective functions

The selected optimal control objective functions used as a basis for the composite criterion are the ones usually encountered when studying the human arm motion tasks. Our basis consists of the following objective functions already discussed in Sect.3.1: the Cartesian jerk criterion which is related to hand motion smoothness, the joint angle acceleration and angle jerk criteria which characterize joint angle motion smoothness, and the torque, torque change, geodesic, energy (absolute work of forces) and effort related criteria. The eight basis objective functions are gathered in table 3.3, seven of which are differentiable, whereas the energy criterion is non-smooth. The latter function is usually considered when studying human arm movements and has been shown to be related to the inactivation principle [69]; it was found that during fast arm movements simultaneous inactivation periods of both antagonistic and agonistic muscles can be predicted using a non-smooth criterion. We assume as in [69], that the CNS can minimize the non-smooth function to predict muscle inactivation, along with some integral costs for smoothness and precision of the arm movements.

The direct optimal control problem that needs to be solved in order to generate human arm displacements, boils down to solving the following optimization problem:

$$\begin{aligned} \underset{w}{\text{minimize}} \quad & \sum_{i=1}^{8} c_i f_i(w), \\ \text{subject to} \quad & g_j(w) \leq 0 \;\; j = 1, \ldots, 8. \end{aligned} \tag{3.3}$$

Note that now the decision variables are the B-spline knots gathered in vector $w \in \Re^n$. The constraint and objective functions depends on the interpolated joint angle trajectories, which in turn are function of knots vector w.

3.3.2 The inverse approximately optimal control problem

We can now address the inverse approximately optimal control problem using the method described in Chapter 2. We just need to specify matrix $A \in \Re^{m \times n}$ in Eq. (2.19) and vector $b \in \Re^m$ in Eq. (2.20), composed of criteria gradient's vectors. For this case, the A matrix is a tall not singular one having more columns than rows ($m \geq n$). Moreover, we checked the correlation (see eq.(2.24)) between each criteria gradient's vectors and they were found uncorrelated, for both artificial and experimental data. So, the criteria will be imputed by solving the overdetermined least square problem (2.22).

TABLE 3.3: The pre-selected basis of objective functions;
N: number of time samples

Criterion	**Cost function** (f_i)	References
Cartesian jerk	$f_1 = \frac{\sum_{i=1}^{N} \dddot{x}_j^2 + \dddot{y}_j^2 + \dddot{z}_j^2}{N}$	[59]
Angular jerk	$f_2 = \frac{\sum_{i=1}^{N} \sum_{i=1}^{4} \dddot{\theta}_{ij}^2}{N}$	[60]
Angle acceleration	$f_3 = \frac{\sum_{i=1}^{N} \sum_{i=1}^{4} \ddot{\theta}_{ij}^2}{N}$	[61]
Torque	$f_4 = \frac{\sum_{i=1}^{N} \sum_{i=1}^{4} \tau_{ij}^2}{N}$	[62]
Torque change	$f_5 = \frac{\sum_{i=1}^{N} \sum_{i=1}^{4} \dot{\tau}_{ij}^2}{N}$	[63]
Geodesic	$f_6 = \frac{\sum_{i=1}^{N} (\dot{\theta}^T M(x) \dot{\theta})^{1/2}}{N}$	[64] [65]
Energy	$f_7 = \frac{\sum_{i=1}^{N} \sum_{i=1}^{4} \left\lvert \dot{\theta}_{ij} \tau_{ij} \right\rvert}{N}$	[66] [67] [68] [69]
Effort	$f_8 = \frac{\sum_{i=1}^{N} \sum_{i=1}^{4} \ddot{\tau}_{ij}^2}{N}$	[69]

Secondly, we must choose which basis objective function will act as pivot i^*. As previously discussed, the choice of the pivot relies on prior knowledge of the sought composite criterion. In order not to corrupt any conclusion to be derived when analyzing the industrial screwing task, we consider that there is no such prior knowledge. As a consequence, we will have to consider any basis function as potential pivot. Then, comparing the solutions of the problem (2.22) we will keep the solutions that show good consistency with the experimental data, those which minimize both the *residuals norm* (3.4) and the root mean square (RMSE) (3.5) described below.

The residuals norm is defined as

$$\frac{1}{n}\|\nabla_w L(\hat{c})\| = \frac{1}{n}\|A\hat{c} - b\|^2, \tag{3.4}$$

and the RMSE is defined as

$$\text{RMSE} = \sqrt{\frac{\sum_{j=1}^{N}(\theta_{mes_j} - \theta_{est_j})^2}{N}} \tag{3.5}$$

where θ_{mes_j} represents the actual observed joint angle positions, θ_{est_j} represents some estimated joint angle position and N is the number of time samples of the joint angle position trajectory.

Finally, our algorithm for solving the inverse problem is as follows:

Algorithm **IAOC** (input: x^*, output: $\{\hat{c}\}$)

- For pivot $i^* = 1$ to k (here $k = 8$)
  1. build matrix A as in Eq. (2.19),
  2. build vector b as in Eq. (2.20),
  3. solve problem Eq. (2.22) and obtain vector $\hat{c}$,
  4. compute residuals norm $\frac{1}{n}\|\nabla_w L(\hat{c})\|$ as defined by Eq. (3.4),
  5. use $\hat{c}$ and solve DOC problem Eq. (3.3) to generate planned joint angle trajectories θ_{est},
  6. compute RMSE defined by Eq. (3.5).
- Keep solution vectors $\hat{c}$ that minimize both residuals norm and RMSE.

3.4 Evaluation on artificial data

In this section, we perform the evaluation of the performance of our method using artificial data. Using the 4 DOF thorough dynamical model of the human arm (introduced in Sect.3.2), we solve DOC problem (3.3) with vector c tuned such that only one single basis objective function is active at the time. We come with eight planned joint trajectories, each minimizing a single basis objective function given in Table 3.3.

For each artificial data generated, we apply our algorithm **IAOC** as defined in Sect.3.3.2. When the objective function used as pivot is the actual objective function, we obtain the smallest residuals norm and an RMSE of 0. The results are gathered in Table 4.2.

TABLE 3.4: The results obtained on artificially generated optimal trajectories; $I = \{1, \ldots, 8\}$

Optimal trajectory generated using :	A	b	$\frac{1}{n}\|\nabla L(\hat{c})\|$	RMSE [deg]
$\min f_1$	$[\nabla f_i],\ i \in I \setminus \{1\}$	$-\nabla f_1$	0.0001	0
$\min f_2$	$[\nabla f_i],\ i \in I \setminus \{2\}$	$-\nabla f_2$	0.0007	0
$\min f_3$	$[\nabla f_i],\ i \in I \setminus \{3\}$	$-\nabla f_3$	0.00003	0
$\min f_4$	$[\nabla f_i],\ i \in I \setminus \{4\}$	$-\nabla f_4$	0.0001	0
$\min f_5$	$[\nabla f_i],\ i \in I \setminus \{5\}$	$-\nabla f_5$	0.0001	0
$\min f_6$	$[\nabla f_i],\ i \in I \setminus \{6\}$	$-\nabla f_6$	0.000004	0
$\min f_7$	$[\nabla f_i],\ i \in I \setminus \{7\}$	$-\nabla f_7$	0.001	0
$\min f_8$	$[\nabla f_i],\ i \in I \setminus \{8\}$	$-\nabla f_8$	0.002	0

TABLE 3.5: The results obtained for the optimal trajectory number 6 generated by minimizing f_6 criterion; $A = [\nabla f_i], i \in \{1, \ldots, 8\} \setminus \{i^*\}$, $b = -\nabla f_{i^*}$

	Contribution [%]										
i^*	f_1	f_2	f_3	f_4	f_5	f_6	f_7	f_8	$\frac{1}{n}\|\nabla L(\hat{c})\|$	RMSE [deg]	γ
1	67.78	0	0	0	0	0	32.22	0	0.362	14.59	+
2	0	0.18	0	0.04	0	99.78	0	0	1	5.78	-
3	0	0	0.33	0.13	0	99.53	0.01	0	0.058	4.76	-
4	0	0	0.45	99.55	0	0	0	0	0.489	35.18	+
5	0	0	0	0	100	0	0	0	0.282	15.71	+
6	0	0.01	0	0	0	99.99	0	0	0.000004	0	
7	0.34	0	0	0	0	0	99.65	0	0.03	13.05	+
8	0	0	0	0	0	0	0	100	2.601	15.43	+

Analyzing further the results, there were some cases where the imputed composite criterion included the correct objective function even if the actual one is not used as pivot. However, in such cases, the residuals norms were too large. Let us illustrate in details the case of the artificial data generated by minimizing f_6. Thorough results are gathered in Table 3.5. The first column indicates the pivot used, and for each case, the line contains the imputed composite criterion thus obtained. The contribution of each basis objective function is given as relative contribution in percentage computed as:

$$f_j = 100 \frac{c_j f_j}{\sum_{i=1}^{8} c_i f_i} [\%], \quad j = 1 : 8. \tag{3.6}$$

Each line contains also the residuals norm and the RMSE. The last column contains the sign of the inner product

$$\gamma = \text{sign}\langle \nabla_w f_{i^*}, \nabla_w f_6 \rangle. \tag{3.7}$$

Table 3.5 clearly shows three types of results.

- When one sets pivot i^* to 6, the inverse optimal control problem emphasizes that the imputed composite criterion includes f_6 which contribution is larger than

99.99% with very small residuals norm and zero RMSE.

- When one sets pivot i^* to 2 or 3, the inverse optimal control problem emphasizes that the imputed composite criterion includes f_6 which contribution is larger than 99.53%. However, both the residuals norm thus computed and the RMSE are large. In particular, the residuals norms are 1000 times larger than the case $i^* = 6$.

- When one sets pivot i^* to 1, 4, 5, 7 or 8, then none of the imputed composite criterion contains f_6, and even more both residuals norm and RMSE are large. In particular, RMSE computed are at least three times the ones obtained with i^* set to 2 or 3.

These outcomes can be explained by considering a geometrical perspective. Solving least square problem (2.22) is equivalent to the projection of vector b onto the manifold defined by the span of A matrix column vectors. However, since this projection is constrained to non-negative values of c_*, the true objective function cannot appear if the inner product between the gradient of the pivot objective function (∇f_{i^*}) and the gradient of the true one (∇f_6) is positive.

To clarify, let us consider the case of a basis with two objective functions only, $\{f_{i^*},\ f_6\}$. We have

$$\begin{aligned} (\text{sign}\langle \nabla f_{i^*}, \nabla f_6 \rangle > 0) \quad &\Rightarrow \quad \exists \zeta > 0,\ \nabla f_{i^*} = \zeta \nabla f_6 + \nabla f_{i^*}^{\perp} \\ &\Rightarrow \quad \exists \zeta > 0,\ \nabla f_{i^*} - \zeta \nabla f_6 = \nabla f_{i^*}^{\perp} \end{aligned} \tag{3.8}$$

where $\nabla f_{i^*}^{\perp}$ is such that $\langle \nabla f_{i^*}^{\perp}, \nabla f_6 \rangle = 0$. In this case, the imputed composite function weights are $c = \{1,\ -\zeta\}$ which contradicts the constraint $c_i \geq 0$. Satisfying the latter positivity constraints, the only feasible solution is $\zeta = 0$. The inner product γ is negative for $i^* = 2$ or 3, therefore objective function f_6 can appear in the imputed composite criterion. To the contrary, the inner product γ is positive for $i^* = 1$, 4, 5, 7 or 8, therefore objective function f_6 cannot appear in the imputed composite criterion.

This emphasizes the necessity to test each basis objective function as a potential pivot and to retain the solutions which minimizes both the residuals norm and the RMSE.

The computation time for realizing these tests on a Intel(R) Core(TM) i7-3630QM CPU@2.40GHz breaks down as follows. The computation of the eight gradients using finite differentiation takes less than 10s. Solving the eight inverse problems (2.22) (one per pivot) takes less than 25s. Solving one DOC for either generating the artificial data or validating the imputed composite objective function takes an average of 1200s. Finally, once the data are generated, solving one inverse optimal control using our **IAOC** algorithm, i.e. computing gradients and solving problem (2.22) takes less than 35s.

These results clearly demonstrate the nice performance of the inverse approximately optimal approach.

3.5 Experimental results

In this section, we use our algorithm as defined in Sect. 3.3.2 to analyze actual joint position data gathered during the screwing task described in Sect.3.2 using the objective functions basis given in Table 3.3.

The outcomes of the **IAOC** algorithm are gathered in Table 3.6. Each line contains the results obtained for a given choice of pivot i^*, as indicated in the first column. It also contains the imputed composite criterion thus obtained, where the contributions are given as in (4.1), the residuals norm as defined in (3.4) and the RMSE as defined in (3.5). The DOC problem (3.3) performed for computing the RMSE uses the knots vector fitting the actual data as initial guess for the optimization algorithm.

Using the residuals norm as a measure of consistency, Table 3.6 clearly shows two possible candidates :

- The best candidate, i.e. the one which yields minimal residual norm, is R_6. It uses f_6 as pivot and obtains 100% contribution for the geodesic criterion;
- The second best candidate with a small residual norm, 10 times larger, is R_{78}. It uses f_7 as pivot and yields 99.66% contribution for the energy expenditure and 0.34% contribution for the effort criterion.

The other combinations all exhibit larger residuals norms (more than 20 times the norm obtained for the best candidate) and should be discarded.

Now, using the RMSE as a measure of consistency, Table 3.6 also clearly shows two possible candidates :

- The best candidate, i.e. the one which yields minimal RMSE is R_{78}.
- The second best candidate with an acceptable RMSE is R_6.

The other combinations all exhibit very large RMSE (10 times the best RMSE) and should be discarded.

The first conclusion is that the two measures derive consistent results as they both exclude all results computed using pivot $i^* \in I \setminus \{6, 7\}$ and both point at candidate

TABLE 3.6: The **IAOC** algorithm results obtained for actual data. $A = [\nabla f_i], i \in \{1, \ldots, 8\} \setminus \{i^*\}$, $b = -\nabla f_{i^*}$

i^*	Contribution [%]								$\frac{1}{n}\|\nabla L(\hat{c})\|$	RMSE [deg]	
	J_1	J_2	J_3	J_4	J_5	J_6	J_7	J_8			
1	8.89	0	0	6.02	0	0	85.09	0	275.122	21.93	
2	0	79.18	0	20.82	0	0	0	0	11239	24.15	
3	0	0	68.03	31.97	0	0	0	0	8	20.58	
4	0	0	0	99.92	0.01	0	0	0.07	0.3	35.61	
5	0	0	0	30.61	58.78	0	10.62	0	2.245	21.58	
6	0	0	0	0	0	100	0	0	0.005	4.07	R_6
7	0	0	0	0	0	0	99.66	0.34	0.059	2.56	R_{78}
8	0	0	0	19.82	0	0	77.99	2.19	867.145	27.85	

solutions R_6 and R_{78} as obtained with pivot $i^* \in \{6, 7\}$. For the latter candidate solutions, Table 3.7 shows the RMSE repartition onto of the four joint angles. The table also shows the correlation coefficient between the reconstructed trajectories and the actual one, a coefficient we use as a measure of similarity.

Since the RMSE obtained for the two candidate solutions, R_6 and R_{78}, are quite close, and since the DOC (3.3) is convex, this suggests that almost any combination of the two candidate solutions may also be a solution. To assess this claim, we have performed DOC computations for several combination of the two solutions. The results are gathered in Table 3.7 : combination $T_1 \equiv 75\%R_6 + 25\%R_{78}$, $T_2 \equiv 50\%R_6 + 50\%R_{78}$ and $T_3 \equiv 28\%R_6 + 72\%R_{78}$. Figures 3.4-3.5 gather all the joint trajectories reconstructed along with the actual data. These results suggest that all the combinations of R_{78} and R_6 tested could be acceptable by considering an RMSE bound of 7 degrees.

Nevertheless, the smallest residuals norm obtained with the actual data ($5 \cdot 10^{-3}$, solution R_6) remains quite large when compared to the best residuals norm obtained with the artificial data ($4 \cdot 10^{-6}$, Table 3.5, line $i^* = 6$). This suggests that the pre-selected objective functions basis is incomplete and may be enriched with other criteria.

To summarize, the inverse approximately optimal control approach presents a significant advantage when compared with the results of the bi-level method used on this paradigm and as reported in [44]. The inverse approximately optimal approach results can naturally provide a subset of composite cost functions that contribute to the movement. Within the subset selected, one could further investigations by solving direct optimal control problems and determine which combination is the best in term of average RMSE, for instance. Moreover, the structure of the bi-level approach yields an unique composite criterion without any proof that this is the global minimum while requiring a huge computation time, reported larger than 30h on this paradigm [44].

TABLE 3.7: RMSE evaluation for DOC using candidate solutions R_6 and R_{78} and combination $T_1 = 75\%R_6+25\%R_{78}$, $T_2 =50\%R_6+50\%R_{78}$ and $T_3 = 28\%R_6+72\%R_{78}$

	R_6		T_1		T_2		T_3		R_{78}	
	RMSE [deg]	Corr	RMSE [deg]	Corr	RMSE [deg]	Corr	RMSE [deg]	Corr	RMSE [deg]	Corr
θ_1	2.06	0.99	10.05	0.97	1.75	0.99	1.66	0.99	1.11	0.99
θ_2	1.64	-0.42	0.96	-0.10	0.96	0.05	0.97	-0.18	1.19	0.26
θ_3	6.52	0.60	4.88	0.79	4.57	0.81	4.62	0.81	4.73	0.81
θ_4	4.11	0.99	5.74	0.98	2.08	0.99	1.89	0.99	1.15	0.99
RMSE total [deg]	4.07		6.30		2.70		2.67		2.56	

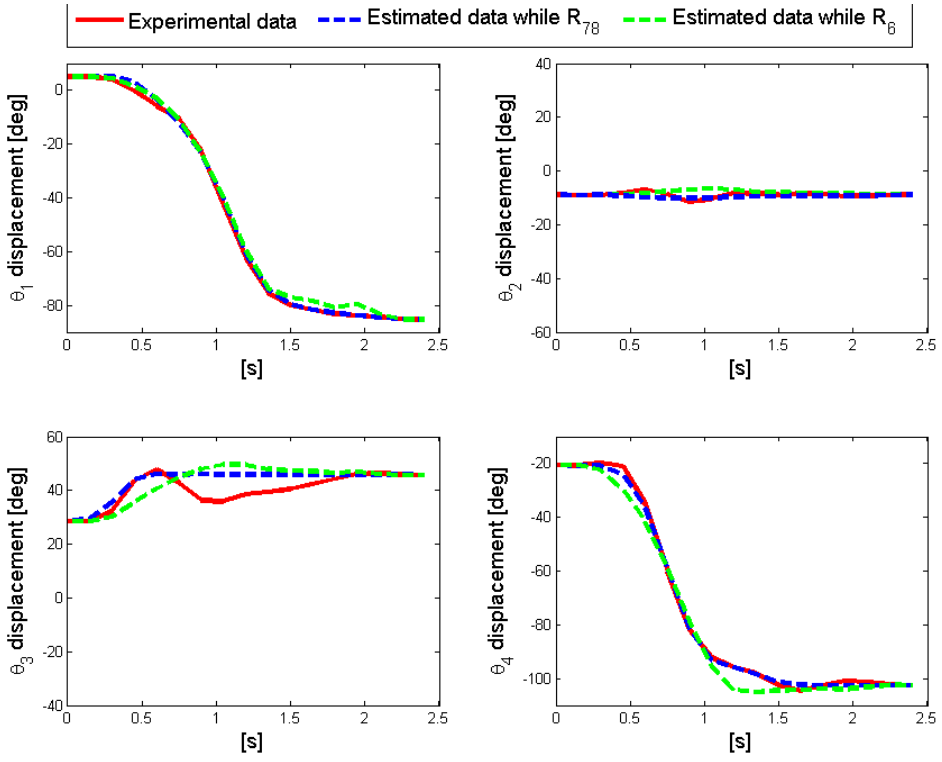

FIGURE 3.4: The observed angle displacements (red line) and the estimated angle displacement(doted blue line and doted green line) while minimizing the exhibited criteria from the inverse optimal control while using f_7 and f_6 as pivots

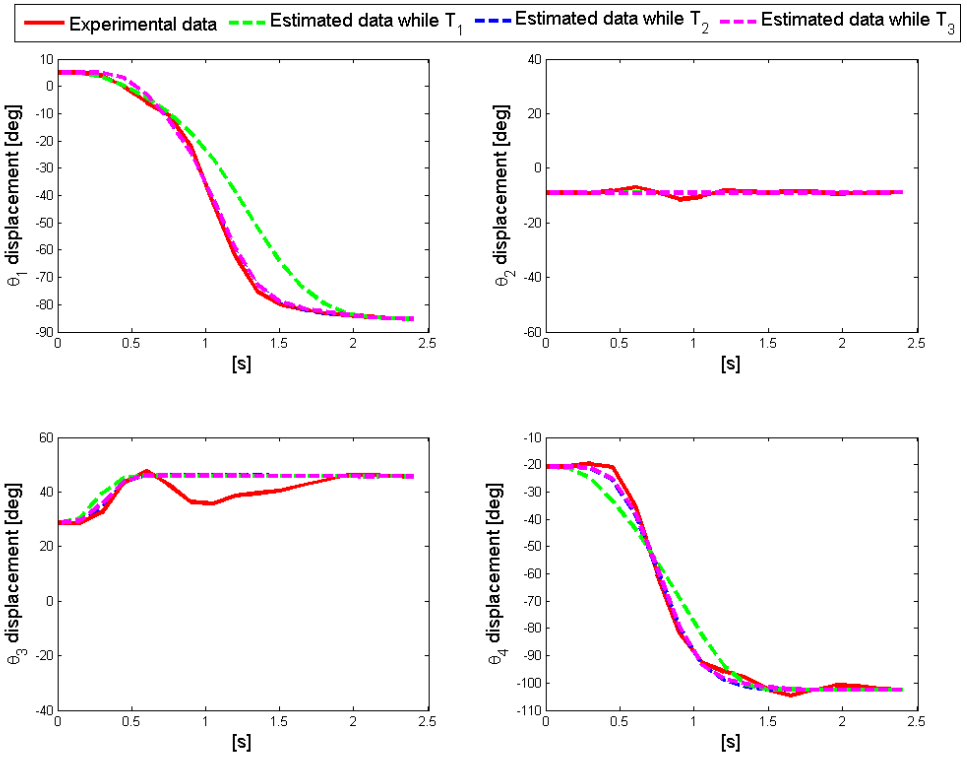

FIGURE 3.5: The observed angle displacements (red line) and the estimated angle displacement: doted green line in the T_1 case, doted blue line in the T_2 case and the doted magenta line in the T_3 case

3.6 Summary

In this chapter, we introduced a general procedure to efficiently impute the composite criterion that can explain the human movement. We used our procedure to analyze the human arm movement within an industrial screwing task.

We manage to successfully solve the inverse optimal control problem in a very fast and efficient way. Our procedure, built upon the inverse approximately optimal control approach, yields results 3000 times faster than the bi-level approach, when used on the same experimental paradigm. Including the verification steps, consistent results can be obtained more than 60 times faster than the bi-level approach.

This significant reduction in computation time makes it now possible to consider using the inverse optimal control approaches for online applications. One can apply this new procedure for inverse optimal control within clinical studies involving a large number of patients as well as within ergonomic studies in industrial environments.

The reduction in computation time will also make it possible to embed motion capture systems with online and adaptive capabilities for quantitative movement analysis based on inverse optimal control approaches. The inverse approximately optimal control approach is able to provide within 35s the subset of the weight coefficients involved in the human movement.

Moreover, our procedure can naturally exhibit a set of candidate solutions for the composite criterion, if they exist. Therefore, it may be used as a fast on-line classification tool to build human movement categories.

This method is to be considered a good candidate for clinical studies with a large number of patients as well as for ergonomic studies in industrial environment to evaluate the impact of exoskeletons or specific movements in assembly lines [43]. Indeed, in the clinical studies, the assessment of movement rehabilitation protocol on patients could use this approach to provide the therapist with a fast result showing the trend in the way of recovery. In conclusion, we can underline the efficiency of the method to provide quickly a subset of cost function candidates attached to a specific movement. Then, the result can be refined by using forward optimal control to find the best combination of all contributions minimizing the average of RMSE.

Finally, this significant reduction in computation time clears the limitations preventing from using a basis with a larger number of objective functions. It is now tractable to consider some other objective function basis, for instance by computing one basis

objective function per joint angle, thus allowing to break down the contribution of each joint angle optimal control model to the whole movement.

Chapter 4

The analysis of the postural coordination in a visual tracking task

4.1 Related literature

In the study of the human movement, the experimental paradigm consisting in tracking a visual moving target in a balanced stance has often been a subject of interest [77, 78, 79, 80, 81].

[78] considered a visual tracking task in the sagittal plane and examined the full body joint coordination. The experiment implied having participants moving back and forth in the sagittal plane in order to track a virtual target. This experimental paradigm emphasized key properties for the human postural control system, such as phase transition, multistability, critical fluctuations, hysteresis, and critical slowing down.

In [82], two postural strategies are observed when the whole body reacts to an external perturbation: ankle and hip strategies. In the ankle strategy, the oscillation of the body is around the ankle joint, and in the hip strategy the upper body leans backward and forward. This result inspired the development of balance controllers that helped humanoids recover from a disturbances while still maintaining an upright posture [83]. The latter it also presented a model tracking control algorithm to make humanoids robots behave in a similar way to humans.

After a more detailed study, the experimental paradigm proposed by [78], [84] implemented the obtained coordination modes on the HOAP3 and HRP2 humanoid robots.

They show that the in-phase mode corresponds to the minimum energy mode, and that only the anti-phase mode was able to maintain balance for high frequencies. A control framework for humanoid robots was presented in [85]; it includes both a balance and a tracking controller that use all joints simultaneously to track motion capture data while maintaining balance. [86] developed a standing balance controller that handles unexpected pushes. The linear quadratic regulator was compared to an optimal controller, using the same optimization criterion, to demonstrate the performance of their proposed method.

An offline optimization of a dynamical model prediction is proposed in [80] in order to analyze the experimental findings reported in [78]. The joint angles trajectories were approximated with a Fourier series, then an integral torque change criterion was minimized under a balance constraint. The results show that the optimization process predicts two coordination modes that depended on the target's motion frequency: the ankle strategy (or the in phase mode) and the hip strategy (or the anti phase mode), as discussed above. They also evaluate the influence of two constraints, an environmental and intentional one, on postural strategy.

Taking into account these remarks, [87, 78] analyzed the ankle-hip joint relative phase transition in an experimental paradigm consisting in tracking a moving target with the head while maintaining balance (we will refer to this experience as Bardy's paradigm), and found that a phase shift is produced as a response to the biomechanical system constraints, namely environmental i.e. support surface properties, intrinsic i.e. height of different body segments, height of center of mass or intentional i.e. task constraint.

Bardy's paradigm, studied by several researchers [80, 81, 87, 78], brings to light important aspects on human postural control system such as: phase transition, multistability, hysteresis and critical slowing down [78].

[80] studied Bardy's paradigm, in an open loop situation. They investigated whether the postural planning process is related to an optimization method that minimizes a dynamic criterion under balance constraints. Indeed their results confirmed Bardy's conclusions: in-phase and anti-phase coordination modes were found, visual task was achieved while maintaining balance and also it was emphasized that the phase shift was induced by the balance constraint.

In this chapter, we aim to provide a class of criteria that can explain Bardy's paradigm. We are interested in doing this, because in the previous studies this paradigm was analyzed by the means of an optimization process that minimized different criteria, torque or torque change, where similar results were obtained.

In order to do so, we collected experimental data and we applied the inverse approximately optimal control, as described in Chapter 2 to the Fourier interpolated collected data. Also, we propose a richer basis of criteria, composed of five optimal models, i.e. the kinematics, the dynamics, the neural and the energetic models, already discussed in Chapter 3 along with one criterion that ensures balance, keeping the Center of Pressure (CoP) within the base of support (BoS).

4.2 The postural coordination in a visual tracking task

4.2.1 The task description

Following previous studies [88, 79], the experiment consists in tracking a moving target with the head while standing. Participants stood on a force platform in front of a physical target moved by a linear motor in antero-posterior direction, with the knees locked and the soles constantly in contact with the ground (Fig. 4.1-4.2).

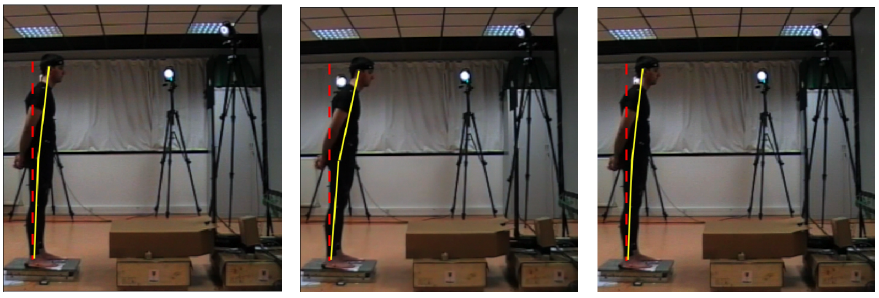

(a) t=0 sec (b) t=1 sec (c) t=2.5 sec

FIGURE 4.1: The human typical experiments at 0.2Hz. Coordinative in-phase small displacement of the ankle and the hip.[2]

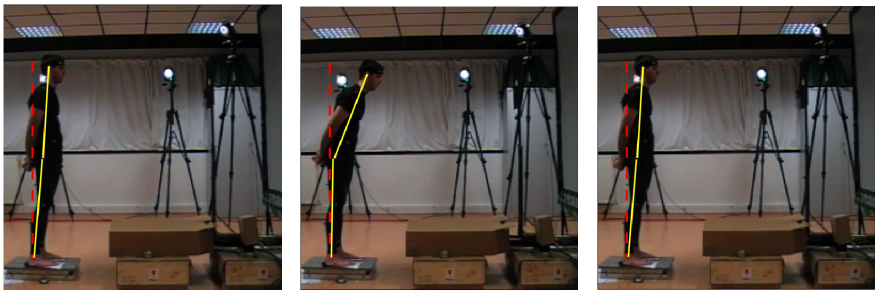

(a) t=0 sec (b) t=0.5 sec (c) t=1.3 sec

FIGURE 4.2: The human typical experiments at 0.6Hz. Coordinative anti-phase displacement of the ankle and the hip. The hip amplitude is larger than the ankle one.[2]

The experiment was performed on 10 healthy male subjects, 1 trial for each, with an average age of 25, average weight of 75kg and average height of 1.79m. Target motion was sinusoidal with 10cm as amplitude, the frequency increases from 0.1Hz to 0.65Hz by 0.05Hz steps and during 12 periods. To capture the joint positions, a motion capture system (VICON NEXUS) was used, with 8 cameras (MX13) tracking 15 makers on the right side of the subject.

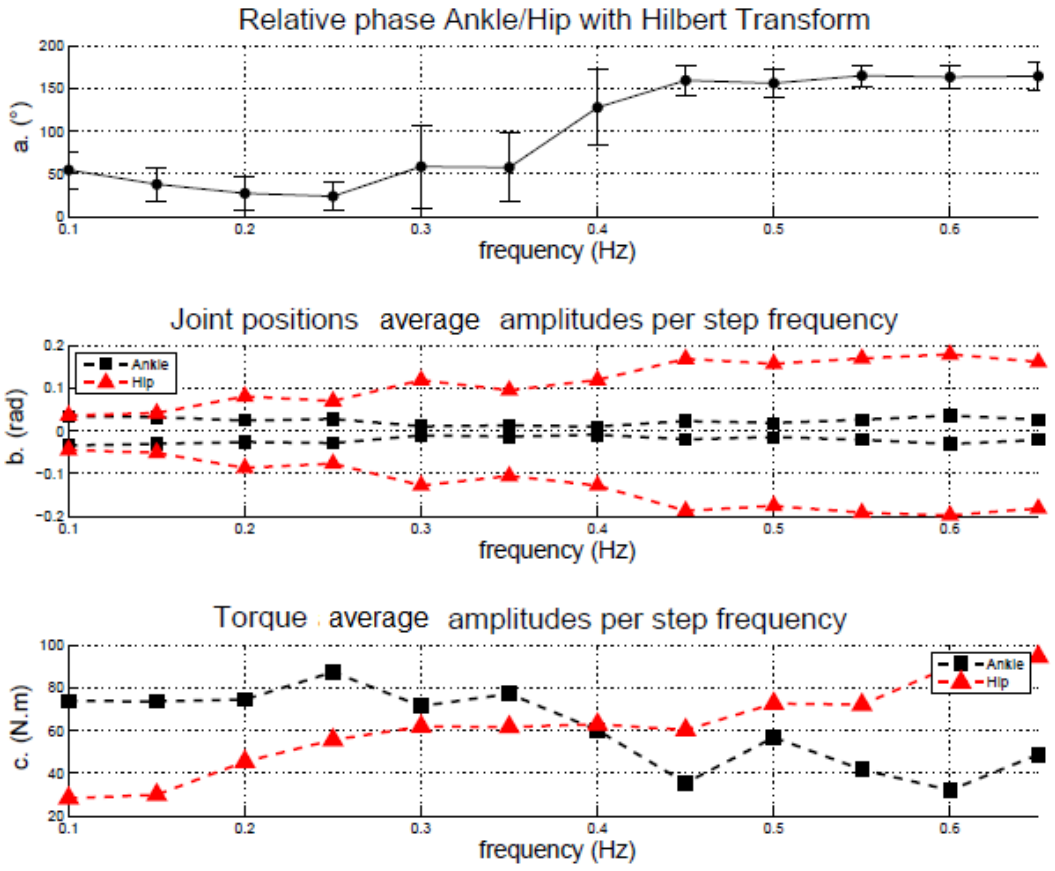

FIGURE 4.3: [2] Typical human experimental results. (a) The ankle/hip relative phase, showing a transition frequency around 0.4Hz (b) Peak to peak joint positions. (c) The estimation of joint torque amplitudes.

4.2.2 Experimental measurements

Fig.4.3 shows typical results for a representative subject (weight 75kg, height 1.80m). In Fig. 4.3a, the average values of the relative phase (Hilbert-transformed) between ankle and hip positions are represented as a function of the frequency step. The depicted error bars correspond to the standard deviations during the 12 oscillations achieved at each frequency step. A transition is observed from in-phase to anti-phase mode around 0.4Hz. Joint positions are presented on Fig. 4.3b by minimum and maximum values.

Each point is the average value of the maximum (or minimum) joint position reached during the 12 oscillation periods performed at each frequency step. For the in-phase mode, i.e. at low frequencies, the joint positions amplitude difference are small, with individual differences in terms of joint amplitude. At the transition frequency, the ankle amplitude becomes very small, and the relative phase between ankle and hip is difficult to estimate. This strong reduction of the ankle amplitude is typical for the human phase transition [88, 79, 89]. The hip amplitude is larger than the ankle amplitude for the anti-phase mode as mentioned in [88, 79, 89]. Fig. 4.3(c) depicts average values for torque amplitude estimation at each frequency step. Torque values were estimated by using the inverse dynamical model of the double inverted pendulum. They indicate a larger ankle torque amplitude for in-phase mode and a larger hip torque amplitude for anti-phase in agreement with the ankle and hip strategy reported in [82] and by Runge *et al.* [90].

These observations hold for all participants and are in accordance with [88, 91, 89], even though the actual transition frequency and joint amplitudes depend on the specific subject body type.

In order to do the average joint displacements, the 10 joint measurements collected for the 10 subjects will be separated into 2 sets. This separation was done after analyzing the way the subjects behaved during the trials. We observed that 6 of the subjects have similar behavior so they will be part of the first set, while the remaining 4 will be part of the second set due to their similar behavior during the trial.

For each set we will take the average joint displacements and we will analyze only the fourth period out of the total of 12 oscillations achieved at each frequency step, because during the 12 oscillations the subjects behavior was constant.

4.3 The choice of the model

When analyzing the human balance control, the human body can be modeled as one or multi-dimensional inverted pendulum chain.

The one-dimensional inverted pendulum modeling ([92], [93], [94]) is accepted if the movements in the other joints are artificially blocked ([93]), so the biomechanical system will be described only by-one variable: the angle of the ankle joint. Even so [95] argued that a single chain inverted pendulum approximation is not sufficient to completely explain balance properties, even for standing balance. In this regard, a common model

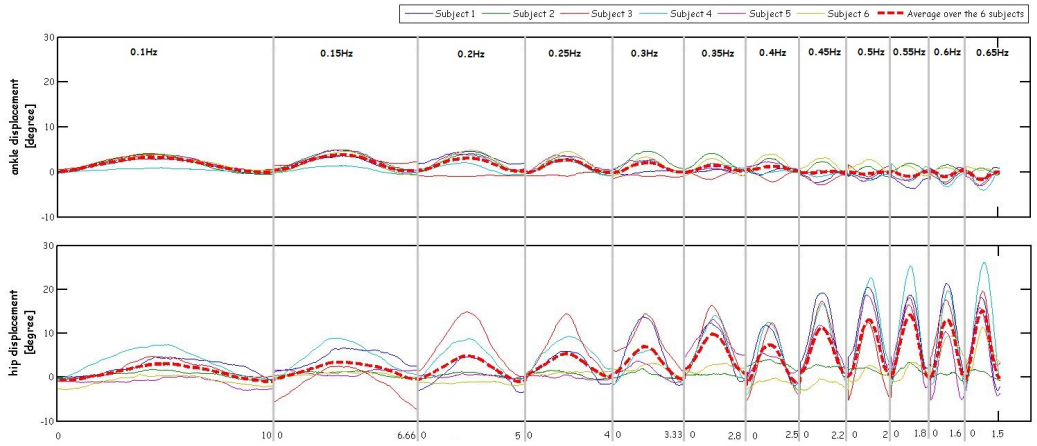

(a)

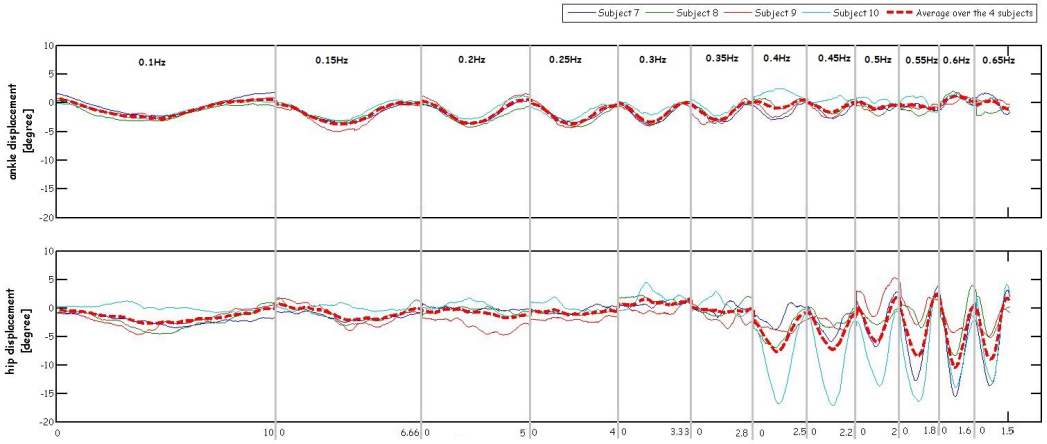

(b)

FIGURE 4.4: The fourth period achieved at each frequency step (0.1Hz: 0.05 :0.65Hz) for the measured joint displacements and its average. (a) corresponds to the first set and (b) to the second one

used in several studies is the double inverted pendulum model [96, 80, 97]. Also a three-dimensional inverted pendulum chain was used, by including the knee [98], to model human body.

Modeling the human body as a multi-dimensional inverted pendulum chain permitted to study human postural responses for simple task experimental paradigms as forward pushes applied to the back of a standing subject [99], fast backward perturbations to the force platform while human quite stance [97] or sudden perturbations of humans in quite stance by backward displacement of the support platform [98] and also for dual-task experimental paradigm as tracking a target with the head while balance [96, 81, 80, 100].

When modeling human body as multi-dimensional inverted pendulum chain, dependency of torques on joint angles and angular velocities is determined by the biomechanical model.

4.3.1 The biomechanical model

During the visual head tracking task, the biomechanical model is represented as a two-link inverted pendulum (DIP). The two rigid links represent the head, arms, torso, both legs and both feet. The head, arms and torso were represented by a link according to the minimal motion observed between these segments [101].

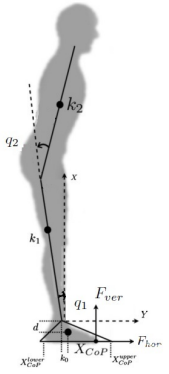

FIGURE 4.5: The double inverted pendulum representation for postural coordination modeling in sagittal plane

The nonlinear motion equations have the following form:

$$M(q, \dot{q})\ddot{q} + C(q)\dot{q} + G(q) = \tau \tag{4.1}$$

Where q, $\dot{q}$, $\ddot{q}$ are the vector of joint angles, the angular velocities and accelerations, τ is the vector of joint torques, the inertia matrix M, the coriolis matrices C and the gravity vector G of the double inverted pendulum are composed of the mass m, length of the segments l, k, center of mass position kl, gravity constant g.
The nonlinear motion equations were linearized with respect to the horizontal axis [99]:

$$M\ddot{q} - Gq = \tau \tag{4.2}$$

where M is the inertial matrix and G is the gravity matrix. τ is the joint torque where muscles act as actuators.

4.3.2 The balance constraint

The balance, maintained during the tracking task in the sagittal plane, depends on the position of the Center of Pressure (CoP) in the Base of Support (BoS). Balance is ensured when the sum of total momentum is equal to zero, hence:

$$F_{ver}X_{CoP} + F_{hor}d - \tau_1 - m_0k_0g = 0 \tag{4.3}$$

where F_{ver} and F_{hor} represent the vertical and horizontal ground reaction force components and τ_1 is the ankle torque.

These two components can be calculated using Euler's equations as showed in [102]. They can be related to the change of the respective horizontal and vertical linear momenta of the whole system at each time t.

$$\begin{cases} F_{ver} = (m_1k_1l_1 + m_2l_1)cos(q_1)\ddot{q_1} + m_2k_2l_2cos(q_1+q_2)(\ddot{q_1}+\ddot{q_2}) - (m_1k_1l_1 + m_2l_1)sin(q_1)(\dot{q_1}^2) \\ \quad -m_2k_2l_2(sin(q_1+q_2))(\dot{q_1}+\dot{q_2})^2 + (m_0+m_1+m_2)g \\ F_{hor} = -(m_1k_1l_1 + m_2l_1)(sin(q_1))\ddot{q_1} - m_2k_2l_2(sin(q_1+q_2))(\ddot{q_1}+\ddot{q_2}) \\ \quad -(m_1k_1l_1 + m_2l_1)(cos(q_1))\dot{q_1}^2 - m_2k_2l_2(cos(q_1+q_2))(\dot{q_1}+\dot{q_2})^2 \end{cases}$$

The position of the CoP on the x-axis is finally given by

$$X_{CoP} = \frac{\tau_1 + m_0k_0g - F_{hor}d}{F_{ver}} \tag{4.4}$$

4.4 The inverse optimal control problem solution

In this section, we apply the IAOC algorithm to experimental data in order to recover the class of criteria that can explain the task.

Our focus is to do this in the context of humanoid robot control in order to implement it on a humanoid robot and to give it the ability of accomplishing the task in an autonomous way. One can find in literature [11], a HRP2 robot that is capable of generating locomotion trajectories by itself, by solving the inverse optimal control via 'bi-level' optimization methods. This approach worked and the HRP2 robot is the prove of it. Still due to the expensive computationally time it is difficult to be used for online applications. As underlined in Chapter 3, our IAOC algorithm has an efficient computational time, so we will analyze the angular displacements collected during the

steady-state postural sways by it means. To do this, we need to formulate the direct optimal control (DOC) problem and to underlie KKT optimality conditions.

4.4.1 The direct optimal control problem

The direct problem is formulated as a planning problem, where joint angle trajectories are the ones which minimize a given composite criterion and satisfy the constraints. To curb the planning problem complexity, we will use joint trajectories described by a N-harmonic Fourier series interpolation as done in [80]. Finally, the optimal planning problem will be solved with respect to the $2(2n+1)$ coefficients of the Fourier series vectors $F_c = [a_{01}, \ldots, a_{n1}, b_{01}, \ldots, b_{n1}, a_{02}, \ldots, a_{n2}, b_{02}, \ldots, b_{n2}]$.

Interestingly, Fourier interpolation will act as a filtering procedure and should prevent any distortion in the estimation that can be due to the presence of correlated noise in the regressor of the least square problem (2.22). In addition, the angular positions and their derivatives are deduced afterwards from the coefficients of the Fourier series by using $n = 3$ harmonics in the optimization research.

Finally, the direct optimization problem is formulated as follows: *"Find the* $2(2n+1)$ *coefficients of Fourier vector* F_c*, such as the Fourier-interpolated joint trajectories described by the coefficients of Fourier can achieve the postural sway during head tracking task and minimize a given composite criteria while the head had to move in phase and with the same amplitude with the target".*

The direct optimal control problem that needs to be solved comes down to solving the following optimization problem:

$$\begin{aligned} \underset{F_c}{\text{minimize}} \quad & \sum_{i=1}^{8} c_i f_i(F_c), \\ \text{subject to} \quad & h_j(F_c) = 0 \;\; j = 1, \ldots, N. \end{aligned} \tag{4.5}$$

where N is the number of time samples.

Note that now the decision variables are the Fourier coefficients gathered in vector $F_c \in \Re^n$. The constraint and objective functions depends on the interpolated joint angle trajectories, which in turn are function of Fourier coefficients vector F_c.

4.4.1.1 The equality constraints

The head had to move in phase and with the same amplitude with the target , during the postural sway:

$$h_j(F_c) = -head_{ref_{x,j}} + h_{x,j}, \quad j = 1 : N, \tag{4.6}$$

where the head position on horizontal axes h_x is calculated using the direct kinematic model:

$$h_{x,j} = l_1 sin(\theta_{1,j}) + l_2 sin(\theta_{1,j} + \theta_{2,j}),\ j = 1 : N \tag{4.7}$$

$head_{ref_x}$ represents the subject head position on the horizontal axes, θ_1 and θ_2 are the ankle and hip displacements, while l_1,l_2 are the lower and upper body lengths and N the number of time samples.

4.4.1.2 The choice of the objective functions

The selected optimal models used as a basis for the composite criterion are the Cartesian jerk criterion which is related to the motion smoothness, the joint angle acceleration and angle jerk criteria. They characterize joint angle motion smoothness, and the torque, torque change, energy (absolute work of forces) and effort related criteria, already discussed and used in Chapter 3. To ensure that the center of pressure remains within the base of support i.e to assure balance during the task, another criterion will be considered to the basis of criteria, consisting in the difference between the center of pressure and the middle value of the base of support. The eight basis objective functions are gathered in table 4.1 and the list of criteria is composed of 7 differentiable functions and one non-smooth (non-differentiable) represented by the energy expenditure.

To summarize, a composite criterion will be build from this eight basis objective functions and the inverse optimal control algorithm will estimate among the Lagrange coefficients, the weight corresponding to each criterion proposed in table 4.1.

TABLE 4.1: The pre-selected basis of objective functions; N: number of time samples

Criterion	**Cost function (f_i)**	References
Torque	$f_1 = \frac{\sum_{i=1}^{N}\sum_{i=1}^{2}\tau_{i_j}^2}{N}$	[62]
Torque change	$f_2 = \frac{\sum_{i=1}^{N}\sum_{i=1}^{2}\dot{\tau}_{i_j}^2}{N}$	[63]
Effort	$f_3 = \frac{\sum_{i=1}^{N}\sum_{i=1}^{2}\ddot{\tau}_{i_j}^2}{N}$	
Energy	$f_4 = \frac{\sum_{i=1}^{N}\sum_{i=1}^{2}\left\lvert\dot{\theta}_{i_j}\tau_{i_j}\right\rvert}{N}$	
Center of pressure	$f_5 = \frac{\sum_{i=1}^{N}(X_{CoP}-\frac{x_a-x_b}{2})^2}{N}$	
Angle acceleration	$f_6 = \frac{\sum_{i=1}^{N}\sum_{i=1}^{2}\ddot{\theta}_{i_j}^2}{N}$	
Angular jerk	$f_7 = \frac{\sum_{i=1}^{N}\sum_{i=1}^{2}\dddot{\theta}_{i_j}^2}{N}$	
Cartesian jerk	$f_8 = \frac{\sum_{i=1}^{N}\dddot{head}_x^{\,2}+\dddot{head}_y^{\,2}}{N}$	

4.4.1.3 The postural coordination responses: the in-phase and the anti-phase modes

In this subsection we want to see the dependance between the Lagrangian and the Fourier coefficients by representing the contour of the obtained Lagrangian value for 100 trajectories. We generated these trajectories by minimizing the f_1 criterion (with different values for the Fourier coefficients F_c). As it can be seen in fig. 4.6 two transition modes were obtained: in-phase and the anti-phase one, this being in accordance with previous study [100].

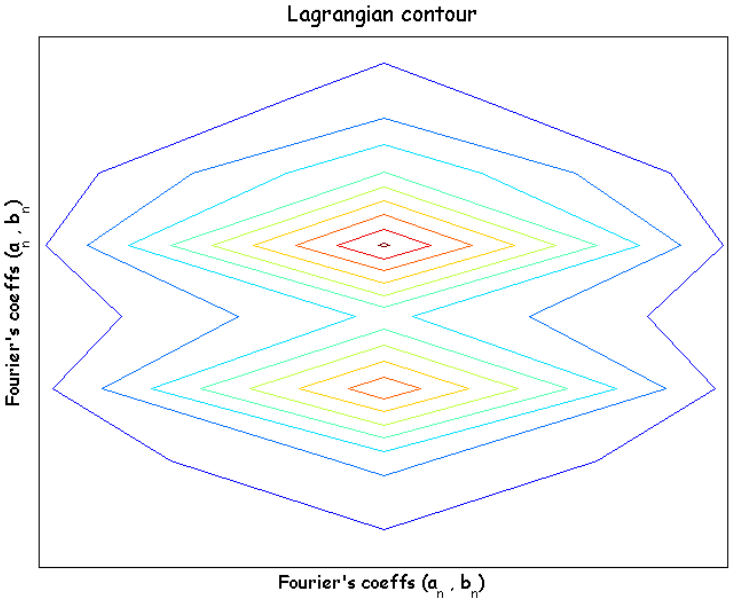

FIGURE 4.6: Lagrangian contour for 100 different values of Fourier's coefficients

This paradigm is a bistable one, due to the phase mode and the anti-phase mode, and it is known to be locally convex, only at the minimum values. In this study, we are only interested in locally analyzing it, at the in-phase mode and the anti-phase one.

4.4.2 The inverse approximately optimal control problem

Now, we can address the inverse approximately optimal control problem using the method described in Chapter 2.

We specify the matrix $A \in \Re^{m \times n}$ as in Eq.(2.19), which is composed of the criteria and equality gradient's vectors with respect to the Fourier's coefficients, and the vector $b \in \Re^m$ as in Eq.(2.20) which contains the chosen objective function gradient vector to act as pivot i^*. For this paradigm the A matrix is a 'wide' one (has more columns than

rows $m \prec n$) so the criteria will be imputed by solving the underdetermined problem (2.23).

As previously discussed, the choice of the pivot relies on prior knowledge of the wanted composite criterion. In order to derive accurate conclusions when analyzing the postural sway during head tracking task, we consider that there is no such prior knowledge. As a consequence, we will have to consider all the basis function as potential pivot. Then, comparing the solutions of problem (2.23) we will keep the solutions that show good consistency with the experimental data, those which minimize both the *residuals norm* (3.4) and the root mean square error (RMSE) (3.5) described below.

4.5 Evaluation on artificial data

In this section, we perform the evaluation of the performance of our method using artificial data. Using the 2 DOF dynamical model of the task (introduced in Sect. 4.3), we solve the DOC problem (4.5) with vector $\overrightarrow{c}$ tuned so that only one single basis objective function is active at the time. We come with eight planned joint trajectories, each minimizing a single basis objective function given in Table 4.1.

When analyzing the correlation (see eq (2.24)) between each calculated criteria gradient's vectors we found strong correlation between them, and we formed groups of correlated criteria gradient's vectors for each artificial data generated while the in-phase mode ($freq = 0.1Hz$) and the anti-phase mode ($freq = 0.5Hz$).

All the criteria gradient's vectors that are correlated and the ones that were kept for the next steps of the **IAOC** algorithm have been gathered in table 4.2:

- For in-phase mode the followings were obtained:
  1. minimizing f_i, $i = 2, 3, 5, 6, 7, 8$: for these cases were found a strong correlation between all criteria gradient's vectors, therefore any of these criteria can be used to explain the artificial optimal trajectories generated by minimizing any f_i.
  2. minimizing f_i, $i = 1, 4$: two groups of correlated criteria gradient's vectors were reported, therefore for this cases we'll keep only one criterion from each group and we continue testing the IAOC algorithm, as following: we keep (∇f_1, ∇f_8) when working with data generated by minimizing f_1 and (∇f_1, ∇f_4) when working with data generated by minimizing f_4.

TABLE 4.2: The groups of correlated gradients. For simplicity we use ∇ instead of ∇_{F_c}

in-phase mode 0.1Hz				
Data generated by	Groups of correlated gradients			Retained gradients
	G_1	G_2	G_3	
$\min f_1$	∇f_1 to ∇f_7	∇f_8		$\nabla f_1, \nabla f_8$
$\min f_2$	∇f_1 to ∇f_8			∇f_2
$\min f_3$	∇f_1 to ∇f_8			∇f_3
$\min f_4$	∇f_1 to ∇f_3, ∇f_5 to ∇f_8	∇f_4		$\nabla f_1, \nabla f_4$
$\min f_5$	∇f_1 to ∇f_8			∇f_5
$\min f_6$	∇f_1 to ∇f_8			∇f_6
$\min f_7$	∇f_1 to ∇f_8			∇f_7
$\min f_8$	∇f_1 to ∇f_8			∇f_8
anti-phase mode 0.5Hz				
Data generated by	Groups of correlated gradients			Retained gradients
	G_1	G_2	G_3	
$\min f_1$	∇f_1 to ∇f_5, ∇f_8	$\nabla f_6, \nabla f_7$		$\nabla f_1, \nabla f_6$
$\min f_2$	∇f_1 to ∇f_5, ∇f_8	$\nabla f_6, \nabla f_7$		$\nabla f_2, \nabla f_6$
$\min f_3$	∇f_1 to ∇f_5, ∇f_8	$\nabla f_6, \nabla f_7$		$\nabla f_3, \nabla f_6$
$\min f_4$	∇f_1 to ∇f_5, ∇f_8	$\nabla f_6, \nabla f_7$		$\nabla f_4, \nabla f_6$
$\min f_5$	∇f_1 to ∇f_3, ∇f_5, ∇f_8	$\nabla_{F_c} f_6, \nabla f_7$	∇f_4	$\nabla f_4, \nabla f_5, \nabla f_6$
$\min f_6$	∇f_1 to ∇f_3, ∇f_5, ∇f_8	$\nabla f_6, \nabla f_7$	∇f_4	$\nabla f_1, \nabla f_4, \nabla f_6$
$\min f_7$	∇f_1 to ∇f_3, ∇f_5, ∇f_8	$\nabla f_6, \nabla f_7$	∇f_4	$\nabla f_1, \nabla f_4, \nabla f_7$
$\min f_8$	∇f_1 to ∇f_3, ∇f_5, ∇f_8	$\nabla f_6, \nabla f_7$	∇f_4	$\nabla f_4, \nabla f_6, \nabla f_8$

- and for the anti-phase mode the results are the following:

  1. minimizing f_i, $i = 1, 2, 3, 4$: two groups of correlated criteria gradient's vectors were found and we will keep (∇f_1, ∇f_6) when working with data generated by minimizing f_1, (∇f_3, ∇f_6) when working with data generated by minimizing f_3 and (∇f_4,∇f_6) for minimizing f_4.
  2. minimizing f_i, $i = 5, 6, 7, 8$: three groups of correlated criteria gradient's vectors were found and we will keep: (∇f_5, ∇f_6, ∇f_4) when working with data generated by minimizing f_5, (∇f_1, ∇f_6, ∇f_4) when working with data generated by minimizing f_6, (∇f_1, ∇f_7, ∇f_4) when working with data generated by minimizing f_7 and (∇f_8, ∇f_6, ∇f_4) when working with data generated by minimizing f_8.

For each artificial data generated, we apply our algorithm **IAOC** as defined in Chapter 3. We applied the steps of the algorithm to the kept criteria gradient's vectors, proposed in table 4.2, and the results were gathered in table 4.3. The first column indicates the criteria that were minimized to obtain the artificial data, the second one the used A matrix, while the b vector is presented in the table's caption, the third one contains the

TABLE 4.3: The results obtained on artificially generated optimal trajectories;$b = -[\nabla_{F_c} f_{i^*}]$. For simplicity we use ∇ instead of ∇_{F_c}

in-phase mode 0.1Hz					
	A	i^*	γ	$\frac{1}{n'}\|\nabla L(\hat{c})\|$	RMSE [deg]
min f_1	$[\nabla f_8\ \nabla h_j]$	1	+	$5.6e^{-07}$	0
	$[\nabla f_1\ \nabla h_j]$	8	+	0.029	0.1
min f_2	$[\nabla h_j]$	2		$1.1e^{-08}$	0
min f_3	$[\nabla h_j]$	3		$4.9e^{-13}$	0
min f_4	$[\nabla h_j]$	1	+	0.026	0.1
	$[\nabla h_j]$	4	+	$6e^{-05}$	0
min f_5	$[\nabla h_j]$	5		3.5^{-15}	0
min f_6	$[\nabla h_j]$	6		6.1^{-15}	0
min f_7	$[\nabla h_j]$	7		2.3^{-15}	0
min f_8	$[\nabla h_j]$	8		2.4^{-13}	0
anti-phase mode 0.5Hz					
	A	i^*	γ	$\frac{1}{n'}\|\nabla L(\hat{c})\|$	RMSE [deg]
min f_1	$[\nabla f_6\ \nabla h_j]$	1	+	$5.3e^{-07}$	0
	$[\nabla_{F_c} f_1\ \nabla h_j]$	6	+	$9.2e^{-05}$	0
min f_2	$[\nabla f_6\ \nabla h_j]$	2	+	$9.2e^{-06}$	0
	$[\nabla f_2\ \nabla h_j]$	6	+	0.2	0.06
min f_3	$[\nabla f_6\ \nabla h_j]$	3	+	$2e^{-06}$	0
	$[\nabla f_3\ \nabla h_j]$	6	+	0.003	0.06
min f_4	$[\nabla f_6\ \nabla h_j]$	4	+	$1.5e^{-07}$	0
	$[\nabla f_4\ \nabla h_j]$	6	+	0.2	0.06
min f_5	$[\nabla f_5\ \nabla f_6\ \nabla h_j]$	4	+	0.2	0.06
	$[\nabla f_4\ \nabla f_6\ \nabla h_j]$	5	+	$6e^{-06}$	0
	$[\nabla f_4\ \nabla f_5\ \nabla h_j]$	6	+	$1e^{-05}$	0.06
min f_6	$[\nabla f_4\ \nabla f_6\ \nabla h_j]$	1	+	$1.9e^{-05}$	0
	$[\nabla f_1\ \nabla f_6\ \nabla h_j]$	4	+	0.2	$1.7e^{-04}$
	$[\nabla f_1\ \nabla f_4\ \nabla h_j]$	6	+	$1.9e^{-07}$	0
min f_7	$[\nabla f_4\ \nabla f_7\ \nabla h_j]$	1	+	$1.9e^{-05}$	0.06
	$[\nabla f_1\ \nabla f_7\ \nabla h_j]$	4	+	0.2	0.06
	$[\nabla f_1\ \nabla f_4\ \nabla h_j]$	7	+	$1e^{-06}$	0
min f_8	$[\nabla f_6\ \nabla f_8\ \nabla h_j]$	4	+	0.2	0.06
	$[\nabla f_4\ \nabla f_8\ \nabla h_j]$	6	+	0.0043	0.06
	$[\nabla f_4\ \nabla f_6\ \nabla h_j]$	8	+	$6e^{-08}$	0

pivot used, the fourth column contains the sign of the inner product (proposed in eq. (3.7)) while the last two columns contain the residuals norm and the RMSE values.

The contribution of each basis objective function, given as relative contribution in percentage computed as in (4.1), was found of 100% for the objective function used as pivot, due to the positive sign found in all the presented cases.

Also, table 4.3 clearly shows that when using as pivot the criterion that was minimized to obtain the artificial data the residuals norm is the smallest and the RMSE is equal

to 0.

Let's take for example the trajectory generated while minimizing f_1. We kept only f_1 and f_8 as potential criteria (the other ones were found correlated, as explained above). When we tested the approach, the residuals norm and RMSE has the smallest value when f_1 is used as pivot. What it is interestingly is that when f_8 is used as pivot, it obtained a RMSE equal to 0.1, even if its residual norm values is 4 times larger than when f_1 was used as pivot. Even so, our algorithm will discharge the case when f_8 is used as pivot, keeping only the case where the residual norm and RMSE values are the smallest i.e. the one when f_1 is used as pivot that is the correct one.

This results clearly show the nice performances of the inverse approximately optimal approach.

4.6 Experimental results

The focus of our analysis in this section, is the use of the IAOC algorithm onto the two average joint displacements presented in section 4.2.2 and represented in fig.4.4(a) and fig.4.4(b). Out of all the shown frequencies for the two average joint displacements, we are only interested in analyzing the in-phase mode ($freq = 0.1Hz$), the transition frequency between in-phase and anti-phase mode ($freq = 0.4Hz$) and the anti-phase mode ($freq = 0.6Hz$).

4.6.1 One at the time criterion analysis

Firstly, we test the IAOC algorithm onto each criterion from table 4.1 and we solve a direct optimization problem by minimizing them and by comparing the estimated trajectories with the measured ones.

The DOC problem, performed for computing the RMSE values, uses the Fourier's coefficients that fit the actual data to which a 5% of error is added as initial guess for the optimization problem. In table 4.4 and table 4.5, the obtained results are gathered and it can be seen that for both sets of average joint displacements, each criterion from table 3.3 exhibits small residuals norm values. This means that each criteria can be a good candidate for explaining the two sets of average joint displacements. Also, by using the RMSE values as a measure of consistency and accepting an estimation error smaller than 2 degree, each criterion from the chosen pre-selected basis of criteria can be considered potential candidate to explain the observations. The fig. 4.8 and the fig. 4.7

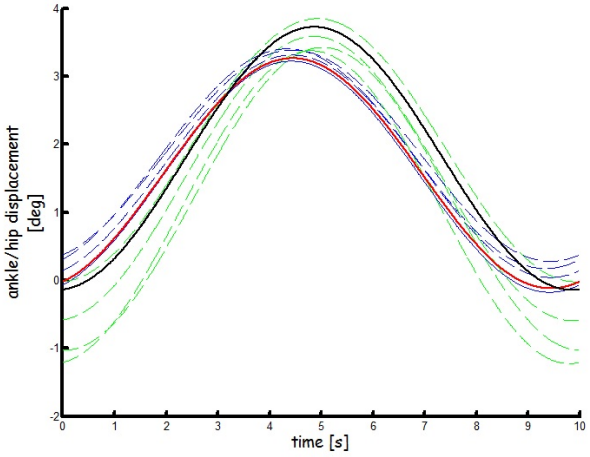

(a)

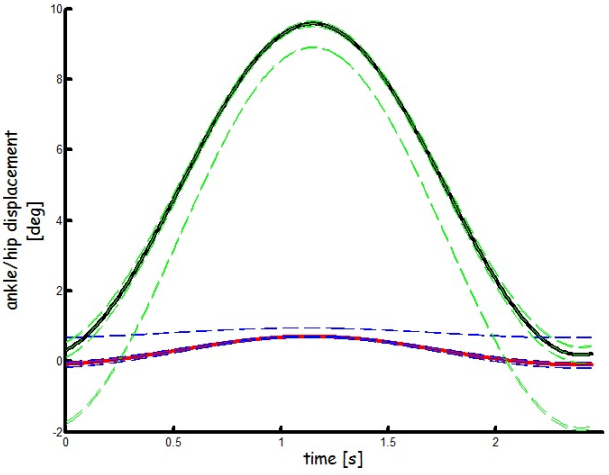

(b)

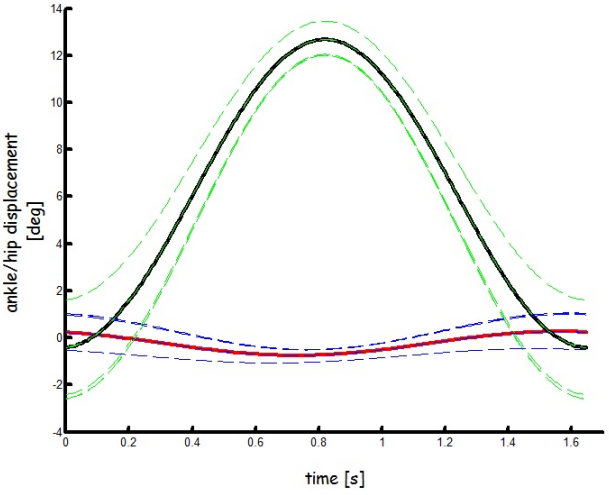

(c)

FIGURE 4.7: The 1^{st} set of average joint displacements: Measured average joint displacements (black trajectory for the hip joint displacement and red trajectory for the ankle joint displacement) with the estimated joint displacements while minimizing each criterion from table 3.3 (doted blue trajectory for the ankle joint displacements and doted green trajectory for the hip joint displacements), for (a) the in-phase mode ($0.1Hz$), (b) the in-phase mode to the anti-phase mode shift ($0.4Hz$) and (c) the anti-phase mode ($0.6Hz$)

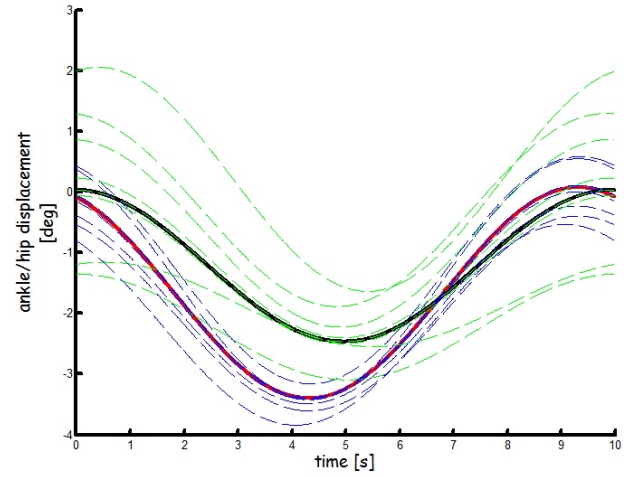

(a)

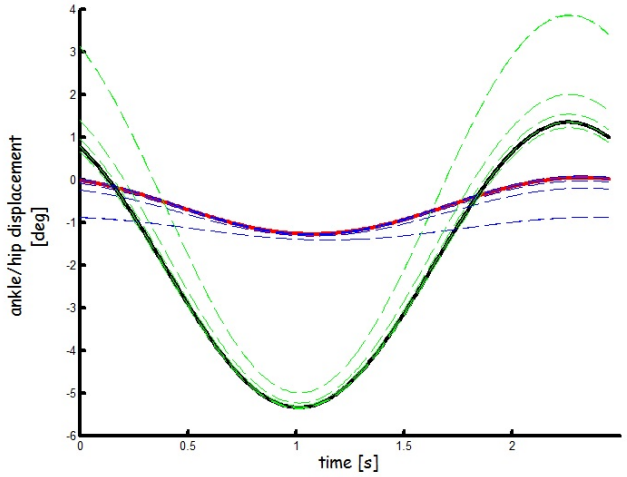

(b)

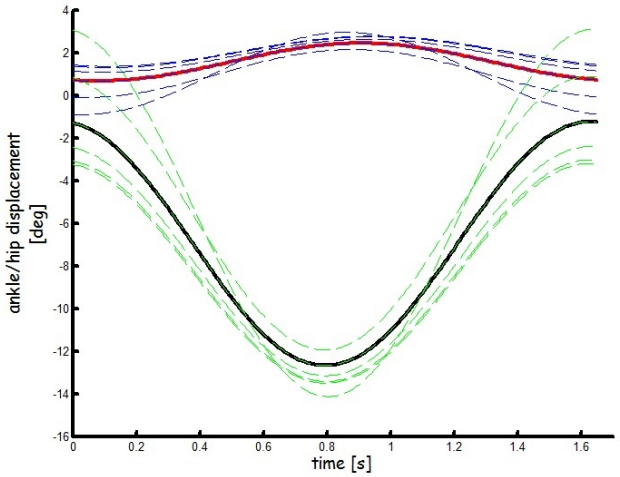

(c)

FIGURE 4.8: The 2^{nd} set of average joint displacements: Measured average joint displacements (black trajectory for the hip joint displacement and red trajectory for the ankle joint displacement) with the estimated joint displacements while minimizing each criterion from table 3.3 (doted blue trajectory for the ankle joint displacements and doted green trajectory for the hip joint displacements), for (a) the in-phase mode ($0.1Hz$), (b) the in-phase mode to the anti-phase mode shift ($0.4Hz$) and (c) the anti-phase mode ($0.6Hz$)

TABLE 4.4: The 1^{st} set of average joint displacements: Results while testing the IAOC algorithm and the DOC for each of the criterion presented in table 3.3, consisting in the residuals norm and RMSE values for the in-phase mode ($0.1Hz$), the in-phase mode to the anti-phase mode shift ($0.4Hz$) and the anti-phase mode ($0.6Hz$)

$A = \nabla_{F_c} h_j$ $j = 1 : N$	$b = -\nabla_{F_c} f_{i^*}$	$0.1Hz$		$0.4Hz$		$0.6Hz$	
		$\frac{1}{n}\|\nabla L(\hat{c})\|$	RMSE	$\frac{1}{n'}\|\nabla L(\hat{c})\|$	RMSE	$\frac{1}{n'}\|\nabla L(\hat{c})\|$	RMSE
	$i^* = 1$	$3.4e^{-12}$	0.23	$3.5e^{-10}$	1.11	$5.2e^{-10}$	1.14
	$i^* = 2$	$6.1e^{-08}$	$1.7e^{-05}$	$2.1e^{-05}$	1.08	$1.1e^{-04}$	1.14
	$i^* = 3$	$5e^{-13}$	$1.5e^{-08}$	$1.4e^{-08}$	0.1	$9.8e^{-08}$	1.14
	$i^* = 4$	$3.2e^{-08}$	$2.3e^{-06}$	$6.8e^{-06}$	$3.1e^{-04}$	$1e^{-05}$	$4.2e^{-05}$
	$i^* = 5$	$9.8e^{-15}$	0.001	$2.4e^{-12}$	0.11	$1.7e^{-12}$	1.05
	$i^* = 6$	$3.7e^{-15}$	0.48	$1.6e^{-12}$	0.12	$6e^{-12}$	0.003
	$i^* = 7$	$1.6e^{-15}$	0.57	$1.2e^{-11}$	$1.6e^{-05}$	$7.8e^{-11}$	1.1
	$i^* = 8$	$2e^{-13}$	0.10	$8e^{-09}$	0.11	$3.9e^{-08}$	$3e^{-06}$

TABLE 4.5: The 2^{nd} set of average joint displacements:Results while testing the IAOC algorithm and the DOC for each of criterion presented in table 3.3, consisting in the residuals norm and RMSE values for the in-phase mode ($0.1Hz$), the in-phase mode to the anti-phase mode shift ($0.4Hz$) and the anti-phase mode ($0.6Hz$)

$A = \nabla_{F_c} h_j$ $j = 1 : N$	$b = -\nabla_{F_c} f_{i^*}$	$0.1Hz$		$0.4Hz$		$0.6Hz$	
		$\frac{1}{n}\|\nabla L(\hat{c})\|$	RMSE	$\frac{1}{n}\|\nabla L(\hat{c})\|$	RMSE	$\frac{1}{n}\|\nabla L(\hat{c})\|$	RMSE
	$i^* = 1$	$9.3e^{-12}$	$6e^{-07}$	$2.3e^{-09}$	0.09	$9.7e^{-09}$	1.13
	$i^* = 2$	$3.8e^{-07}$	0.43	$4.3e^{-05}$	1.21	$8.7e^{-05}$	1.13
	$i^* = 3$	$1.3e^{-12}$	0.78	$9.9e^{-08}$	1.2	$1.9e^{-06}$	1.88
	$i^* = 4$	$2e^{-07}$	0.1	$3.7e^{-06}$	0.3	$3.1e^{-05}$	0.64
	$i^* = 5$	$2.1e^{-14}$	0.05	$5e^{-12}$	$3.5e^{-05}$	$1.5e^{-11}$	$9e^{-12}$
	$i^* = 6$	$4e^{-15}$	0.58	$1e^{-12}$	0.06	$5.6e^{-12}$	1.09
	$i^* = 7$	$1.5e^{-15}$	0.71	$6e^{-12}$	0.06	$7.6e^{-11}$	0.99
	$i^* = 8$	$2.6e^{-13}$	1.14	$2.7e^{-09}$	$4.6e^{-11}$	$3.7e^{-08}$	$9.1e^{-07}$

present the measured joint displacements and the joint displacements ones estimated by minimizing each criterion from the selected basis of criteria.

4.6.2 The basis of criteria analysis

We test our algorithm, for all the criteria proposed in the basis of criteria. The correlation between the criteria gradient's vectors is verified (see eq. (2.24)) and the results of the correlated groups of criteria gradient's vectors are gathered in table 4.6. For both sets of average joint displacements, the followings were found:

1. For the in-phase mode, $0.1Hz$: two groups of correlated criteria gradient's vectors were found, the G_1 group and the G_2 group (see table 4.6). We keep only one gradient vector out of the first group, let's say the ∇f_1 criterion gradient vector, and the ∇f_4 criterion gradient vector out of the second group.

2. For the in-phase mode to the anti-phase mode shift, $0.4Hz$ and the anti-phase mode, $0.6Hz$: three groups of correlated criteria gradient's vectors were found, G_1, G_2 and G_3 groups (see table 4.6). We keep only one gradient vector out of the three groups, let's say the ∇f_1, the ∇f_4 and the ∇f_6 gradient's vectors.

TABLE 4.6: The 1^{st} and the 2^{nd} set of average joint displacements: Results obtained after verifying the form correlation between each criteria gradient's vectors. For simplicity we use ∇ in place of ∇_{F_c}

1^{st}	Groups of correlated gradients			
	G_1	G_2	G_3	Retained gradients
$0.1Hz$	$\nabla f_1$to∇f_3, $\nabla f_5$to∇f_8	∇f_4		$\nabla f_1, \nabla f_4$
$0.4Hz$	$\nabla f_1$to∇f_3, ∇f_5, ∇f_8	$\nabla f_6, \nabla f_7$	∇f_4	$\nabla f_1, \nabla f_4, \nabla f_6$
$0.6Hz$	$\nabla f_1$to∇f_3, ∇f_5, ∇f_8	$\nabla f_6, \nabla f_7$	∇f_4	$\nabla f_1, \nabla f_4, \nabla f_6$
2^{nd}	Groups of correlated gradients			
	G_1	G_2	G_3	Retained gradients
$0.1Hz$	$\nabla f_1$to∇f_3, $\nabla f_5$to∇f_8	∇f_4		$\nabla f_1, \nabla f_4$
$0.4Hz$	$\nabla f_1$to∇f_3, ∇f_5, ∇f_8	$\nabla f_6, \nabla f_7$	∇f_4	$\nabla f_1, \nabla f_4, \nabla f_6$
$0.6Hz$	$\nabla f_1$to∇f_3, ∇f_5, ∇f_8	$\nabla f_6, \nabla f_7$	∇f_4	$\nabla f_1, \nabla f_4, \nabla f_6$

We finally applied the next steps of the IAOC algorithm to the kept criteria gradient's vectors, as explained above, and the outcomes were gathered in table 4.7 for the first set and in table 4.8 for the second one. We obtained similar results for both sets, such as:

For the in-phase mode (0.1Hz):

- The 1^{st} set of average joint displacements: when using as pivot f_1 or f_4, their contribution will be 100%, due to the positive inner product γ sign; moreover, when using as pivot the f_1, the residuals norm value is smaller than when using the f_4. While the RMSE value is larger than when using the f_4 as a pivot.
- The 2^{nd} set of average joint displacements: when using as pivot f_1 or f_4, their contribution will be 100%, due to the positive inner product γ sign; moreover, when using as pivot the f_1, the residuals norm and the RMSE values are smaller than when using the f_4,

and for the in-phase mode/anti-phase mode shift (0.4Hz) and for the anti-phase mode (0.6Hz) the findings are similar as follows:

- When pivoting after f_4, the residual norm is 8 times larger for $0.4Hz$ and 7 times larger for $0.6Hz$, therefore this case will be discharged. When pivoting after f_1 and f_6, the residuals norm values are the smallest and the RMSE values are the ones obtained when minimizing them one at the time, as reported in the previous subsection.

TABLE 4.7: The 1^{st} set of average joint displacements: Results while testing the IAOC algorithm and the DOC for the retained uncorrelated criteria gradient's vectors, consisting in criteria contribution, the inner product sign and the residuals norm and RMSE values for in-phase mode ($0.1Hz$), the in-phase mode to the anti-phase mode shift ($0.4Hz$) and the anti-phase mode ($0.6Hz$).. For simplicity we use ∇ in place of ∇_{F_c}

1^{st} group	A	b	Contribution [%]			γ	$\frac{1}{n}\|\nabla L(\hat{c})\|$	RMSE [deg]
			f_1		f_4	γ_{14}		
$0.1Hz$	$[\nabla h_j \nabla f_4]$	$-\nabla f_1$	100		0	+	$3e^{-08}$	0.23
	$[\nabla h_j \nabla f_1]$	$-\nabla f_4$	0		100	+	0.01	$2.3e^{-06}$
			f_1	f_4	f_6			
$0.4Hz$	$[\nabla h_j \nabla f_4 \nabla f_6]$	$-\nabla f_1$	100	0	0	γ_{14} =-, γ_{16} =+	$6.1e^{-07}$	1.11
	$[\nabla h_j \nabla f_1 \nabla f_6]$	$-\nabla f_4$	73.76	26.24	0	γ_{41} =-,γ_{46} =+	1.03	0.008
	$[\nabla h_j \nabla f_1 \nabla f_4]$	$-\nabla f_6$	0	0	100	γ_{61} =+,γ_{64} =+	$1.7e^{-08}$	0.12
			f_1	f_4	f_6			
$0.6Hz$	$[\nabla h_j \nabla f_4 \nabla f_6]$	$-\nabla f_1$	100	0	0	γ_{14} =+,γ_{16} =+	$2.1e^{-05}$	1.14
	$[\nabla h_j \nabla f_1 \nabla f_6]$	$-\nabla f_4$	0	18.64	81.36	γ_{41} =+,γ_{46} =-	2.1	$7.8e^{-07}$
	$[\nabla h_j \nabla f_1 \nabla f_4]$	$-\nabla f_6$	0	0	100	γ_{61} =+,γ_{64} =-	$2e^{-07}$	0.003

TABLE 4.8: The 2^{nd} set of average joint displacements: Results while testing the IAOC algorithm and the DOC for the retained uncorrelated criteria gradient's vectors, consisting in criteria contribution, the inner product sign and the residuals norm and RMSE values for in-phase mode ($0.1Hz$), the in-phase mode to the anti-phase mode shift ($0.4Hz$) and the anti-phase mode ($0.6Hz$). For simplicity we use ∇ in place of ∇_{F_c}

2^{nd} group	A	b	Contribution [%]			γ	$\frac{1}{n}\|\nabla L(\hat{c})\|$	RMSE [deg]
			f_1		f_4	γ_{14}		
$0.1Hz$	$[\nabla h_j \nabla f_4]$	$-\nabla f_1$	100		0	+	$3.2e^{-04}$	$6e^{-07}$
	$[\nabla h_j \nabla f_1]$	$-\nabla f_4$	0		100	+	0.02	0.1
			f_1	f_4	f_6			
$0.4Hz$	$[\nabla h_j \nabla f_4 \nabla f_6]$	$-\nabla f_1$	100	0	0	γ_{14} =-, γ_{16} =+	0.002	0.09
	$[\nabla h_j \nabla f_1 \nabla f_6]$	$-\nabla f_4$	73.76	26.24	0	γ_{41} =-,γ_{46} =+	1.04	0.1
	$[\nabla h_j \nabla f_1 \nabla f_4]$	$-\nabla f_6$	0	0	100	γ_{61} =+,γ_{64} =+	$1.6e^{-08}$	0.06
			f_1	f_4	f_6			
$0.6Hz$	$[\nabla h_j \nabla f_4 \nabla f_6]$	$-\nabla f_1$	100	0	0	γ_{14} =+,γ_{16} =+	$2.1e^{-05}$	1.13
	$[\nabla h_j \nabla f_1 \nabla f_6]$	$-\nabla f_4$	0	100	0	γ_{41} =+,γ_{46} =+	2.3	0.64
	$[\nabla h_j \nabla f_1 \nabla f_4]$	$-\nabla f_6$	0	0	100	γ_{61} =+,γ_{64} =+	$2e^{-07}$	1.09

The results exhibited by our algorithm are coherent with the findings, when analyzing each criterion one at the time. This means that, for the choice of selecting to keep the f_1, f_4 and f_6 in our algorithm, they were found as possible candidates for the task. If a combination between this criteria was found they were discharged, due to a large residuals norm value.

4.6.3 Summary

In this study, we tested each criterion one at the time and the obtained results suggest that any criterion from the basis of criteria can be a possible candidate for the visual tracking task. Moreover, when applying our algorithm the same conclusions were drawn. This findings are consistent with previous studies, where this paradigm was analyzed while minimizing the torque or the torque change and, in both cases similar results were obtained.

In the next section we proposed a closed loop modeling with feedback gain synthesis, on artificial data.

4.7 The closed-loop modeling with gain synthesis on simulated data

In this section, we aim to investigate whether the human biomechanical model, represented by a linearized double inverted pendulum, in a closed loop optimal control can efficiently model the visual tracking task. More precisely, we will close the loop with the help of two PD feedback loops: a short loop that will address the balancing issue, and a long loop that will address the visual tracking task. The two PD feedback control gains are synthesized by using three different integral criterion (torque, torque change and head jerk presented in table 4.1).

The idea of using feedback loops to model the human motor control system is not new. In [97], human postural responses to platform perturbations during standing are described in terms of a linear dynamical model with Proportional-Derivative (PD) feedback loops were control gains are scaled and selected by the central nervous system (CNS). The appropriate values for the gains are obtained via model-data fitting using actual experimental data. Moreover, [99] showed that a PD feedback loop with scaled gains can accurately model the postural response to a forward push recovery, the scaling depending on the type of perturbation. During the trials, for backward ([97], [98]) and forward

([99]) push recoveries studies, it was observed that when the perturbation magnitude increases, the ankle torque control gain decreases while hip torque control gain increases.

For the same experimental paradigm, [81] proposed a non-linear closed-loop optimal model that predicted changes between the in-phase and the anti-phase postural coordination. In the latter study, the control torque related to the tracking task was obtained by using a pseudo-inverse Jacobian matrix while an adaptive saturation of ankle torque was used to satisfy the balance constraint.

[80] and [81] used a similar constraint in the optimization algorithm that ensured balance: the Center of Pressure(CoP) had to remain within the base of support (BoS)[103]. Balance issue was also studied on humanoids for different purposes. For example, a hydraulic humanoid was used in [104] to have a practical exploration of the effects of modeling error and unknown forces on state estimation for dynamic humanoids balance. In [105] a feedback controller for the joint position was designed, where a switching was performed between gains according to the Zero Moment Point (ZMP) location in order to maintain balance.

Previous studies presented human postural responses to a sudden and impulsive backwards perturbation of the support platform in quiet stance. This situation can be described in terms of feedback loop control. Feedback control gains, represented by stiffness and viscosity coefficients, obtained as the optimal parameters of a regression model, were found scaling with the perturbation's type ([97]). This result brings to light suggestions from previous studies ([106]) where it was supposed that the CNS selects muscle activation, not only because of some type/magnitude of perturbation, but also because of the biomechanical constraints. For the same experimental paradigm used in [97], [98] modeled postural responses as a triple inverted pendulum in feedback paradigm; they obtained the stiffness and viscosity gains with the eigenmovements approach, which is a special case of feedback full state control. They concluded that the study did not exhibit a significant dependence of the stiffness gains on perturbation amplitude, while the viscosity ones were found decreasing with the perturbation amplitude. For forward impulsive pushes onto human body's back while in a quiet stance ([99]), human postural responses were described in terms of feedback control gains, and as in [97] the feedback control gains were found scaling with the perturbation's type.

Describing the human postural responses in terms of feedback control gains, all the presented studies obtained realistic human postural responses i.e ankle/hip strategies and moreover some of these studies exhibited fully or partially the selection of feedback gain and the scaling was dependent on the type of perturbation [99, 97, 98]. The ankle and hip strategies appeared while increasing perturbation/target magnitude.

By investigating the same experimental paradigm and by modeling it as a double inverted pendulum, operated in a closed feedback framework, [81] exhibited realistic human coordination modes. The method proposed by [81] is able to predict the in-phase and the anti-phase coordination modes. Firstly, they solved the redundancy problem using the pseudo-inverse Jacobian matrix, and secondly they use an adaptive ankle torque saturation to ensure balance. This saturation ensures human stance, while the pseudo-inverse Jacobian minimize the instantaneous norm of the torque vector.

The use of continuous feedback ensures some advantages as it provides dynamic stability for the quiet stance when there are no external perturbations, and reacts to multiple perturbations because the response represents the outcome of the interactions between the perturbation and the feedback system. Although feedback control has these advantages, human postural responses depend on biomechanical properties, such as body and surface configuration as well as task objectives. Therefore strategies should change and different sets of feedback control gains may be required.

We modeled Bardy's paradigm as a two-dimensional inverted pendulum, as presented in section 4.3.1, operated by two independent PD feedback loops, one to ensure balance while the visual task is realized, and another to achieve the tracking task while the balance task is accomplished. We also want to go further and claim a predictive constrained optimization algorithm. Our method investigates human postural responses and optimizes the viscosity, stiffness and the cross gain coefficients in a closed loop framework situation. The redundancy is solved by transposing the operational space into an articular one without using an explicit inverted Jacobian matrix. The feedback control gains, necessary to accomplish our experimental paradigm, are synthesized and selected frequency by frequency for different target magnitudes in 3 optimization cases: (a) minimizing a torque criterion, (b) minimizing a torque change criterion and (c) minimizing a head jerk one, under both tracking (or environmental) and balance (or intentional) constraints.

4.7.1 The closed-loop modeling

While performing the visual tracking task in a closed loop situation, a corrective joint torque is applied to the ankle and hip joints. Our modeling paradigm relies on two PD controllers, one to maintain balance while doing the task and another, to achieve the target tracking task while keeping balance. The state space vector θ of the joint kinematics is defined as:

$$\theta = [q_1 \quad q_2 \quad \dot{q_1} \quad \dot{q_2}]^T$$

where q_1, q_2 are the ankle and hip angular positions, while $\dot{q_1}$, $\dot{q_2}$ are the ankle and hip angular velocities, respectively.

The feedback control input τ is represented by the ankle and hip joint torques $\tau = [\tau_1 \quad \tau_2]^T$. It is generated by a full-state feedback, that has the following form:

$$\tau = \begin{bmatrix} A_p & A_d \end{bmatrix} \Delta\theta + H \begin{pmatrix} \Delta h \\ \Delta\dot{h} \end{pmatrix} \tag{4.8}$$

where $A_p = \begin{pmatrix} k_{p11} & k_{p12} \\ k_{p21} & k_{p22} \end{pmatrix}$ and $A_d = \begin{pmatrix} k_{d11} & k_{d12} \\ k_{d21} & k_{d22} \end{pmatrix}$ are the proportional and derivative gains matrices ($A_p \in \Re^{2x2}$, $A_d \in \Re^{2x2}$) respectively for the balancing PD controller, while $H = \begin{pmatrix} k_{p1} & k_{d1} \\ k_{p2} & k_{d2} \end{pmatrix}$ is the proportional and derivative gain matrix ($H \in \Re^{2x2}$) for the PD controller that accomplishes the visual tracking task. $\Delta\theta = \theta_0 - \theta$, where θ_0 represents quiet standing (angular position and velocity are equal to 0). $\Delta h = h_{ref}(t) - h$, where h_{ref} is the system input represented by the target's position and h is the subject head position on the horizontal axes.

The direct kinematic model used to calculate the head position on horizontal h_x and vertical h_y axes, is given by:

$$\begin{aligned} h_x &= l_1 \sin q_1 + l_2 \sin (q_1 + q_2) \\ h_y &= l_1 \cos q_1 + l_2 \cos (q_1 + q_2) \end{aligned} \tag{4.9}$$

4.7.2 The gain synthesis method

Considering human postural activity as composed of two-joint motion, postural responses are transformed into a mathematical optimization problem with an objective function, that firstly, specifies the minimization of the sum of joint torque changes, secondly, the minimization of the sum of joint torques and thirdly, the minimization of the sum of head jerk.

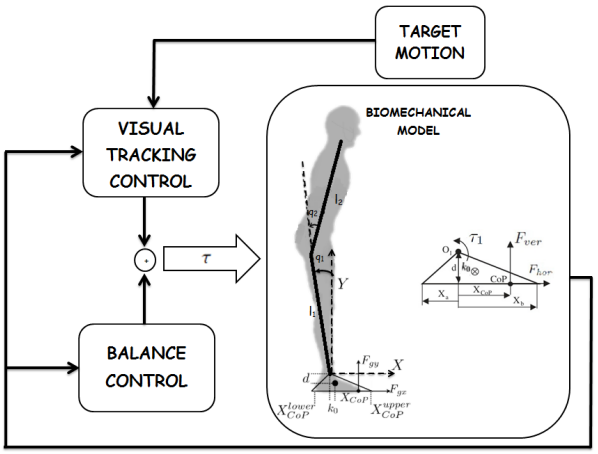

FIGURE 4.9: The controller block diagram for postural coordination (DIP model in sagittal plane. Characteristics of ankle-foot group)

$$\underset{K}{\text{minimize}} \quad J(K) = \frac{1}{2} \begin{cases} (a) \int_0^{T_c} \left(\left(\frac{d\tau_1}{dt} \right)^2 + \left(\frac{d\tau_2}{dt} \right)^2 \right) dt, \\ (b) \int_0^{T_c} \left((\tau_1)^2 + (\tau_2)^2 \right) dt, \\ (c) \int_0^{T_c} \left(\left(\frac{d^3 h_x}{d^3 t} \right)^2 + \left(\frac{d^3 h_y}{d^3 t} \right)^2 \right) dt, \end{cases} \tag{4.10}$$

$$\text{subject to} \quad h_x(z,t) - a_{ref} = 0, \ t = \frac{T_c}{4} \tag{4.11}$$

$$h_x(z,t) + a_{ref} = 0, \ t = \frac{3T_c}{4} \tag{4.12}$$

$$\frac{dh_x}{dt}(z,t) = 0, \ t = \frac{T_c}{4} \tag{4.13}$$

$$\frac{dh_x}{dt}(z,t) = 0, \ t = \frac{3T_c}{4} \tag{4.14}$$

$$h_y(z,t) \geq 0.5 \cdot \text{body height} \tag{4.15}$$

$$\tau_{ankleMIN} \leq \tau_1(z,k,t) \leq \tau_{ankleMAX}, \ \forall t \in [0, T_c]. \tag{4.16}$$

$$\tau_{hipMIN} \leq \tau_2(z,k,t) \leq \tau_{hipMAX}, \ \forall t \in [0, T_c]. \tag{4.17}$$

$$X_a \leq X_{CoP}(\tau, z, k, t) \leq X_b, \ \forall t \in [0, T_c]. \tag{4.18}$$

where $T_c = 1/f_{ref}$ is the period of the target motion, f_{ref} and a_{ref} are the target's frequency and magnitude and $[X_a, X_b]$ represent the extremal positions of the CoP in forward and backward directions with respect to the ankle joint ([80]).

The nonlinear constrained optimization consists in: 'finding the optimal feedback control gains that minimize a given criterion (4.10) under balance (4.18), horizontal tracking ((4.11)-(4.12)) and vertical tracking ((4.15)) at a null velocity ((4.13)-(4.14)) and bounded torques ((4.16)-(4.17)), equality/inequality constraints'.

4.7.2.1 The numerical experiment

The initial values of joint position and velocity are considered to be equal to 0, hence one should see a transient response that should not be taken into account in the optimization process. Each trial is studied only for the fourth period of the target displacement.

To perform the visual tracking task, specific input data values were chosen [103]. All optimization trials were done for a typical subject: body height $= 1.8\ m$ and $mass = 75\ kg$. The anthropometric parameters values were: $d = 0.07\ m$, $l_1 = 0.88\ m$, $l_2 = 0.85\ m$, $m_0 = 2.18\ kg$, $m_1 = 21.98\ kg$, $m_2 = 50.85\ kg$, $k_0 = 0.07$, $k_1 = 0.55$, $k_2 = 0.63$ and the inertia $I_i = m_i(k_i l_i)^2$.

The input signal is a sine wave in the Cartesian space. In our study, the magnitude for the target's motion used was equal to 10 cm and the length of support base was equal to $\pm 10\ cm$. Taking into account that we have 12 gains to synthesize with the optimization program, it is safer to start from a feasible point. For each magnitude, 70 different frequencies are studied: $0.1\ Hz : 0.01 : 0.79\ Hz$. These frequencies are usually the ones investigated in literature for the same experimental paradigm.

The starting point, taken for the feedback gains in the optimization search is almost the same in all simulations. Considering that we have to find 12 gains with the optimization program, it is wiser for us to start from a feasible point. In fact, the gains are initialized as follows: the initial values for the balance controller's gains correspond to the ones obtained from actual data in [107], whereas the initial values for the tracking controller are adjusted manually, so that the tracking task is approximately satisfied.

4.7.2.2 Analysis

The optimal feedback control gains values obtained via optimization, for $\pm 10\ cm$ support base length, 10 cm for the target displacement and for low/high frequencies ($0.1\ Hz : 0.01 : 0.79\ Hz$), are reported on Fig.4.10, Fig.4.11 and Fig.4.12.

Two different postural coordination strategies, namely the ankle and the hip strategies (Figure 4.14), appear on the joint trajectories when increasing the target's oscillation frequency. The in-phase coordination mode shows that the ankle joint torque and hip torque extend simultaneously, and that the ankle one has a greater impact on the postural coordination mode responses, even when the biomechanical constraints are inactive. Yet, in contrast, the anti-phase coordination mode presents the influence of the hip torque during the activation of the biomechanical constraints.

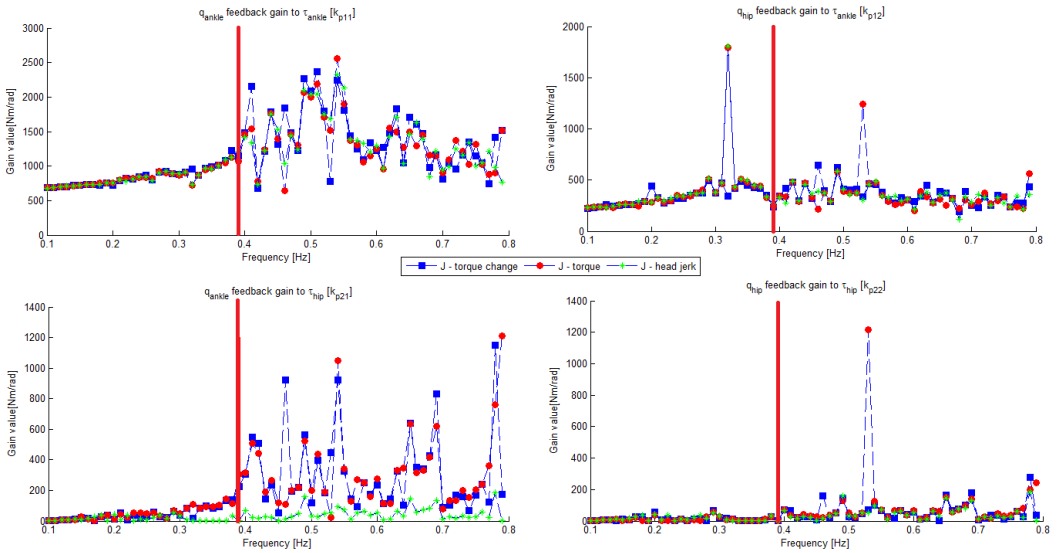

FIGURE 4.10: The proportional gains values for the balance control (A_p). The blue feedback gains resulted while minimizing the torque criterion, the green ones resulted while minimizing the head jerk and the red ones while minimizing the torque change.

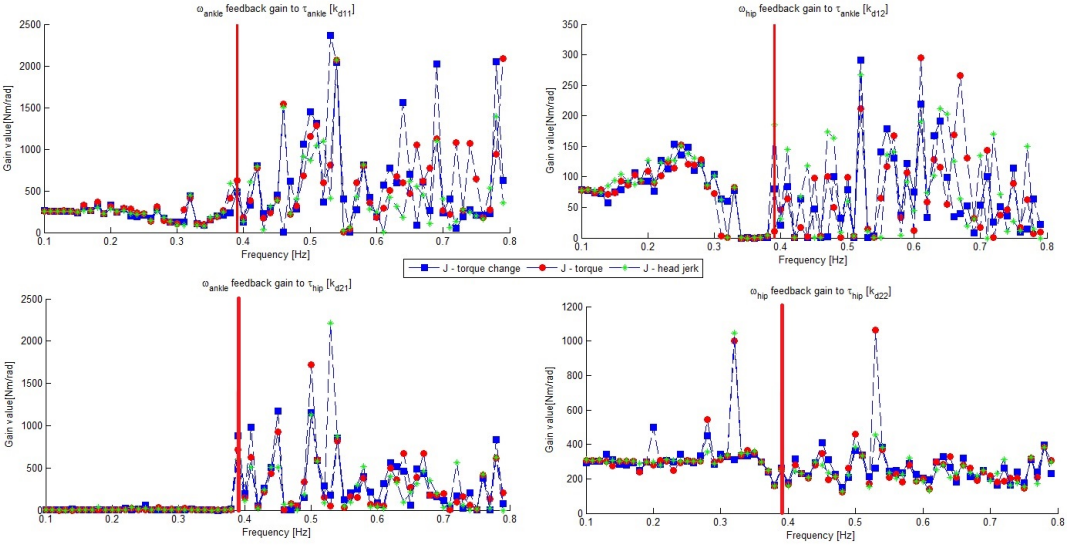

FIGURE 4.11: The derivative gains values for the balance control (A_d). The blue feedback gains resulted while minimizing the torque criterion, the green ones resulted while minimizing the head jerk and the red ones while minimizing the torque change.

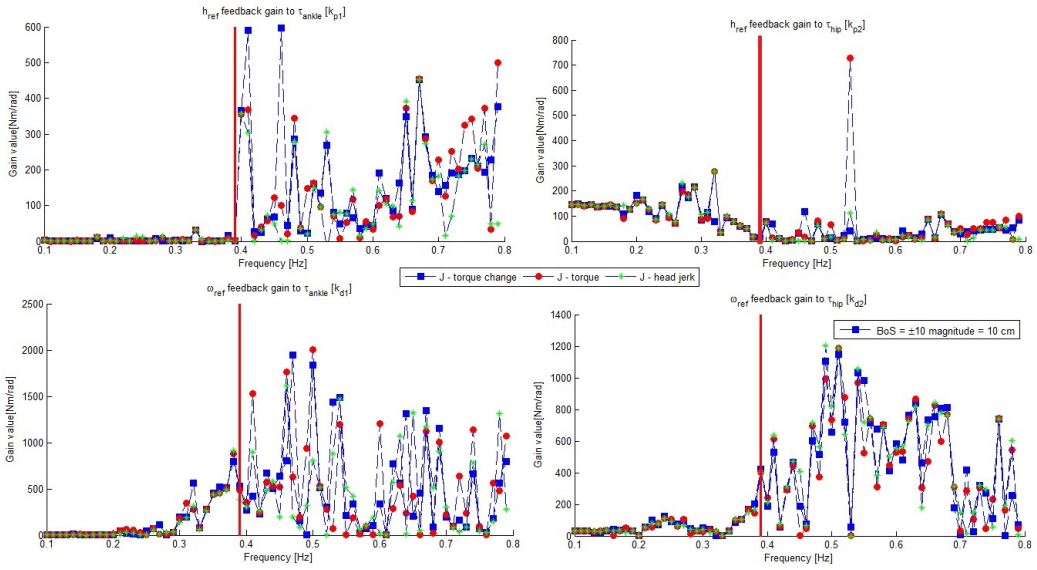

FIGURE 4.12: The proportional and the derivative gains values for the tracking control (H). The blue feedback gains resulted while minimizing the torque criterion, the green ones resulted while minimizing the head jerk and the red ones while minimizing the torque change.

Also, it can be seen that for the in-phase coordination mode, the angular displacement magnitude for the ankle joint is greater than the hip joint. When phase shift happens, in the anti-phase coordination mode case, the angular displacement magnitudes are smaller at ankle joint than at the hip ones (Figure 4.14). Figure 4.13 shows that the visual tracking and the balance constraints are satisfied while increasing the frequency during the synthesis method.

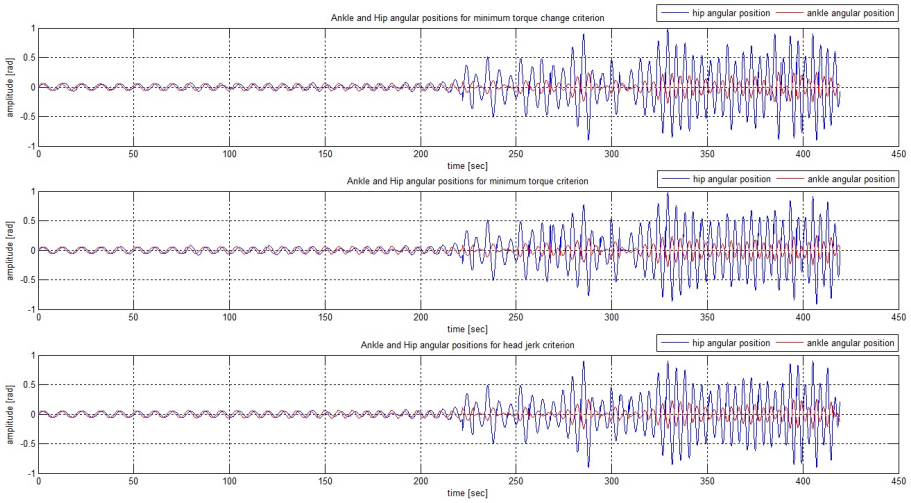

FIGURE 4.13: The angular positions; the target amplitude = 10 cm, the in-phase (until 0.39 Hz) and the anti-phase (after 0.39 Hz) coordination modes

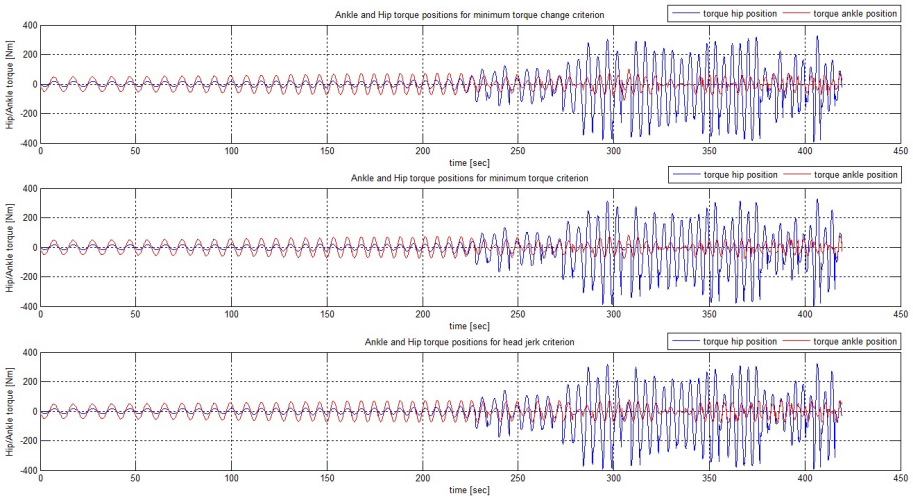

FIGURE 4.14: The joint torque displacement; the target amplitude = 10 cm, the in-phase (until 0.39 Hz) and the anti-phase (after 0.39 Hz) coordination modes

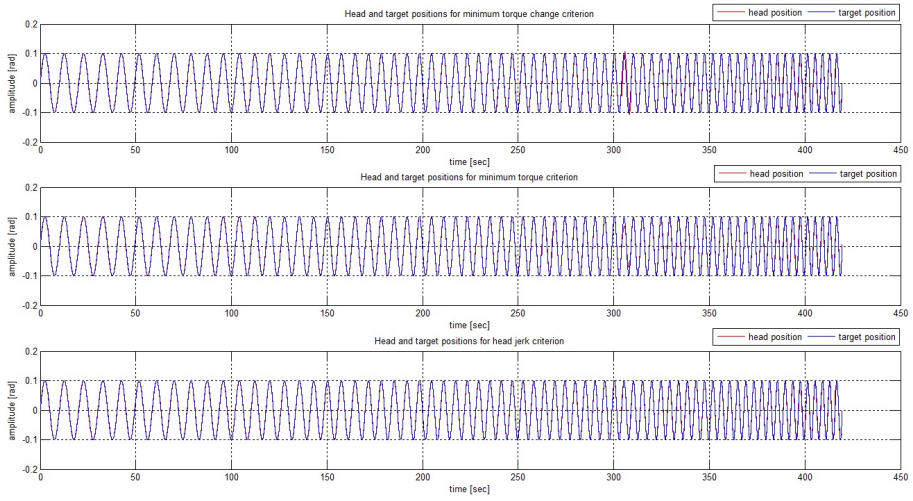

FIGURE 4.15: The head displacement; the target magnitude = 10 cm for all range of frequencies

In terms of feedback control gains, it can be observed that a trend is exhibited until phase shift (until 0.39 Hz) and after the transition frequency, the trend will change (after 0.39 Hz) (see Fig. 4.10, Fig. 4.11 and Fig. 4.12). The feedback control gains were obtained via a constrained optimization programming using a nonlinear equation solver (fmincon, Matlab®).

The synthesis method yields a closed loop feedback framework that exhibits behaviors consistent with the experimental findings, namely the ankle and the hip strategies, the in-phase/ anti-phase coordination modes for low/high frequencies. The minimization of

the torque change [63], torque change and head jerk, provided suitable responses for the chosen experimental paradigm as it was expected and also the feedback control gains behavior is similar.

During the synthesis method, the ankle joint torque is restricted due to it's dependance with the CoP (Fig.4.13) in order to satisfy the balance constraint. For the same experimental paradigm, modeled in the open loop [80] results revealed that during ankle strategy the balance constraints are not active and during the hip strategy the constraints become active.

Feedback gains exhibited smooth, increased, decreased or constant behaviors for the in-phase coordination mode, while for the anti-phase coordination mode, the feedback gains exhibited non smooth increase, decrease or a constant behavior.

During the use of our synthesis method, we considered a sinusoidal wave as the input to our system, but actually, this input consists of a more complex vision model with information coming from the vestibular and somato-sensory systems. In order to synthesize the feedback control gains for the measured data, the input of the system also need to be estimated, therefore the problem becomes more complicated.

Finally, we were able to show that similar conclusions are drawn when applying the inverse optimal control problem and when solving the synthesized method. As presented in the sections that solve the inverse optimal control problem, this paradigm can be explain by using different criteria. Hence, it was not a surprise to obtain similar feedback gains control behaviors when testing different criteria for this paradigm.

4.8 Summary

In this chapter, the postural coordination in a visual tracking task was analyzed. Firstly, the inverse approximately optimal control approach was applied in order to find the class of criteria that can explain this experimental task. The results presented the fact that any criterion, chosen in the basis of criteria, can be a potential candidate for explaining this task. This result is consistent with the literature, meaning that this task was described in literature by minimizing the torque criterion or the torque change criterion and the found results, in terms of postural responses, were the same.

Secondly, we modeled the visual tracking of a target with the head in a closed loop optimal control, consisting in two PD feedback loops: a short loop that addresses the balancing issues, and a long one that addresses the visual tracking task. The closed loop

was used for the simulated data while using three criteria considered candidate by our algorithm. The obtained results where consisting in both an open loop and a closed loop situation: if our IAOC algorithm exhibits certain criteria, the results obtained in the closed loop for this criteria, presents similar behaviors in terms of feedback gains (the PD feedback gains have the same behavior).

Chapter 5

The analysis of the human walking gait initialization task.

5.1 Related literature

One of the hardest phenomenon that come in elderly is the loss of autonomy and this leads to slips or falls. Nowadays, this phenomenon has become common in our society, resulting in injuries and even death each year. Due to its importance, the balance control loss ('BCL') has become a widely studied subject within the research communities such as biology, neuroscience, engineering and so on. All these communities are trying to work together in order to use knowledge from all the fields in order to come up with ways to prevent or to give solutions to this universal problem. The field of our interest are biomechanics, control and robotics, and we are trying to model balance control loss in Parkinson's disease. The latter is a neurodegenerative disorder and it is characterized by progressive loss of muscle control, which leads to tremor in limbs and head while at rest, with stiffness, slowness, and impaired balance [108]. As the symptoms worsen, it may become difficult to walk, talk, and complete simple tasks.

A considerable number of experimental studies have focused on the balance control loss, in order to find simplified models or to enhance our understanding of this phenomenon. Taking into account the amount of experimental observations, the balance recovery strategies presented in Fig. 5.1 can be divided into 2 classes:

- **Fixed-Support strategies**, which include the ankle and hip strategies. In ankle strategy, the oscillation of the body is around the ankle joint and it is commonly used to tackle small external perturbations. In the hip strategy, the upper body

leans backwards and forwards around the hip joint and, it is often used for slightly larger disturbances.

- **Change-of-support strategies**, which can involve the use of compensatory stepping. This strategy is suitable for large disturbances where the fixed-support strategies are not sufficient to recover balance.

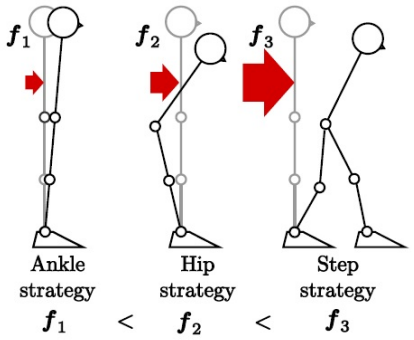

FIGURE 5.1: The fixed-support strategies (the ankle and hip strategies) and the change-of-support or the stepping strategy [3]

The fixed-support strategies for balance recovery

When analyzing human balance control, human body can be modeled as one or multi-dimensional inverted pendulum chain. The one-dimensional inverted pendulum model [92, 93, 94] is accepted, if the movements in the other joints are artificially blocked [93], so the biomechanical system will be described only by-one variable: the angle of the ankle joint. Even so, [95] argued that a single chain inverted pendulum approximation is not sufficient to completely explain balance properties, even for standing balance. When modeling the human body as a multi-dimensional inverted pendulum chain, the dependency of torques on joint angles and angular velocities is determined by the stiffness and the viscosity gain coefficients respectively. Therefore the change of torque in any joints will have an impact on all the joints. Accordingly, a common model used in several studies and also in our study presented in chapter 3 is the double inverted pendulum model [96, 80, 97, 100]. Also a three-dimensional inverted pendulum chain was used, by including the knee joint [98], to model human body.

For more details on how these strategies are modeled can be found in our previous study from chapter 3, where we used, as stated previously, a double inverted pendulum model in order to guarantee balance during postural coordination in a visual tracking task (see chapter 3 for more details and related literature).

The change-of-support strategies for balance recovery

When certain boundary values are exceeded (in angle position or velocity) during the hip strategy a new one called stepping strategy is identified. This strategy is characterized by two variables: the step length (the sum of length preparation) and step time (the leg-swing times). [109] found this 2 variables as factors between failing and successful recoveries in human subjects. The step length and step time are positively correlated, so a larger step requires more time to execute meanwhile the system continues to fall. Conversely, a quicker step cannot be placed beyond a certain distance due to actuation constraints. Hence, a trade-off is to be found between these two variables for a successful balance recovery [110]. It was showed that the stepping strategy is preferred over the fixed-support strategies even before the fixed-support strategies have not reached its theoretical limits [111]. The age-related difference impact in the balance recovery ability was studied for young and elderly subjects during various disturbances paradigms, in order to compare their responses. Elderly prefer the use of the stepping strategy to recover balance and they are more likely to use a higher number of steps in order to recover balance than the young subjects [112].

The most common simplified model for biped robots is the Inverted Pendulum proposed by [113] which assumes telescopic legs and constrains the CoM to move in the horizon plane above the ground, but it neglects the rotational effects of different body parts. The upper body inertia effects are included by using an inertia wheel centered at the CoM level [114]. To incorporate leg compliance, [115] proposed a simplified model consisting in a massless spring attached to a point mass and demonstrate realistic dynamic properties of human walking and running. An improved match of walking data was exhibited while modeling human gait dynamics as a compliant legged bipedal model with continuous pivot translation profile which emulates empirical CoP excursion during the stance phase [116]. By using damping compliant legs inverted pendulum model to match the human ground reaction forces at different gait speed suggested that humans may benefit from spring-like leg mechanics [117]. Moreover, the same way of modeling the human body while walking implies that the human walking dynamics and the variation with respect to age, can be well captured by the spring-like leg mechanics [118]. [119] modeled a leg, while analyzing human walking, as a simple two-link system with two joints at a hip and a knee, where the trunk moves horizontally at a constant speed and it found that the experimental data of human walking showed common characteristics.

Modeling human gait

The human gait requires the maintenance of balance (postural control with ankle and hip strategies) and continuous movement (locomotion with stepping strategy) simultaneously.

There are two ways of modeling human gait by mixing the three sets of strategies:
(a) *Proposing a model while in fixed support strategies and switching to another model while in change of support strategies.*
(b) *Proposing only one model that can take into account the three sets of strategies, namely the ankle, the hip and the stepping.*
The mix between the three sets of strategies can be found modeled when trying to explain human balance recovery while important external perturbations are applied. In this sens, [120] proposed a scheme that predicts multiple step placements, by modeling the dynamics of a running cart on the table [121, 57, 122]. The scheme is composed of a simple balance recovery model, represented by an inverted pendulum with a foot model, based on the Linear Model Predictive Control. This schema is more complex then the one in previous studies, by predicting multiple step recovery while taking into account the step execution time, working in a sagittal plane.

Furthermore, in [123] they improved their mechanical model that explains the human balance recovery, introducing the upper body inertia (UBI) influence on modeling human balance recovery. They studied the recovery paradigm in a model predicted control framework by modeling it as a flywheel linear inverted pendulum plus a foot model and they exhibit realistic step lengths. Their results show the influence of the UBI onto the step lengths. Finally, making use of this model and analyzing different sets of criteria they propose in [124] a single Model Predictive Control scheme for biped humanoid robots. In this study, they propose a schema that minimizes sets of criteria with proper relative weight coefficient values. Along the set of criteria, the penalization of the swing foot acceleration showed an impact to recovery improvement. This scheme improves the balance recovery response to external perturbations while properly combining the ankle, hip and stepping strategies.

[3] implements a method that smoothly shifts between ankle and hip strategies when studying balance control, while continuous external forces are applied to a humanoid robot.

[125] studies the human balance stability while standing and it introduces a new stability condition, the extrapolated center of mass position (XCoM), that requires the center of mass within the base of support in order to accomplish balance.

[126] proposed an online walking motion generation in order to demonstrate the ability of the model predictive control to generate stable walking motions without using predefined foot steps. In [56], the walking motion generation was expanded to enhance its flexibility and independence by controlling appropriate feet and trunk orientation. [127] used this online walking motion generation based on the model predictive control to show that it is possible to obtain a continuous adaptation of the foot placement even in the presence of strong perturbations.

In this chapter, we are focused on finding a suitable model for the walking gait initialization task and the criteria that can explain experimental data collected during the task. The models mentioned above are modeling the human locomotion task and their analysis is not connected to the gait initialization. In our study, we will firstly use the studies mentioned in the subsection 5.1 to achieve the modeling part and, secondly we will address our IAOC algorithm to find the potential criteria candidates that can explain the experimental data collected for parkinsonians and non-parkinsonian subjects.

5.2 The model predictive control scheme

In this section, we start with a brief description of the model predictive control, that will be used in our study. Moreover, here we will present the model predictive optimal control scheme used to model the walking paradigm. But this does not mean that we are going to neglect our objective of modeling the gait initialization, as this one is the initial phase of the walking paradigm.

The Model Predictive Control (MPC) is a control technique which amounts to repeatedly solving online a series of Optimal Control problems, always taking into account the latest observation of the real state of the system. It usually takes the form of minimizing at every time t_k a cost function L, considering a prediction of the dynamics of the system over a time horizon of the length T:

$$min_{u_k} \int_{t_k}^{t_k+T} L(u_k)dt \tag{5.1}$$

The control $u(t_k)$ that results from this optimization is applied to the system until the next observation time t_{k+1} and the process is repeated.

5.2.1 The biomechanical model

The dynamic system used to model the ankle, the hip and the stepping strategies in 2D - sagittal and horizontal plane (with the assumption that the CoM height is constant on the horizontal plane) - is the one proposed and described in [56]. The dynamics are those of a running cart on a table [121]:

$$p_x = c_x - \frac{c_z}{g}\ddot{c}_x \tag{5.2}$$

where c_z is the constant height of the CoM position above the ground, g is the norm of the gravity force, while c_x and p_x are the coordinates on x axes of CoM and CoP.

We consider trajectories of the CoM which have piecewise constant jerk $\dddot{c}_x$ over time intervals of constant length T so that we can compute the corresponding dynamics at a discrete time t_k:

$$\begin{cases} \hat{x}_{k+1} = A\hat{x}_k + B\dddot{c}(t_k) \\ \hat{y}_k = C\hat{x}_k \end{cases} \tag{5.3}$$

with

$$\hat{x}_{k+1} = \begin{pmatrix} c(t_k) \\ \dot{c}(t_k) \\ \ddot{c}(t_k) \end{pmatrix}, \hat{y}_k = p_k \tag{5.4}$$

and

$$A = \begin{pmatrix} 1 & T & T^2 \\ 0 & 1 & T \\ 0 & 0 & 1 \end{pmatrix}, B = \begin{pmatrix} \frac{T^3}{6} \\ \frac{T^2}{2} \\ T \end{pmatrix}, C = \begin{pmatrix} 1 & 0 & -c_z/g \end{pmatrix} \tag{5.5}$$

where c_x and p_x are the coordinates on x axes of COM and COP.

5.2.2 The original MPC controller scheme

The controller proposed in [120, 56] anticipates future motion on a prediction horizon composed of N time intervals of equal length T. During the motion, on the future horizon, the third derivative $\dddot{c}$ over each time interval is considered zero. The CoM position, velocity and acceleration can be related to the corresponding constant third derivative $\dddot{c}$, through simple matrices, by integrating over the whole prediction horizon:

$$X_{k+1} = \begin{pmatrix} x_{k+1} \\ \vdots \\ x_{k+N} \end{pmatrix} = S_p \hat{x}_k + P_p \dddot{c}_k \tag{5.6}$$

$$\dot{X}_{k+1} = \begin{pmatrix} \dot{x}_{k+1} \\ \vdots \\ \dot{x}_{k+N} \end{pmatrix} = S_v \hat{x}_k + P_v \dddot{c}_k \tag{5.7}$$

$$\ddot{X}_{k+1} = \begin{pmatrix} \ddot{x}_{k+1} \\ \vdots \\ \ddot{x}_{k+N} \end{pmatrix} = S_a \hat{x}_k + P_a \dddot{c}_k \tag{5.8}$$

$$p^x_{k+1} = \begin{pmatrix} p^x_{k+1} \\ \vdots \\ p^x_{k+N} \end{pmatrix} = S_{pp} \hat{x}_k + P_{pp} \dddot{c}_k \tag{5.9}$$

with

$$\dddot{c}_k = \begin{pmatrix} \dddot{c}_k \\ \vdots \\ \dddot{c}_{k+N-1} \end{pmatrix}. \tag{5.10}$$

Where $S_p,\ S_v,\ S_a,\ S_{pp} \in \Re^{N\times 3}$ and $P_p,\ P_v,\ P_a,\ P_{pp} \in \Re^{N\times N}$ are matrices that are obtained from a recursive application of the dynamic system.

The original MPC schema, proposed in [121], consists in minimizing over a predictive horizon of length NT the jerk of CoM with the tracking of a reference position (p_{ref}) of the CoP. The CoP is chosen to be in the middle of the base of support, for an enhanced robustness against perturbations. This can be expressed as the following quadratic program:

$$\underset{\dddot{c}_x}{\text{minimize}} \quad \frac{\alpha}{2} \|\dddot{c}_x\|^2 + \frac{\beta}{2} \left\| p^x_{k+1} - p^{xref}_{k+1} \right\|^2. \tag{5.11}$$

5.2.3 The cost function

The choice of criteria

In the original MPC scheme proposed in [121] and described previously, the minimization of the jerk of the CoM is necessary to generate stable motions, but also it was showed that a weakly weighted minimization helps smoothing the contact forces and

therefore the resulting motion. Moreover, the minimization of the tracking of a reference position of the CoP was necessary to generate a feasible motion, but also a weakly weighted minimization allows faster and more robust reactions to changes in the state of the system. These criteria were widely used in robotics to propose a walking pattern generator [128, 121, 57, 122, 129]. Some recent studies analyzed the human balance recovery and ensured standing position based on robotic approaches, by taking into account upper body inertia effects [124]. The minimization of the CoM and the trunk rotation velocities always allow quicker steps.

In this study, we want to model human gait initialization and compare it with experimental data, therefore we'll choose as criteria the jerk, the velocity and the acceleration of CoM in order to guarantee smooth trajectories and the tracking of a reference position of the CoP. We do this in order to ensure balance maintenance while gait initialization.

5.2.4 The kinematic and the dynamic constraints

5.2.4.1 The inequality constraints

Center of pressure

Center of pressure (CoP) is the term given to the point where the ground reaction force is balanced. The ground reaction force vector represents the sum of all forces acting between a physical object and its supporting surface.

The static balance is ensured if the CoP always stays within the base of support (support polygon) during the single and double support while walking (see Fig.5.2). Hence, this constraint is represented in the optimization program by eq (5.12):

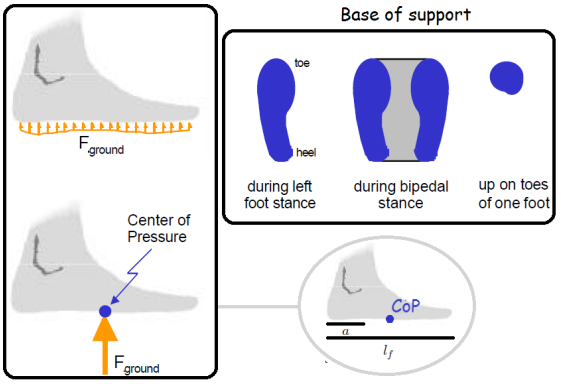

FIGURE 5.2: The CoP and the base of support representation

$$-a \leq CoP \leq l_f - a \tag{5.12}$$

where a is the ankle to heel horizontal distance and l_f represents the foot length.

Foot step placements

To ensure feasible step placements generated by our optimization program algorithm, we'll bound the position of the next foot step depending on the current position of the foot in the air:

$$-Dmax \leq X_f(i) - X_f(i-1) \leq Dmax, \tag{5.13}$$

where

$$Dmax = (t_{touchdown}(i) - t_{touchdown}(i-1))v_{max} \tag{5.14}$$

with $X_f(i)$, the position of the next foot step on x axes, $X_f(i-1)$ the current position of the foot in the air on x axes, v_{max} a vector of approximate maximum Cartesian speed and $t_{touchdown}$ the time when the foot in the air is planned to touch the ground.

5.2.4.2 The equality constraints

Center of mass position and velocity

The center of mass is the geometric point where every particle of a body's mass is equally distributed, as presented in Fig. 5.3, being equal to the product between each body particle position and its mass divided by the sum of each particle's mass.

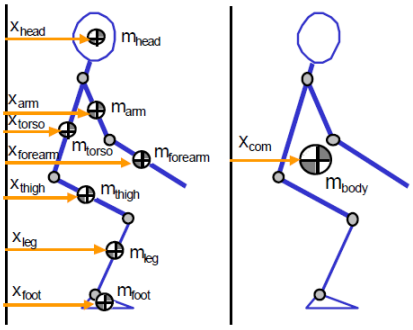

FIGURE 5.3: The CoM representation

During the optimization program algorithm we require the CoM position and velocity to be equal with the ones observed, in order to assure final feasible values:

$$\begin{aligned} c_x(end) &= c_{xdata}(end) \\ \dot{c_x}(end) &= \dot{c_{xdata}}(end) \end{aligned} \tag{5.15}$$

5.2.5 The proposed MPC controller: design and scheme

The MPC scheme proposed in [56] balances over a prediction horizon, the minimization of the jerk of the CoM with the tracking of a reference position of the CoP which is chosen to lie in the middle of the base of support for an enhanced robustness against perturbations. In this study, we are analyzing human gait and because we do not need to recover after perturbations we'll balance over the entire horizon the minimization of the jerk of the CoM and the positions of the following steps while maintaining the CoP within the base of support with a prior final position and velocity of the CoM. We can express this minimization problem in the corresponding quadratic program to be solved:

$$\begin{aligned} \underset{u_k}{\text{minimize}} \quad & \frac{\alpha}{2}\left\|\dddot{c}_x\right\|^2 + \frac{\beta}{2}\left\|\dot{c}_x\right\|^2 + \frac{\delta}{2}\left\|\ddot{c}_x\right\|^2 + \frac{\gamma}{2}\left\|p^x_{k+1} - p^{xref}_{k+1}\right\|^2. \\ \text{subject to} \quad & h_i(u_k) = 0, \quad i = 1, \ldots, 2.(5.15) \\ & g_i(u_k) \leq 0, \quad i = 1, \ldots, 4.(5.12), (5.13) \end{aligned} \tag{5.16}$$

where

$$u_k = \begin{pmatrix} \dddot{c}_x \\ X^f \end{pmatrix}, \tag{5.17}$$

and $\dot{c}_x$, $\ddot{c}_x$, p^x_{k+1} are the state vector defined in (5.7), (5.8) and (5.9), while $\dddot{c}_x$ represents the optimization decision variable. Because we do not want the CoP to track a trajectory fixed in advance, we define:

$$p^{xref}_{k+1} = U^c X^{fc} + U_{k+1} X^f, \tag{5.18}$$

so that it can lie in the middle of the foot positions actually decided by the optimization algorithm. X^{fc} is the current position of the foot on the ground (which can not be

changed) and X^f are the positions of the next steps, where:

$$U^c = \begin{pmatrix} 1 \\ \vdots \\ 1 \\ 0.5 \\ 0 \\ \vdots \\ 0 \\ 0 \\ \vdots \\ 0 \end{pmatrix} \in \Re^N, U_{k+1} = \begin{pmatrix} 0 & 0 & \\ \vdots & \vdots & \\ 0 & 0 & \\ 0.5 & 0 & \\ 1 & 0 & \\ \vdots & \vdots & \\ 0.5 & 0.5 & \\ 0 & 1 & \\ \vdots & \vdots & \\ 0 & 1 & \ddots \end{pmatrix} \in \Re^{N \times m}. \tag{5.19}$$

The 1 values from the above matrices indicates which sampling times t_k fall into which step and the 0.5 values indicate the fact that during the double support phase the sampling times t_k fall in the middle of the feet and m represent the number of steps defined in advanced.

5.3 Experimental data: the center of mass reconstruction

5.3.1 Description

We tested 6 non-parkinsonian subjects, by asking them to start (one trial per subject) a normal and a quick walk on a force platform. Also, 5 parkinsonian subjects were asked to perform a normal walk before and after Levadopa (or L-dopa) treatment and a quick one before and after Levadopa (or L-dopa) treatment on the force platform, one trial per subject. While analyzing the CoP observed trajectories for each subject, we saw that every subject has a different behavior, showing different step length values and step duration, therefore we need to apply our algorithm for each subjects' observed trajectory.

For each subject, in the CoP position was observed and the CoM position needs to be recontructed in order to analyze and model walking gait initialization task. The CoM position is reconstructed by using the following pattern generator scheme.

5.3.2 The pattern generator scheme

Due to the fact that observed outputs are sampled and noisy we interpolated the measurements by applying a spline-fitting of the observed outputs as proposed in [55]. Therefore the observed output, the CoP position in our case, is interpolated with a 7th order spline with 60 knots.

On the interpolated CoP position we apply the pattern generator proposed and presented in [57], in order to reconstruct the CoM position and its derivatives. The pattern generator consists in minimizing the error between the reference position of the CoP (in this case it is the observed CoP and interpolated with a spline curve) and the obtained CoP from the running cart on a table dynamics ([121]).

The pattern generator comes down to minimizing the following criteria:

$$\underset{z}{\text{minimize}} \quad \sum_{j=1}^{N_L} \left(CoP_j^{ref} - CoP_j \right). \tag{5.20}$$

where N_L is the future step at every sampling time, z represent the state vector of the following system representation:

$$\begin{cases} \begin{bmatrix} \dot{CoM} \\ \ddot{CoM} \\ \dot{CoP} \end{bmatrix} = \begin{bmatrix} 0 & 1 & 0 \\ \frac{g}{h_{CoM}} & 0 & -\frac{g}{h_{CoM}} \\ 0 & 0 & 0 \end{bmatrix} \begin{bmatrix} CoM \\ \dot{CoM} \\ CoP \end{bmatrix} + \begin{bmatrix} 0 \\ 0 \\ 1 \end{bmatrix} \dot{CoP} \\ CoP = \begin{bmatrix} 0 & 0 & 1 \end{bmatrix} \begin{bmatrix} CoM \\ \dot{CoM} \\ CoP \end{bmatrix} \end{cases} \tag{5.21}$$

where g is the norm of gravity force and h_{CoM} represents the height of the center of mass.

5.3.3 Results

Fig. 5.4(a) and fig. 5.4(b) present the results of one trial for one of the subjects, while performing two steps (fig. 5.4(b)) and three steps (fig. 5.4(a)). It can be seen that we have dynamic stability, namely the CoP is directly below the body CoM.

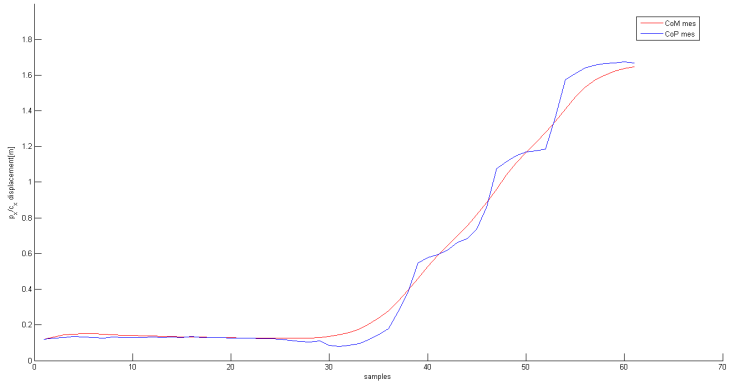

(a) One subject performing 3 steps

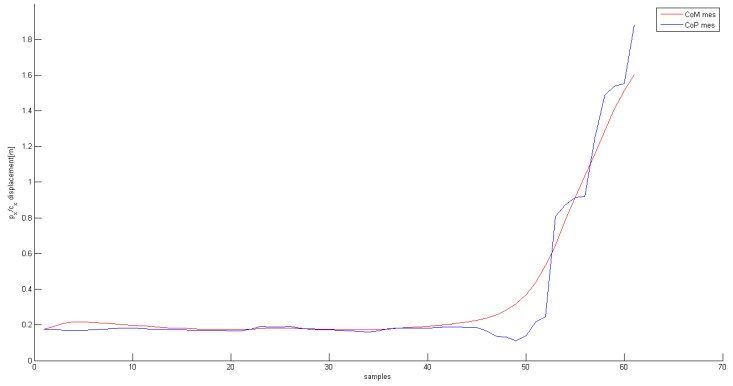

(b) One subject performing 2 steps

FIGURE 5.4: The measured CoP trajectory (the blue line) and the reconstructed CoM trajectory (the red line) with the pattern generator

5.4 The inverse optimal control solution

We first formulate the direct optimal control (DOC) problem and the KKT optimality conditions. Secondly, we address our IAOC algorithm described in Chapter. 2 and solving Eq.(2.22).

5.4.1 The direct optimal control problem

The used direct optimal control problem is formulated in section 5.2, eq. (5.16), and minimizes a given composite criterion while satisfying constraints.

Before applying the direct optimal control, the CoP collected trajectories are interpolated by b-spline curves. After this interpolation, the resulted CoP trajectories are used to reconstruct the CoM trajectories by applying the pattern generator described above.

Finally, the direct optimization problem which helps us to obtain the walking task is formulate.

The direct optimal control problem for walking task: "Find the CoM jerk trajectory and the foot steps positions,while minimizing a given composite criteria as in table 5.1 while maintaining balance (eq. (5.12)), ensuring feasible step placements (eq. (5.13)) and a feasible final CoM position and velocity values (eq. (5.15))".

TABLE 5.1: The pre-selected basis of objective functions;
N: number of time samples

Criterion	**Cost function (f_i)**	References
CoM jerk	$f_1 = \frac{\sum_{i=1}^{N} \dddot{CoM}(i)^2}{N}$	[126, 127]
CoM velocity	$f_2 = \frac{\sum_{i=1}^{N} \dot{CoM}(i)^2}{N}$	[126, 127]
CoM acceleration	$f_3 = \frac{\sum_{i=1}^{N} \ddot{CoM}(i)^2}{N}$	[126, 127]
CoP tracking	$f_4 = \frac{\sum_{i=1}^{N} (CoP(i) - CoP^{ref}(i))^2}{N}$	[126, 127]

The inequality constraints $g_j(u_k)$ are presented and explained in subsection 5.2.4.1, where j have different length for each subject.

5.4.2 The inverse approximately optimal control problem

Firstly, we need to specify matrix $A \in \Re^{m \times n}$ as in Eq. (2.19), which is composed of criteria and equality gradient's vectors, and the vector $b \in \Re^m$ as in Eq. (2.20), composed of the criterion gradient vector chosen as pivot. The A matrix is a 'tall' one (it has more columns than rows $m \geq n$), therefore we impute the criteria by solving the overdetermined least square problem (2.22).

Secondly, we must choose which basis objective function will act as pivot i^*. As previously discussed, the choice of the pivot relies on the prior knowledge of the sought composite criterion. In order not to corrupt any conclusion to be derived when analyzing the industrial screwing task, we consider that there is no such prior knowledge. As a consequence, we will have to consider any of the basis function as potential pivot. Then,

comparing the solutions of the problem (2.22) we will keep the solutions that show good consistency with the experimental data, those which minimize both the *residuals norm* (3.4) and the CoP and CoM root mean square (RMSE CoP and RMSE CoM) (3.5) described below.

5.4.2.1 Evaluation on the artificial data

In this section, we perform the evaluation of the performance of our method using artificial data. Using the human walking gait initialization model (introduced in subsection 5.4.1), we solve a DOC problem 5.16 with vector $\vec{c}$ tuned so that only one single basis objective function is active at the time. We come with four optimal trajectories, each minimizing a single basis objective function given in Table 3.3.

Firstly, we verified if the A matrix columns are correlated (see eq. (2.24)) for each optimal trajectory, and we concluded that:

- for 3 out of 4 optimal trajectories (min f_1, f_3 and f_4) there were found 2 groups of correlated criteria gradient's vectors $(\nabla_{u_k} f_2, \nabla_{u_k} f_3)$ and $(\nabla_{u_k} f_2, \nabla_{u_k} f_4)$. For these cases, we kept only three criteria: f_1, f_3 and f_4 and we continued the following steps of the algorithm.
- for the case, where f_2 is minimized, the same groups of correlated criteria gradient's vectors were found, therefore, for this case, we kept only the f_1 criterion and the f_2 one.

Secondly, we apply the steps of our algorithm **IAOC** as defined in the previous chapters and the results are gathered in Table 5.2. The first column indicates the optimal trajectory analyzed, the second and the third ones indicate the A matrix and the pivot used. The contribution of each basis objective function is given in the next columns as a relative contribution in the percentage computed as in (4.1).

Following the contribution result columns, is the sign of the inner product, as defined in eq. (3.7). Finally, the last columns contain the residuals norm and the RMSE values.

Table 5.2 clearly shows the following types of results:

- min f_1, min f_2 and min f_4 cases: When pivot i^* is set to be the true minimized objective function, the inverse optimal control problem emphasizes that the imputed composite criterion includes the true criteria whose contribution is 100% for

TABLE 5.2: The results obtained by our algorithm for the artificial data. $b = -[\nabla_{F_c} f_{i^*}]$

data while:	A	i^*	Contributions [%]			γ			$\frac{1}{n}\|\nabla L(\hat{c})\|$	RMSE com [m]	RMSE cop [m]
			f_1	f_3	f_4	γ_{13}	γ_{14}	γ_{34}			
min f_1	$[\nabla_{u_k} f_3 \nabla_{u_k} f_4]$	1	100	0	0	+	-	-	0.06	0	0
	$[\nabla_{u_k} f_1 \nabla_{u_k} f_4]$	3	0	100	0				0.1	0.08	0.1
	$[\nabla_{u_k} f_1 \nabla_{u_k} f_3]$	4	0	0	100				0.09	0.08	0.09
min f_3	$[\nabla_{u_k} f_3 \nabla_{u_k} f_4]$	1	4.45	39.56	55.99	+	-	-	0.04	0.02	0.02
	$[\nabla_{u_k} f_1 \nabla_{u_k} f_4]$	3	3.72	40.36	55.92				0.001	0.01	0.01
	$[\nabla_{u_k} f_1 \nabla_{u_k} f_3]$	4	3.77	40.12	56.11				0.01	0.02	0.02
min f_4	$[\nabla_{u_k} f_3 \nabla_{u_k} f_4]$	1	0.33	0.69	98.98	+	-	-	0.03	0.01	0.01
	$[\nabla_{u_k} f_1 \nabla_{u_k} f_4]$	3	0.33	0.7	98.97				0.002	0.01	0.01
	$[\nabla_{u_k} f_1 \nabla_{u_k} f_3]$	4	0.33	0.68	98.99				$3.7e^{-05}$	0.01	0.01
min f_2			f_1		f_2	γ_{12}					
	$[\nabla_{u_k} f_2]$	1	99		1	-			1.45	0.10	0.13
	$[\nabla_{u_k} f_1]$	2	5.6		94.4	-			0.2	0.001	0.009

the first case, 94.4% for the second one and 98.99% for the final one, with small residuals norm and RMSE values.

- min f_3 case: When pivot i^* is set to be 1, 4 or 3, the inverse optimal control problem emphasizes that the imputed composite criterion includes the true criteria whose contribution is 39.56% for $i^* = 1$, 40.36% for $i^* = 3$ and 40.12% for $i^* = 4$. However, both the residuals norm thus computed and the RMSE values when choosing the pivot to be 1 or 4, are 10 to 40 times for the residual norm and 2 times in term of RMSE rather than the case $i^* = 3$, which is the true criterion.

For the case where we min f_3, the inner product between $(\nabla f_1, \nabla f_4)$ and $(\nabla f_3, \nabla f_4)$ is negative, therefore the objective function f_3 can appear in the imputed composite criterion. To the contrary, the inner product γ_{13} is positive for the case where f_1 is minimized, therefore objective function f_1 cannot appear in the imputed composite criterion when pivoting after the other criteria gradient's vectors.

To conclude, our algorithm on artificial optimal trajectories shows that when using the true objective function as pivot, the residuals norm and RMSE values are smaller than in the other cases.

5.4.2.2 Experimental results

In this section, we use our algorithm as defined in Chapter 3 to analyze the gait initialization data gathered during the walking task described in Sect.5.3, using the objective functions basis given in Table 5.1.

After verifying the A matrix column's correlation (see eq. (2.24)), for both non-parkinsonian and parkisonian subjects, it turned out that there are three groups of correlated gradients: (∇f_2,∇f_3), (∇f_2,∇f_4) and (∇f_3,∇f_4). In our study, we will choose to keep f_1 and f_4 criteria in order to apply our algorithm. But f_1 and f_4 are not the only solution, we can also choose to replace f_4 by f_2 or f_3 according to our will, thus not changing our outcomes as f_2, f_3 and f_4 are correlated at the minimum. Hence, the outcomes of the **IAOC** algorithm are gathered in Table 5.3 for the 6 non-parkinsonian subjects while gait initialization during normal and quick walk, and for the parkinsonian subjects while gait initialization during normal and quick walk before and after L-dopa treatment in Table 5.4 and Table 5.5, respectively.

In Table 5.3 each line contains the results obtained for all the non-parkinsonian subjects, the number of trials, the criteria contribution, the sign between the criteria gradient's vectors, and the residuals norm, RMSE CoM and RMSE CoP values.

Comparing the obtained results for all subjects, both parkinsonians and non-parkinsonians, while using as pivot $i^* = 1$ with the ones obtained in the other case, we can conclude:

- for non-parkinsonian subjects: the results obtained while pivoting after $i^* = 4$ were found in terms of residuals norm value between 10000 and 40000 higher than when pivoting after $i^* = 1$, and 2 times higher in terms of RMSE than when pivoting after $i^* = 1$, and it should be discarded.
- for parkinsonian subjects: the results obtained while pivoting after $i^* = 4$ were found in terms of residuals norm value between 10000 and 20000 higher than when pivoting after $i^* = 1$, and 2 times higher in terms of RMSE than when pivoting after $i^* = 1$, and it should be discarded.
- for all subjects the results obtained in terms of RMSE are smaller while using as pivot $i^* = 1$ than in the other case.

We randomly choose the second parkinsonian subject and we graphically represented the cop and com trajectories, estimated via direct optimal control with the results obtained when the pivot is $i^* = 1$ (the green dotted trajectory in the CoP fig. 5.7(b) and CoM fig. 5.7(a) cases) and $i^* = 4$ (the blue dotted trajectory in the CoP and CoM cases).

After analyzing the results we decided that the best option is to keep the case where the pivot is f_1 i.e. the com jerk gradient vector, because as we can see from the explanations above, the results are the one that comply with the requirements of our algorithm.

As far as the contributions are concerned, the followings are obtained for the non-parkinsonian subjects, (see Table 5.3):

- the algorithm found 2 out of 6 subjects for which the CoM jerk criterion is the best candidate with a value equal to 100 %, for both the normal and the quick walk. During the normal walk task, our algorithm found a combination between the CoM jerk and the CoP tracking criteria for all the other 4 subjects. On the other hand, during the quick walk task, the CoP tracking criterion contribution will decrease while the CoM jerk increases for 3 out of 4 subjects. During the quick walk task for S5, our algorithm found that the combination consisting in half of the CoM jerk criterion and of the CoP tracking one can be a good candidate for this subject.

and for the parkinsonian subjects (see Table 5.4 for the normal and the quick walk before L-dopa treatment and Table 5.5 for the normal and the quick walk after Ldopa treatment):

- for S1 and S2 the algorithm found that the CoM jerk criterion can explain the observed trajectories in all 4 cases, i.e. the normal walk and the quick walk before L-dopa treatment and after L-dopa treatment. To simplify, we denote the normal walk before L-dopa treatment with NWBL, the quick walk before L-dopa treatment with QWBL, the normal walk after L-dopa treatment with NWAL, and the quick walk after L-dopa treatment with QWAL.
- NWBL case: for S3 and S4 it was found that the combination between the CoM jerk and CoP tracking criteria is considered to be a good candidate, while in the case of S5 the algorithm returned only the CoM jerk.
- NWAL case: for S3 it was found that the combination between the CoM jerk and CoP tracking criteria is considered to be a good candidate, while in the case of S4 and S5 the algorithm returned only the com jerk.
- QWBL case: for S3 and S5 it was found that the combination between the CoM jerk and CoP tracking criteria is considered to be a good candidate, while in the case of S4 the algorithm returned only the CoM jerk.
- QWAL case: for S3 it was found that the combination between the CoM jerk and CoP tracking criteria is considered to be a good candidate, while in the case of S4 and S5 the algorithm returned only the CoM jerk.

In the case of the parkinsonian subjects for which a combination between the CoM jerk and CoP tracking criteria was found: such as S3 and S4, a change between the NWBL and QWBL cases can be seen, meaning that the CoP tracking contribution is decreasing

for both subjects. The same behavior can be observed in the case of S3 and S5 for the NWAL and QWAL cases, in the case of S3 ,S4 and S5 for the NWBL and NWAL cases and also in the case of S3 and S5 for the QWBL and QWAL cases.

The inverse approximately optimal approach results can naturally provide a single criterion (the S4 and S6 non-parkinsonian subjects and the S1 and S2 parkinsonian subjects) or a composite one (for the other subjects) that can be considered as candidates to the walking gait initialization task.

The obtained residuals norm values are very small and this can suggest that the selected basis of criteria is sufficient to explain the studied task. We should mention the fact that the direct optimal control program used in the estimation of the step length, CoP and CoM trajectories considers the step duration as a known value and equal for all the steps. A way of improving the RMSE values is considered to be a future research study, by taking into account the step duration as an optimization variable to the direct optimal control problem. This means that the step duration will be refined through the optimization problem and not chosen in advanced.

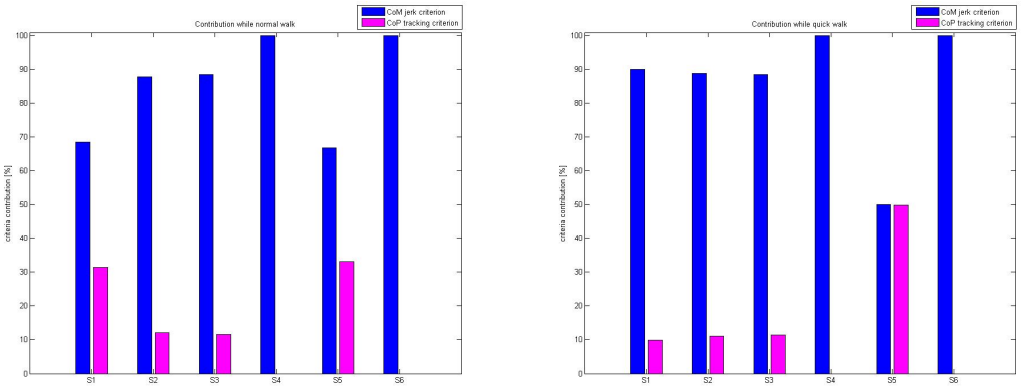

(a) (b)

FIGURE 5.5: The contribution found for the 6 non parkinsonian subjects during the normal walk (a) and during the quick walk (b). The blue bars correspond to the com jerk criterion while the magenta ones correspond to the cop tracking criterion.

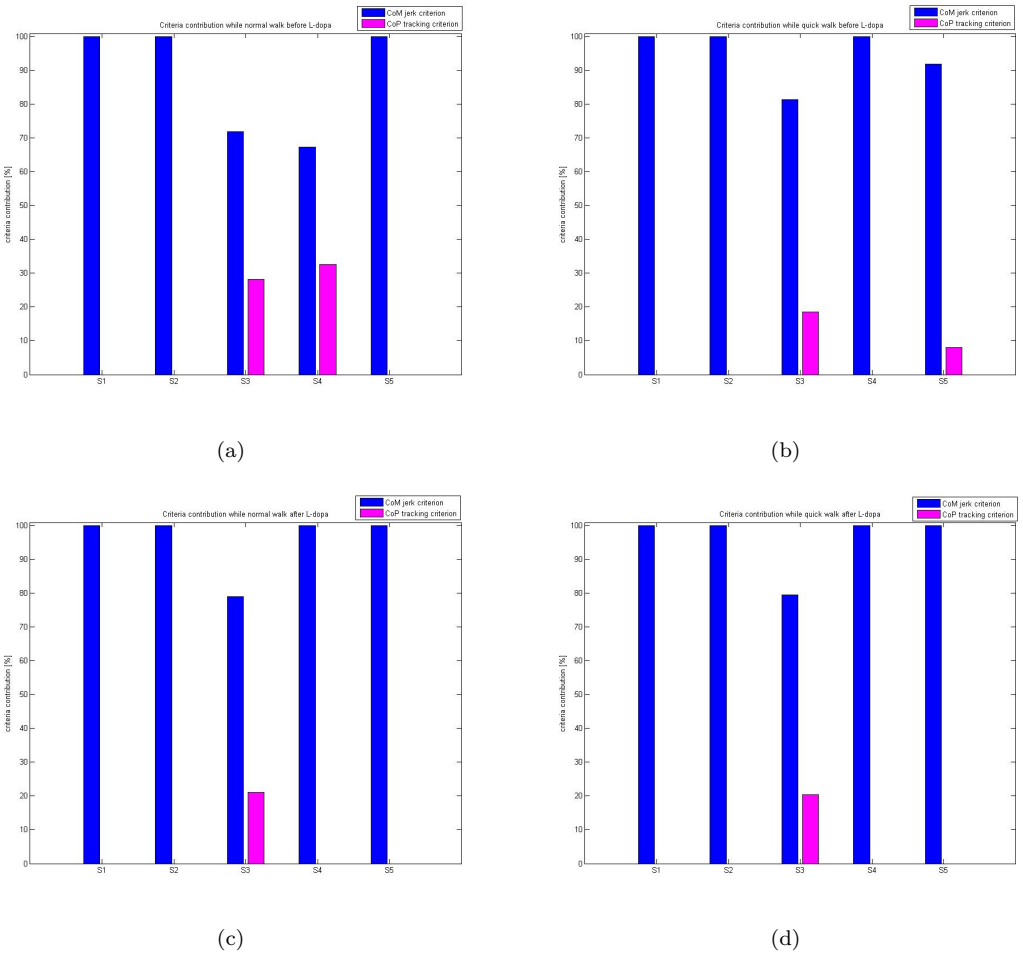

(a) (b)

(c) (d)

FIGURE 5.6: The contribution found for the 5 parkinsonian subjects during the normal walk before L-dopa treatment (a), the quick walk before L-dopa treatment (b), the normal walk after L-dopa treatment (c) and the quick walk after L-dopa treatment (d). The blue bars correspond to the com jerk criterion while the magenta ones correspond to the cop tracking criterion.

TABLE 5.3: The results obtained by our algorithm for the 6 non-parkinsonian subjects during the normal and the quick walk

normal walk							
Subject nb	i^*	contribution [%]		γ	$\frac{1}{n}\|\nabla L(\hat{c})\|$	RMSE [m]	
		f_1	f_4			com	cop
S_1	1	68.59	31.41	-	$5e^{-04}$	0.02	0.07
	4	0.07	99.93		2.8	0.06	0.09
S_2	1	87.82	13.18	+	$4e^{-04}$	0.02	0.06
	4	0.07	99.93		1.1	0.03	0.07
S_3	1	88.46	11.54	+	$4e^{-04}$	0.03	0.05
	4	0.07	99.93		1	0.04	0.06
S_4	1	100	0	+	$4e^{-04}$	0.09	0.11
	4	0.07	99.93		1.1	0.10	0.12
S_5	1	66.79	33.21	+	$5e^{-04}$	0.02	0.07
	4	50.13	49.87		1.9	0.05	0.12
S_6	1	100	0	+	$3e^{-04}$	0.03	0.07
	4	0	100		1.4	0.09	0.12
quick walk							
Subject nb	i^*	contribution [%]		γ	$\frac{1}{n}\|\nabla L(\hat{c})\|$	RMSE [m]	
		f_1	f_4			com	cop
S_1	1	90.08	9.92	-	$8e^{-04}$	0.04	0.11
	4	0.07	99.93		2.1	0.08	0.13
S_2	1	88.86	11.14	-	$6e^{-04}$	0.03	0.09
	4	0.1	99.99		3.3	0.08	0.12
S_3	1	88.49	11.51	-	$6e^{-04}$	0.03	0.09
	4	0.02	99.98		3.4	0.10	0.15
S_4	1	100	0	+	$5e^{-04}$	0.04	0.10
	4	0	100		2.5	0.06	0.12
S_5	1	50.13	49.87	-	$5e^{-04}$	0.03	0.10
	4	0.09	99.91		1.3	0.04	0.11
S_6	1	100	0	+	$4e^{-04}$	0.03	0.07
	4	0	100		1.8	0.05	0.09

TABLE 5.4: The results obtained by our algorithm for the 5 parkinsonian subjects during the normal walk before and after the L-dopa treatment

normal walk before L-dopa							
Subject nb	i^*	contribution [%]		γ	$\frac{1}{n}\|\nabla L(\hat{c})\|$	RMSE [m]	
		f_1	f_4			com	cop
S_1	1	100	0	+	$4.9e^{-04}$	0.02	0.05
	4	0	100		1.4	0.04	0.07
S_2	1	100	0	+	$3e^{-04}$	0.09	0.08
	4	0	100		1.3	0.10	0.11
S_3	1	71.85	28.15	+	$5e^{-04}$	0.01	0.06
	4	0.2	99.98		1	0.03	0.07
S_4	1	67.4	32.6	+	$3e^{-04}$	0.03	0.08
	4	0.02	99.98		3.3	0.05	0.09
S_5	1	100	0	+	$4e^{-04}$	0.04	0.06
	4	0	100		1	0.05	0.07
normal walk after L-dopa							
Subject nb	i^*	contribution [%]		γ	$\frac{1}{n}\|\nabla L(\hat{c})\|$	RMSE [m]	
		f_1	f_4			com	cop
S_1	1	100	0	+	$9e^{-04}$	0.006	0.06
	4	0	100		3.2	0.06	0.09
S_2	1	100	0	+	$4e^{-04}$	0.03	0.07
	4	0	100		1.8	0.04	0.09
S_3	1	78.98	21.02	+	$6e^{-04}$	0.03	0.08
	4	0.2	99.98		1.2	0.05	0.09
S_4	1	100	0	+	$7e^{-04}$	0.01	0.04
	4	0	100		2.7	0.04	0.07
S_5	1	100	0	+	$5e^{-04}$	0.08	0.12
	4	0	100		1.8	0.09	0.13

TABLE 5.5: The results obtained by our algorithm for the 5 parkinsonian subjects during the quick walk before and after the L-dopa treatment

quick walk before L-dopa							
Subject nb	i^*	contribution [%]		γ	$\frac{1}{n}\|\nabla L(\hat{c})\|$	RMSE [m]	
		f_1	f_4			com	cop
S_1	1	100	0	+	$9.4e^{-04}$	0.007	0.07
	4	0	100		2.5	0.04	0.09
S_2	1	100	0	+	$4e^{-04}$	0.05	0.09
	4	0	100		0.9	0.06	0.10
S_3	1	79.57	20.43	+	$7e^{-04}$	0.02	0.07
	4	0.2	99.98		1.3	0.07	0.09
S_4	1	100	0	+	$3e^{-04}$	0.10	0.12
	4	0	100		0.4	0.11	0.14
S_5	1	100	0	+	$5.7e^{-04}$	0.04	0.08
	4	0	100		1.9	0.06	0.10
quick walk after L-dopa							
Subject nb	i^*	contribution [%]		γ	$\frac{1}{n}\|\nabla L(\hat{c})\|$	RMSE [m]	
		f_1	f_4			com	cop
S_1	1	100	0	+	0.001	0.02	0.07
	4	0	100		4	0.06	0.09
S_2	1	100	0	+	$5.3e^{-04}$	0.03	0.06
	4	0	100		1.5	0.04	0.08
S_3	1	81.49	18.51	+	$7.6e^{-04}$	0.03	0.09
	4	0.1	99.99		1.3	0.07	0.10
S_4	1	100	0	+	$5.6e^{-04}$	0.01	0.04
	4	0	100		2.1	0.04	0.06
S_5	1	92	8	-	$5.3e^{-04}$	0.04	0.09
	4	0.03	99.97		2.5	0.06	0.07

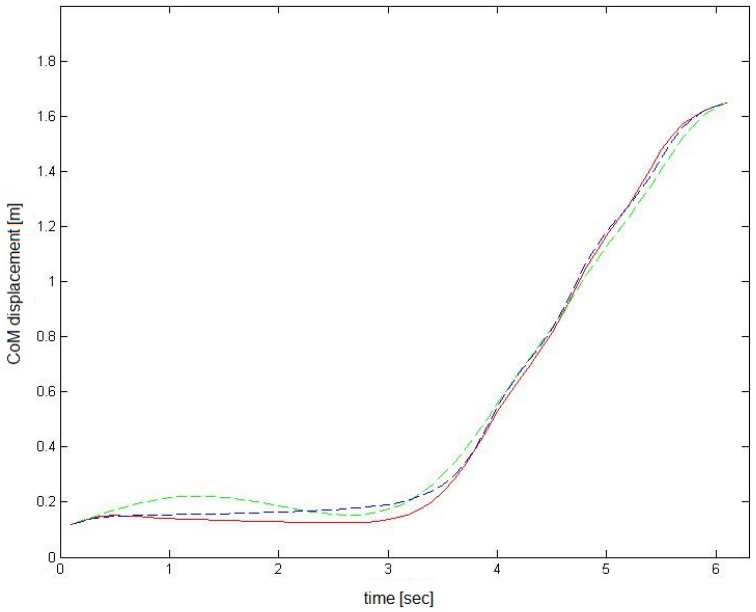

(a) The com representation for the cases when the com jerk criterion is chosen as pivot (the green dotted trajectory) and when the cop tracking criterion is chosen as pivot (the blue dotted trajectory)

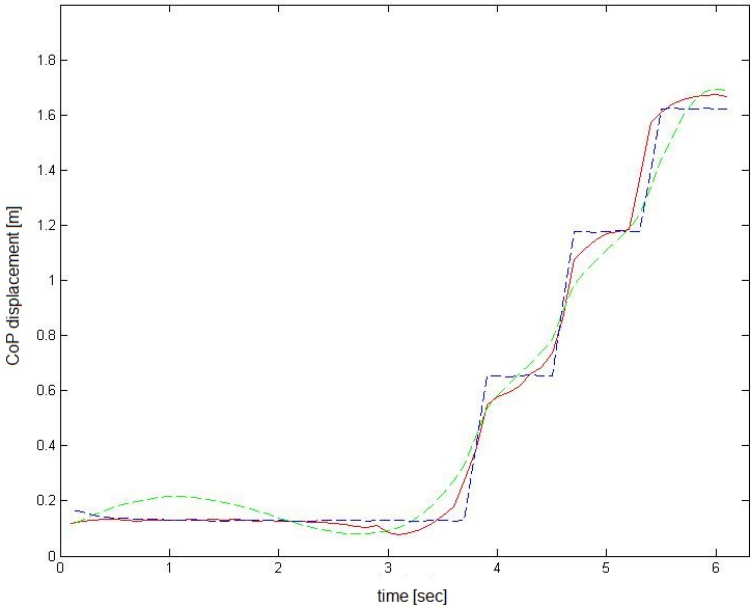

(b) The cop representation for the cases when the com jerk criterion is chosen as pivot (the green dotted trajectory) and when the cop tracking criterion is chosen as pivot (the blue dotted trajectory)

FIGURE 5.7: The com (a) and the cop (b) estimated by the direct optimal control problem for the results obtained by our algorithm with the observed com and cop trajectories (the red trajectory in the com (a) and cop (b) representation)

5.5 Summary

In this chapter, we propose a pilot study for the human walking gait initialization task for 6 non-parkinsonian subjects and 5 parkinsonian ones. We applied our algorithm to one trial per subject and it found as a good candidate one criterion or a combination between two criteria: CoM jerk and CoP tracking criteria. Further investigations on this matter will be the subject of future work and we will describe our intentions in the chapter dedicated to the perspectives of this thesis.

To summarize, in this chapter as in the previous ones, the inverse approximately optimal control approach presents a significant advantage due to its computational time (testing one subject one trial takes less then 85s for solving the inverse optimal control and a forward optimal control one).

Chapter 6

The inverse optimal control in a bounded-error framework

Due to the barely known nature of the errors and uncertainties acting on the system and observations while trying to estimate unknown criteria that can explain the observations, in this chapter we aim at working into a bounded-error framework [130]. The bounded error framework approach was widely used and studied over the years. It has been applied to state and parameters estimation for nonlinear discrete time systems ([130] and reference there in), continuous-time systems [131, 132] or to show how to deal with the presence of uncertainty in the model and data, located within prior intervals [133].

In this chapter, we introduce our bounded-error approach to solve inverse optimization problems. We validate this approach in simulation by using the discretized unicycle robot type model to generate uniformly distributed noisy data.

6.1 Problem formulation

The approximately optimal framework, presented in Chapter 2, assumes that the human motor is an imperfect optimal control process, while all the imperfections resides in the observation. To the contrary, in our new appoach we assume that the human motor control is a perfect optimal control process and we will explicitly consider noise and disturbance on the observations or any modeling error and only assume that the errors are bounded with known bounds, otherwise unknown. As it can be seen in fig. 6.1(b), all trajectories passing through the feasible tube of optimal measurements will be solution to our problem.

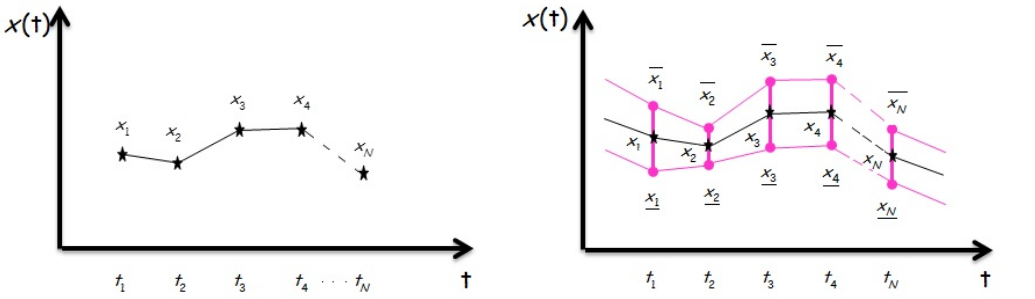

(a) Optimal measurements (b) Feasible domain/tube of optimal measurements

FIGURE 6.1: Example of unbounded optimal measurements 6.1(a) and feasible domain/tube of optimal measurements 6.1(b)

In the sequel, we assume that the actual optimal variables are measured with bounded uncertainties, i.e. the optimal variables x^* are not exactly known but merely contained in a bounded set with known bounds. Here, we consider simple bounds on vector x^* components, i.e. bounded intervals $[x^*] = [\underline{x}^*, \overline{x}^*]$, where $\underline{x}^*$ denotes the lower bounds of variable x^* and $\overline{x}^*$ the upper bounds. Therefore we are trying to find the feasible set of the objective functions that can explain all the measurements from the feasible tube (see Fig. 6.1(b)).

We use the bounded-error framework to find the feasible set of objective function weights vector $c \in \Re_+^k$ and the dual variables $\lambda \in \Re_+^{m_2}$ and $\nu \in \Re^{m_1}$ solutions such as:

$$\mathbb{S} = \{c \times \lambda \times \nu \times x^* \in \Re_+^k \times \Re_+^{m_2} \times \Re^{m_1} \times [x^*] \text{ s.t. } \text{Eq.}(2.13)\} \quad (6.1)$$

Because of the large number of unknown variables $\mathbb{S} \in \Re^{k \times m_1 \times m_2}$ and for a better understanding of our approach, we will consider below the case $\mathbb{S} \in \Re^3$. This enables us to represent better an outline goal for our method.

Let's suppose we are looking to find the set of feasible solutions:

$$\mathbb{S} = \{c \times \nu \in \Re_+^2 \times \Re^1 \text{ s.t. Property}\} \subset \Re^3, \quad (6.2)$$

composed of the objective function's weight $c \in \Re_+^2$ and the Lagrange multiplier $\nu \in \Re^1$.

As it can be seen in Fig. 6.2, the set $\mathbb{S}$ of feasible solutions is difficult to be characterized, due to its unknown complicated shape. Therefore, we'll reduce our problem by searching only the projection of the feasible set of solutions on the subspace created by

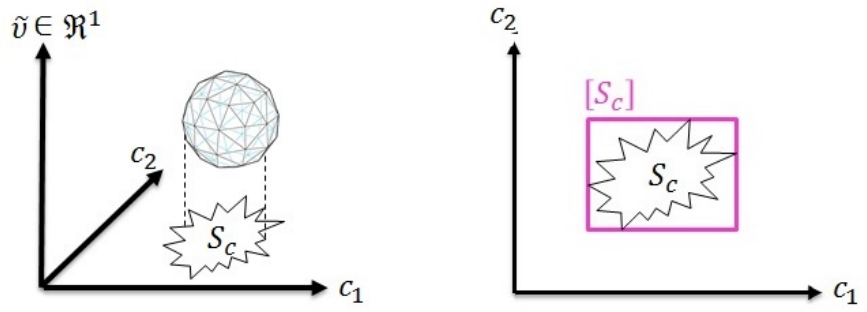

FIGURE 6.2: Fig on the left side: Geometric representation of the $\mathbb{S}$ set of feasible solutions with three unknown variables; Fig on the right side: The set of feasible solutions projected onto the objective function's weight subspace

the parameters of interest c_1 and c_2, i.e objective function's weight:

$$\mathbb{S}_c = \text{proj}_{\vec{c}}(\mathbb{S}) = \{c \in \Re^2_+, \text{ s.t. } \exists \nu \in \Re^1 \text{and Property}\} \in \Re^2 \tag{6.3}$$

Still, the set of feasible solution is not something that can be found easily, but we known how to obtain the smallest box over approximating the solution set, i.e. the convex hull of the set of feasible objective function's weight solutions $[\mathbb{S}_c]$ (represented by the pink box in fig.6.2). And we have the certainty that it contains the set of feasible solutions:

$$\mathbb{S}_c \subseteq [\mathbb{S}_c] = \left[\underline{c_1}, \overline{c_1}\right] \times \left[\underline{c_2}, \overline{c_2}\right] \tag{6.4}$$

The convex hull of the set of solutions is composed of the Cartesian product of $\left[\underline{c_1}, \overline{c_1}\right]$ and $\left[\underline{c_2}, \overline{c_2}\right]$ bounded intervals.

Following the example presented above we'll use the same concept for the case where $\mathbb{S} \in \Re^{k+m_2+m_1}$. Because we are only mainly interested in imputing the weight vector $c \in \Re^k$ the inverse optimization boils down to computing the convex hull approximation of the set of objective function's weight solutions:

$$[\mathbb{S}_c] = \left[\underline{c_1}, \overline{c_1}\right] \times \left[\underline{c_2}, \overline{c_2}\right] \times \ldots \times \left[\underline{c_k}, \overline{c_k}\right], \tag{6.5}$$

where the bounds are computed component-wise [130] as follows.

The constraints that need to be considered while searching the lower and upper bounds consist in satisfying the KKT conditions, the Lagrange multipliers, associated with the inequality constraints, need to be positive as well as the weight vector c, while the

measurements are within a bounded set and are grouped as following:

$$\begin{cases} \lambda_i \geq 0, \quad i = 1, \ldots, m_2 \\ c_i \geq 0, \quad i = 1, \ldots, k \\ x \geq \underline{x}_i^*, \quad i = 1, \ldots, n \\ x \leq \overline{x}_i^*, \quad i = 1, \ldots, n \\ r_s(c, \lambda, \nu, x^*) = 0 \\ \forall i \in \{1, \ldots, m_2\}\, r_{c,i}(\lambda, x^*) = 0 \end{cases} \tag{6.6}$$

The lower bounds of the objective function's weights are obtained by solving k constrained minimization problems, whereas the upper bounds ones are obtained by solving k constrained maximization problems [130][pg. 111]:

$$\begin{gathered} \forall j = 1 \ldots k, \\ \underline{c}_j \leftarrow \min_{c,\lambda,\nu,x} \; c_j \qquad\qquad \overline{c}_j \leftarrow \max_{c,\lambda,\nu,x} \; c_j \\ \text{subject to eq.(6.6)} \qquad\qquad \text{subject to eq.(6.6)} \end{gathered} \tag{6.7}$$

Both lower and upper bounds of the objective function's weight are used to obtain the convex hull approximation of the set of objective function's weight solutions. These can be obtained by taking the Cartesian product of the weight bounded intervals. Also, the feasible set of objective function's weight solutions $\mathbb{S}_c$ is within the determined convex hull:

$$\mathbb{S}_c \subseteq [\mathbb{S}_c] = [\underline{c}_1, \overline{c}_1] \times [\underline{c}_2, \overline{c}_2] \times \ldots \times [\underline{c}_j, \overline{c}_j] \tag{6.8}$$

6.2 Application on simulated data

We consider, as in the previous chapter, the discrete model of the unicycle robot type

$$\begin{cases} x_{i+1} = x_i + \tau u_{1,i} \cos\theta_i \\ y_{i+1} = y_i + \tau u_{1,i} \sin\theta_i \\ \theta_{i+1} = \theta_i + \tau u_{2,i} \\ \zeta_0 = \zeta_{start} \\ \zeta_{N-1} = \zeta_{target} \end{cases} \tag{6.9}$$

where τ is the sampling rate and $i = 0 : N-1$ is the time step, (x, y) the position, θ the orientation and u_1, u_2 the forward (linear) speed and angular speed respectively and $\zeta = \begin{bmatrix} x & y & \theta & u_1 & u_2 \end{bmatrix}^T$.

The optimal artificial trajectories are generated by solving an equality constrained optimization problem:

$$\begin{aligned} \underset{\zeta}{\text{minimize}} \quad & \frac{1}{2}\tau \sum_{k=1}^{n} c^T \chi_n(\zeta) \\ \text{subject to} \quad & eq(6.9) \end{aligned} \tag{6.10}$$

where $c \in \Re^{n\times 1}$ is the criteria's weight vector, χ contains the pre-selected criteria and n is the number of the chosen basis criteria to be minimized.

6.2.1 The three criteria case

We apply the bounded-error approach to estimate the weight of three criteria: the linear velocity and the orientation respectively, where the angular velocities one is used as pivot (its weight will be equal to 1.). Firstly, we generate data solving problem (6.10), where the known basis criteria are

$$\chi(\zeta) = \begin{bmatrix} \|u_2\|^2 \\ \|u_1\|^2 \\ \|\theta\|^2 \end{bmatrix}, \tag{6.11}$$

where $c = [1\ 5\ 1.5]^T \in \Re^3$.

Secondly, an uniformly distributed noise is added to the generated optimal trajectories as follows: $\pm 0.4\%$ of error to the positions and linear velocity and $\pm 0.2\%$ of error on orientation and angular velocity, $\pm 1\%$ of error to the positions and linear velocity and $\pm 0.5\%$ of error on orientation and angular velocity, $\pm 1.8\%$ of error to the positions and linear velocity and $\pm 0.9\%$ of error on orientation and angular velocity and we finish by adding $\pm 3\%$ of error to the positions and linear velocity and $\pm 1.5\%$ of error on orientation and angular velocity, as presented in table 6.1 and represented in fig. 6.3.

We define the KKT conditions

$$\begin{aligned} & h_j(\zeta) = 0 \ j = 1, \ldots, 3N \\ & \nabla_\zeta \|u_2\|^2 + c_1 \nabla_\zeta \|u_1\|^2 + c_2 \nabla_\zeta \|\theta\|^2 + \textstyle\sum_{j=1}^{3N} \nu_j \nabla_\zeta h_j(\zeta) = 0 \end{aligned} \tag{6.12}$$

associated with the forward optimal control problem (6.10) that minimized the criteria from eq.(6.11), used to generate the optimal trajectory.

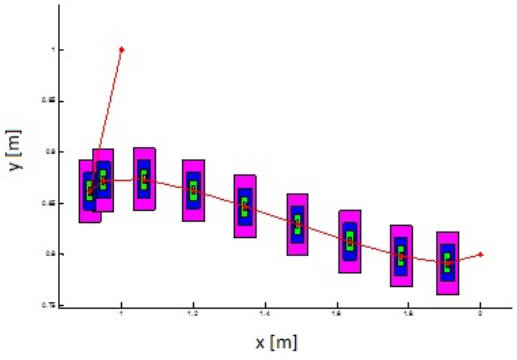

TABLE 6.1: The uniformly distributed noise with four different values for the p variance

Case	Noise added to x,y and u_1 $\times 0.01$	Noise added to θ and u_2 $\times 0.01$
1	± 0.4	± 0.2
2	± 1	± 0.5
3	± 1.8	± 0.9
4	± 3	± 1.5

FIGURE 6.3: Trajectory obtained for $c_1 = 5$ et $c_2 = 1,5$ using the unicycle model (red line) with four different noisy trajectories. Uniformly distributed noise is added to the obtained trajectory as described previously and presented in Table 6.1. The first case is represented by the cyan boxes, the second one by the green boxes, the third one by the blue boxes and the final one by the magenta boxes.

Then the convex hull of the set of feasible objective function's weight solutions is:

$$[\mathbb{S}_c] = [\underline{c}_1, \overline{c}_1] \times [\underline{c}_2, \overline{c}_2] \tag{6.13}$$

where the c_1, c_2 upper and lower bounds are obtained by solving four optimization problems:

$$\begin{array}{cccc}
\underline{c}_1 \leftarrow \min\limits_{z} \ c_1 & \overline{c}_1 \leftarrow \max\limits_{z} \ c_1 & \underline{c}_2 \leftarrow \min\limits_{z} \ c_2 & \overline{c}_2 \leftarrow \max\limits_{z} \ c_2 \\
\text{s.t. } eq.(6.12) & \text{s.t. } eq.(6.12) & \text{s.t. } eq.(6.12) & \text{s.t. } eq.(6.12) \\
c_1 \geq 0 & c_1 \geq 0 & c_1 \geq 0 & c_1 \geq 0 \\
c_2 \geq 0 & c_2 \geq 0 & c_2 \geq 0 & c_2 \geq 0 \\
\zeta^* \in [\zeta^*] & \zeta^* \in [\zeta^*] & \zeta^* \in [\zeta^*] & \zeta^* \in [\zeta^*]
\end{array} \tag{6.14}$$

where $z = [c_1\,, c_2\,, \nu, \zeta]$.

The values obtained for the two criteria's weight are listed in table 6.2, while the smallest box approximation of the objective function's weight solutions are represented in Fig. 6.4. It can be seen that our bounded-error approach returns the true solution within the exhibited convex hull of the set of feasible objective function's weight solutions. Also, while the noise variance increases the obtained convex hull is larger.

Nevertheless, the objective of this chapter is to find the convex hull set of feasible objective function's weight solutions in which we have the certainty that all feasible solutions are included. Fig. 6.5 is presenting a bisection over c_1 parameter that can give a good idea about the set of feasible objective function's weight solutions, represented by the gray colored boxes.

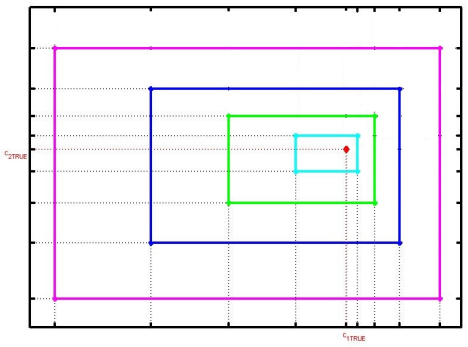

TABLE 6.2: The results obtained with the bounded-error framework approach for the three criteria case

Noise $\times 0.01$	Convex hull of inverse optimal solution $[\mathbf{S}_c] = [\underline{c_1}, \overline{c_1}], [\underline{c_2}, \overline{c_2}]$
Case1	$[\mathbf{S}_c] = [4.6510, 5.0779], [1.4876, 1.5075]$
Case2	$[\mathbf{S}_c] = [4.1809, 5.1995], [1.4698, 1.5187]$
Case3	$[\mathbf{S}_c] = [3.6390, 5.3715], [1.4472, 1.5339]$
Case4	$[\mathbf{S}_c] = [2.9719, 5.6528], [1.4160, 1.5569]$

FIGURE 6.4: The convex hull set of feasible objective function's weight solutions for the four different noisy trajectories, case 1 cyan box, case 2 green one, case 3 blue one and in the last case the magenta one, with the true values for the criteria's weight represented by the red point

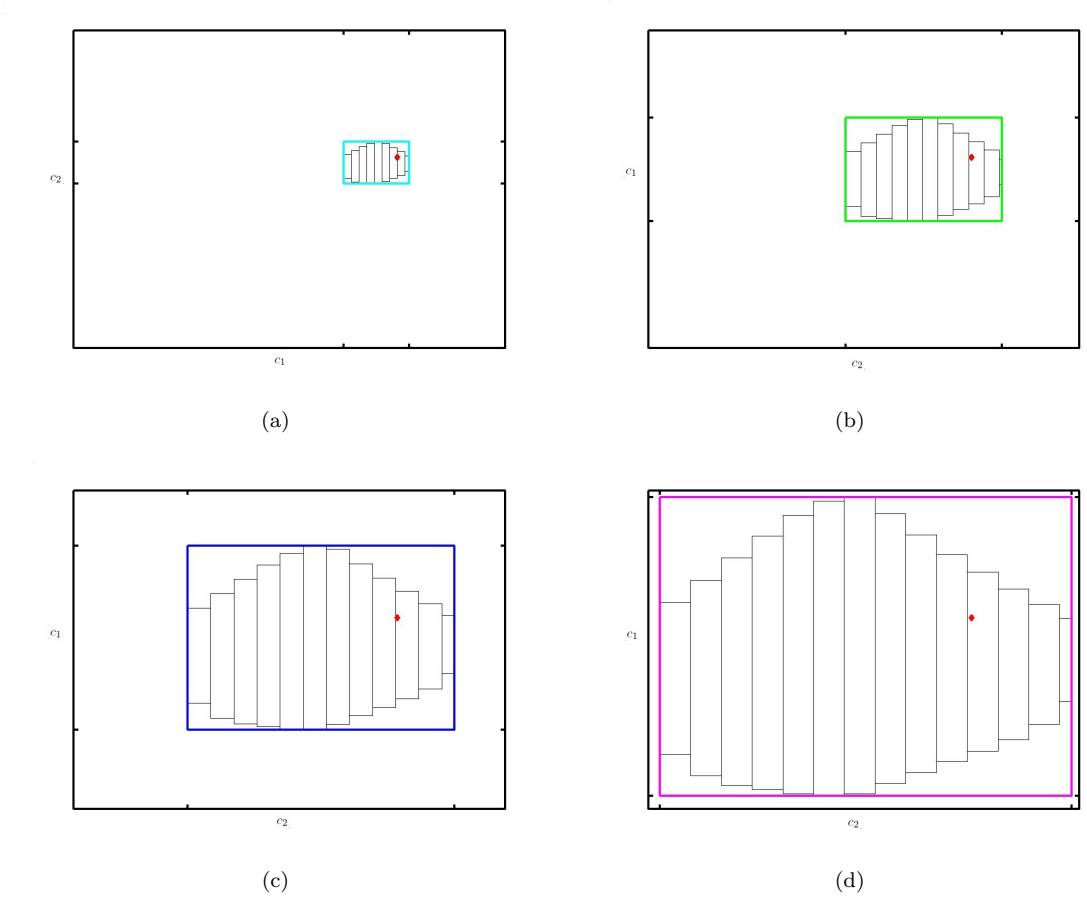

FIGURE 6.5: The convex hull set of objective function's weight solutions for the four different noisy trajectories ((a) case 1, (b) case 2, (c) case 3, (d) case 4) along with the true values for the criteria's weight represented by the red point for the three criteria case; also, the bisection over the c_1 criterion weight represented by the gray boxes for each of the 4 noisy trajectories cases.

We solved 100 forward optimal control problems for each of the four noisy trajectory cases, by selecting random $\{c_1, c_2\}$ values from the obtained set of feasible objective function's weight solutions represented by the gray colored boxes in fig. 6.5. As it can be seen in fig.6.6 the obtained trajectories are passing through the feasible tube/domain of optimal trajectories, representing certain possible solutions to our problem.

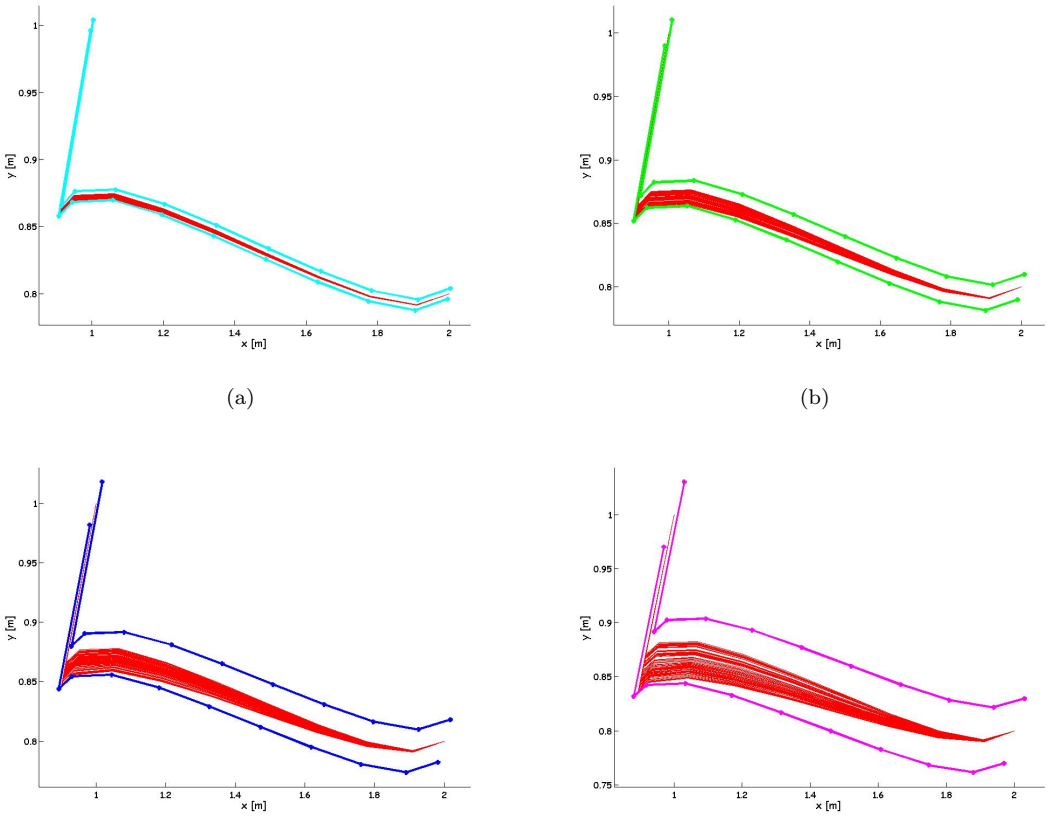

FIGURE 6.6: The trajectories obtained while applying the forward optimal control with 100 random parameter values, for each noisy trajectory case, from the set of feasible solution represented by the red trajectories for the three criteria case.

6.2.2 The four criteria case

In this subsection, we apply the bounded error approach to estimate the weight of four criteria: the linear velocity, the robots orientation and the squared error between orientation and direction to the goal, respectively, where the angular velocities one is chosen as pivot (its weight will be equal to 1). Firstly, we generate data solving problem (6.10) where the known basis criteria are

$$\chi(\zeta) = \begin{bmatrix} \|u_2\|^2 \\ \|u_1\|^2 \\ \|\theta\|^2 \\ \|\varphi(\zeta, \zeta_{target})\|^2 \end{bmatrix} \tag{6.15}$$

where $c = [1\ 1.8508\ 42.0533\ 0.6590]^T \in \Re^4$, N is the number of samples and $\varphi(\zeta, \zeta_{target})$ is the squared error between orientation and direction to the goal:

$$\varphi(\zeta_i, \zeta_{targeti}) = \arctan(\frac{y_{targeti} - y_i}{x_{targeti} - x_i}) - \theta_i \quad i = 0 : N-1$$

Secondly, an uniformly distributed noise is added to the generated optimal trajectories as follows: $\pm 0.4\%$ of error to the positions and linear velocity and $\pm 0.2\%$ of error on orientation and angular velocity, $\pm 1\%$ of error to the positions and linear velocity and $\pm 0.5\%$ of error on orientation and angular velocity, $\pm 1.8\%$ of error to the positions and linear velocity and $\pm 0.9\%$ of error on orientation and angular velocity and we finish by adding $\pm 3\%$ of error to the positions and linear velocity and $\pm 1.5\%$ of error on orientation and angular velocity, as presented in table 6.3 and represented in fig. 6.7.

We define the KKT conditions

$$\begin{aligned} &h_j(\zeta) = 0\ j = 1, \ldots, 3N \\ &\nabla_\zeta \|u_2\|^2 + c_1 \nabla_\zeta \|u_1\|^2 + c_2 \nabla_\zeta \|\theta\|^2 + c_3 \nabla_\zeta \|\varphi(\zeta)\|^2 + \textstyle\sum_{j=1}^{3N} \nu_j \nabla_\zeta h_j(\zeta) = 0, \end{aligned} \tag{6.16}$$

associated to the forward optimal control problem (6.10) that minimized the criteria from (6.15), used to generate the optimal trajectory.

Then the convex hull of the set of feasible objective function's weight solutions is:

$$[\mathbb{S}_c] = [\underline{c}_1, \bar{c}_1] \times [\underline{c}_2, \bar{c}_2] \times [\underline{c}_3, \bar{c}_3] \tag{6.17}$$

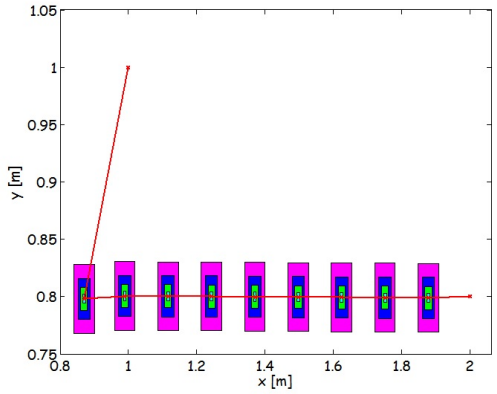

TABLE 6.3: The uniformly distributed noise with four different values for the p variance

Case	Noise added to x,y and u_1 $\times 0.01$	Noise added to θ and u_2 $\times 0.01$
1	± 0.4	± 0.2
2	± 1	± 0.5
3	± 1.8	± 0.9
4	± 3	± 1.5

FIGURE 6.7: Trajectory obtained for $\{c_1, c_2, c_3\} = \{1.8508, 42.0533, 0.6590\}$ using the unicycle model (red trajectory) with four different noisy trajectories. Uniformly distributed noise is added to the obtained trajectory as described previously and presented in Table 6.3. The first case is represented by the cyan boxes, the second one by the green boxes, the third one by the blue boxes and the final one by the magenta boxes.

where the c_1, c_2, c_3 lower and upper bounds are obtained by solving six optimization problems:

$$\begin{array}{ccc}
\underline{c}_1 \leftarrow \min\limits_{z} \; c_1 & \underline{c}_2 \leftarrow \min\limits_{z} \; c_2 & \underline{c}_2 \leftarrow \min\limits_{z} \; c_3 \\
\text{s.t. } eq.(6.16) & \text{s.t. } eq.(6.16) & \text{s.t. } eq.(6.16) \\
c_i \geq 0 \,, i = 1,2,3 & c_i \geq 0 \,, i = 1,2,3 & c_i \geq 0 \,, i = 1,2,3 \\
\zeta^* \in [\zeta^*] & \zeta^* \in [\zeta^*] & \zeta^* \in [\zeta^*] \\
\overline{c}_1 \leftarrow \max\limits_{z} \; c_1 & \overline{c}_2 \leftarrow \max\limits_{z} \; c_2 & \overline{c}_3 \leftarrow \max\limits_{z} \; c_3 \\
\text{s.t. } eq.(6.16) & \text{s.t. } eq.(6.16) & \text{s.t. } eq.(6.16) \\
c_i \geq 0 \,, i = 1,2,3 & c_i \geq 0 \,, i = 1,2,3 & c_i \geq 0 \,, i = 1,2,3 \\
\zeta^* \in [\zeta^*] & \zeta^* \in [\zeta^*] & \zeta^* \in [\zeta^*]
\end{array} \tag{6.18}$$

where $z = [c_1 \,, c_2 \,, c_3 \,, \nu, \, \zeta]$.

TABLE 6.4: The results obtained with the bounded-error framework approach for the four criteria case

Noise $\times 0.01$	Convex hull of inverse optimal solution $[\mathbf{S}_c] = [\underline{c_1}, \overline{c_1}] \times [\underline{c_2}, \overline{c_2}] \times [\underline{c_3}, \overline{c_3}]$
Case1	$[\mathbf{S}_c] = [0.0026, 1.8923] \times [41.5961, 42.8394] \times [1.5959e^{-08}, 0.9254]$
Case2	$[\mathbf{S}_c] = [0.0016, 1.9579] \times [41.4327, 42.9719] \times [1.9987e^{-08}, 0.9601]$
Case3	$[\mathbf{S}_c] = [0.0059, 2.0522] \times [41.2184, 43.1503] \times [3.9545e^{-07}, 1.0059]$
Case4	$[\mathbf{S}_c] = [0.0051, 2.2105] \times [40.9046, 43.4220] \times [1.9989e^{-08}, 1.0736]$

The values obtained for the three criteria's weight are reported in table 6.4, while the set of feasible objective function's weight solutions are represented in Fig. 6.8. It can

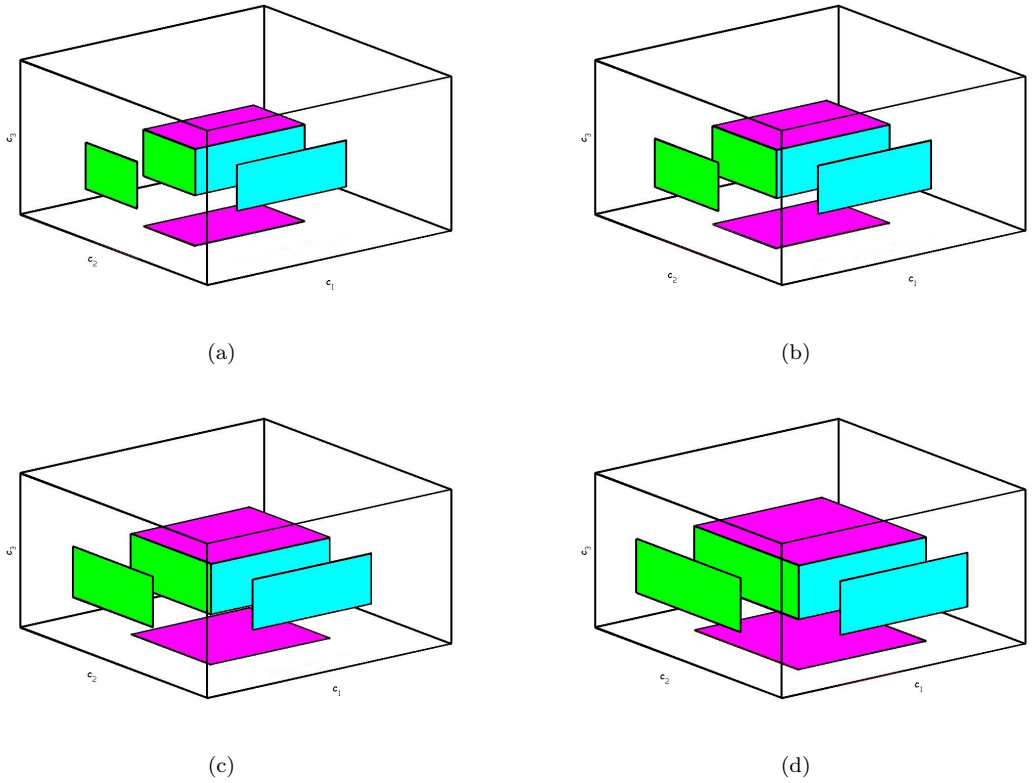

FIGURE 6.8: The computed convex hull set of feasible objective function's weight solutions for the four different noisy trajectories projected on the three criteria's weight subspace along with the true value for the criteria weight represented by the red point, for the case with four criteria

be seen that our bounded error approach returns the true solution within the exhibited convex hull of the set of feasible objective function's weight solutions. Also, while the noise variance increases also the obtained convex hull are larger. We solved 100 forward optimal control problems for each of the four noisy trajectory cases, by selecting random $\{c_1, c_2, c_3\}$ values from the obtained convex hull set of feasible objective function's weight solutions in fig. 6.8. As it can be seen in fig.6.9 the obtained trajectories are passing through the feasible tube/domain of optimal trajectories, representing certain possible solutions to our problem.

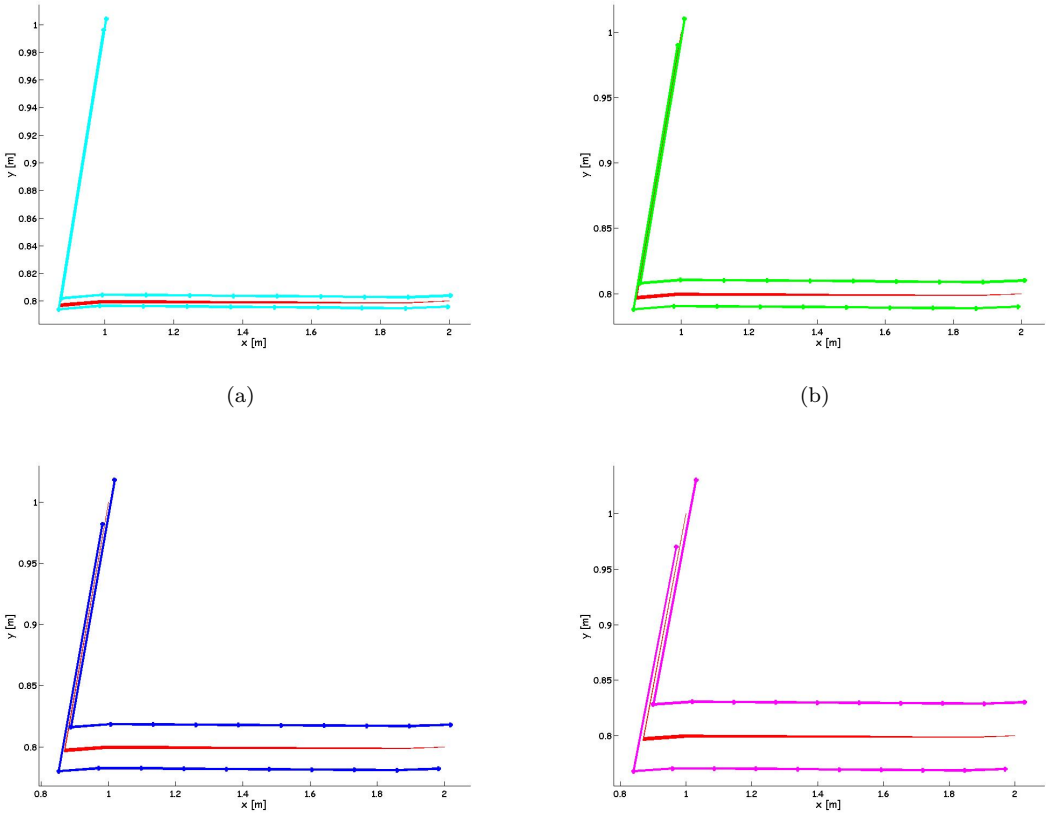

FIGURE 6.9: The trajectories obtained while applying the forward optimal control with 100 random parameter values, for each noisy trajectory case, from the set of feasible solution represented by the red trajectories for the four criteria case.

6.2.3 The guarantee of the computed convex hull set

By applying our method, we simplify the initial problem to a constraint programming one, where KKT constraints need to be satisfied, Lagrange multiplier and criteria's weight are required positive and measurements, placed within a bounded set are stated in the form of constraints. All these constraints are taken into account when minimizing and maximizing the criteria's weight in order to obtain the convex hull set of feasible objective function's weight.

In this section we will numerically guarantee that the computed convex hull set of feasible objective function's weight i.e. $[\mathbf{S}_c]$ is the interval hull i.e. the smallest box that contains the set of feasible objective function's weight. This can be done by using interval arithmetic and contractors programming [130].

All the known tools (e.g. IBEX) that solve this kind of problems are usually used when dealing with small scale problems. The core algorithm of these tools automatically does the following steps: verify if the solution is within the initially selected interval and that the constraints are satisfied and if this is not the case the algorithm will then do the bisection over the unknown variables. Finally the algorithm yields three pavings or union of boxes:

- an *inner approximation* that is included in the solution set,
- an *uncertainty layer* that contains boxes that may contain solutions and
- the *remaining sets* that are proven to contain no solution.

The union of the inner approximation and the uncertainty layer constitutes the *outer approximation.*

A disadvantage of this bisection is the computational time which increases exponentially with the number of unknown variables. Therefore they are not usually employed in solving large scale problems, but they can be efficiently used if the bisection over the unknown variables is not applied. This is our approach to solving out large scale problems, having $\Re^{k+m_1+m_2}$ unknown variables, i.e. we use the known interval analysis tools, without the bisection, to show that the computed convex hull is the smallest box that contains the set of feasible solutions.

There is a possibility for the computed convex hull to encounter two situations, presented in fig. 6.10, as follows:

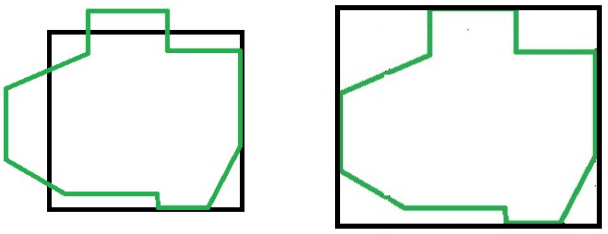

(a) (b)

FIGURE 6.10: The graphical representation of the two possible situations encounter by the convex hull, where the convex hull is represented by the black box and the set of feasible solutions by the green shape: (a) the computed convex hull omitted parts of the set of feasible solutions; (b) the computed set includes all the set of feasible solutions

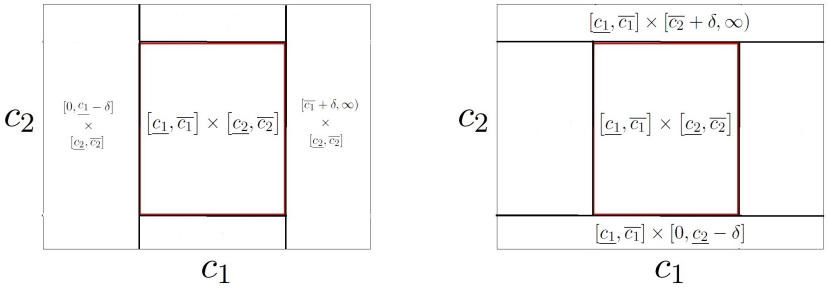

(a) (b)

FIGURE 6.11: The graphical representation of the convex hull and the intervals around it, by adding a small coefficient to the convex hull $\delta = 0.01$: (a) the intervals on the left and on the right of the convex hull; (b)intervals above and below the convex hull

- the computed convex hull omitted parts of the set of feasible solutions (see fig. 6.10(a)).
- the computed set includes all the set of feasible solutions (see fig. 6.10(b)).

At first, we define all intervals which need to be tested. As fig.6.11 shows we test the computed convex hull $[\mathbf{S}_c]$ as well as the intervals around it, where δ has a small value, equal to 0.01 for our cases.

Therefore, by using δ we test the two situations presented above: if the computed convex hull includes or omits some parts of the set of feasible solutions.

First, we define the interval boxes as presented in fig. 6.11, in order to check each of the computed convex hull bounds:

1. Check upper bound of c_1: $\mathbf{Y}_1 = [\overline{c}_1 + \delta, \infty) \times [\underline{c}_2, \overline{c}_2]$.

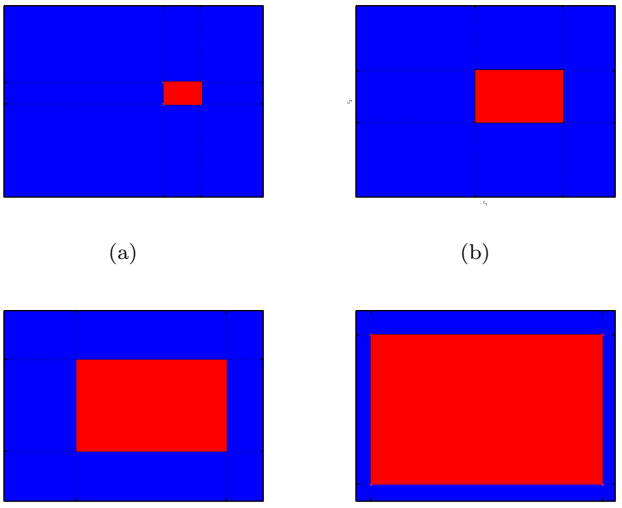

(a) (b)

(c) (d)

FIGURE 6.12: The graphical representation of the results obtained after applying the EASIBEX-MATLAB to the results obtained with our method on the three criteria case: (a) case 1, (b) case 2, (c) case 3, (d) case 4. The blue sets correspond to the remaining set (or sets with no solutions) and the red ones to the inner and the uncertainty sets (or sets with solutions)

2. Check lower bound of c_1: $\mathbf{Y}_2 = [0, \underline{c}_1 - \delta] \times [\underline{c}_2, \overline{c}_2]$.

3. Check upper bound of c_2: $\mathbf{Y}_3 = [\underline{c}_1, \overline{c}_1] \times [\overline{c}_2 + \delta, \infty)$.

4. Check lower bound of c_2: $\mathbf{Y}_4 = [\underline{c}_1, \overline{c}_1] \times [0, \underline{c}_2 - \delta]$.

Second, for each of this five boxes, i.e. the computed convex hull set and the ones around it, we test its intersection with the set of feasible solutions.

Let's consider the case when our algorithm checks the upper bound of c_1 with the associated box $\mathbf{Y}_1 = [\overline{c}_1 + \delta, \infty) \times [\underline{c}_2, \overline{c}_2]$: If the intersection between $\mathbf{Y}_1$ and the set of feasible solutions is empty then there are no solutions in the investigated $\mathbf{Y}_1$ box; otherwise there are still solutions and the initial $\mathbf{Y}_1$ box will increase by doubling the δ's value, i.e. $\mathbf{Y}_1 = [\overline{c}_1 + 2\delta, \infty) \times [\underline{c}_2, \overline{c}_2]$, and the intersection will be repeated until an empty one is obtained. If this is the case, then the computed convex hull encounters the first case presented in fig. 6.12 and stated previously.

The fig 6.12 shows that the convex hull computed with our bounded error inverse optimal control method encounters the second situation, being the smallest approximation at a δ maximum value.

6.3 Summary

The main focus of this chapter was the presentation of a new way of solving the inverse optimal control problem that fosters on ideas developed for approximately inverse optimization. The method deals with errors or uncertainties acting on the observations. This approach was validated using noisy artificial optimal trajectories, generated by solving a direct optimal control problem on an unicycle robot type discrete model and by adding uniformly distributed noise with four different variances. In order to support our approach two cases were considered, where the convex hull set of objective function's weight solutions needed to be found. In both cases one criteria was chosen as pivot (therefore its weight was equal to 1), while the other 2 for the first case and respectively 3 for the second one were estimated. The computed convex hull set of objective function's weight solution was obtained as the Cartesian product between the objective function's weight lower and upper bounds, obtained component-wise by solving k constrained minimization and k constrained maximization problems (where k represents the number of unknown criteria's weight). Finally, we numerically guaranteed that the computed convex hull set is the smallest box that contains the set of objective function's weight solutions.

Chapter 7

Conclusions and Future works

The main focus of this thesis is to address the inverse optimal control problems as they offer us a good opportunity to understand what cost functions are minimized by the human motor control while performing a certain motor control task. In this thesis we assume that the collected experimental observations are in accordance with what the human motor control is planning. This understating can offer new opportunities for the sciences that analyze the human behavior, to bring solutions for people in need as patients with degenerative and locomotion diseases etc. or to obtain humanoid robots with a human-like behavior that can, for example, facilitate the collaboration between human and robots in an industrial environment or in everyday life scenarios.

The inverse optimal control problems can be solved in many ways in literature, as we presented in the related work section, so we prefer to select the approximately inverse optimal control one, that has a nice computation time thus offering the possibility to use it for online applications. This approach assumes that the human motor control, is an imperfect optimal control process, while the observed data is considered perfect. In our study, we proposed an algorithm based on this approach. In the previous studies on the topic, a basis of criteria was proposed for the studied tasks. Even if there is not a prior knowledge of the actual cost functions minimized by the human motor control, they tested a single criterion as a pivot. We propose the basis of criteria that has been already analyzed in literature for the studied tasks, and we went further by testing each criterion to be a pivot in solving the problem. This means that by testing each criterion we do not tamper with the results, allowing the algorithm to find the best candidates that exhibit small residuals norm values and better fit the experimental data. Our proposed algorithm for the inverse optimal control problems was addressed in three human motion examples: human arm movement from an initial point to a final one, represented by screwing tasks in an industrial environment, a cyclic human

movement consisting in visually tracking a target with the head and the human walking gait initialization task for non parkinsonian and parkinsonian subjects.

For the first example, the algorithm obtained two classes of possible criteria. Also we have observed that any combination between these two classes of criteria can be a good choice to explain the collected experimental data for this task. In the second example it was found that any criterion from the selected basis of criteria can be a good candidate for explaining the experimental data. For this task we proposed a closed loop modeling with a gain synthesis method for artificial data. The last example was a pilot study conducted for the non parkinsonian during normal and quick walk and for the parkinsonian subjects during the normal and quick walk before and after the L-dopa treatment. As a first result, the algorithm presented different combination of proposed criteria as possible candidates to explain the variability found in the experimental data.

While applying this method we came upon a new approach of solving the inverse optimal control problem when dealing with errors and uncertainties acting on the system and observations, where the errors are bounded with known bounds, otherwise unknown. In this approach we assume that the human motor control is a perfect optimal control process, while all imperfection resides in the observations. Our method returns the convex hull set of feasible cost functions solutions and we have the certainty that the true solution is within the obtained set.

In the perspective of our future works we have many opportunities and avenues to follow:

- First of all, the new inverse optimal control approach in a bounded error framework can be addressed for the human motions studied in this thesis, but also for new human motion tasks. By doing so we can get an idea about how the human motor control works for a multitude of tasks thus having uncertainty domains of cost functions that can be minimized by it.

- Our inverse approximately optimal control (IAOC) algorithm presented a significant reduction in computation time, for all the presented examples, and it can be applied to clinical studies involving a large number of patients as well as for ergonomic studies in an industrial environment.

- We can extend the pilot study for the human walking gait initialization task, by analyzing it with a hybrid inverse optimal control problem. The literature offers us an approximately optimal control problem for hybrid dynamical systems, addressed on the ParkourBot biped robot [52]. Also, [5] proposed an inverse parametric bi-level optimization with an application to hybrid system control. A new

perspective in solving this matter consists in the use of a bounded error framework for addressing the hybrid inverse optimal control problem to the experimental data.

- Another perspective of the use of the inverse optimal control is to obtain models for human tasks and after to control lower limb prosthetic devices by using impedance control, as in [134] for helping amputee patients, or people with locomotion diseases.

- Nowadays there is a new trend in the robotic innovation, consisting in technologies such as exoskeletons, which help people walk or makes them able of carrying heavy loads. We can find this kind of technology in healthcare (for example: the Hybrid Assistive Limb (HAL) exoskeleton suitable in walking and carrying heavy loads, that detects bio-signals which appear on the skin surface when the user intents to move and generates required forces for effort compensation, having as flaw the complexity of its control i.e. requires calibration up to two month) or in the military field (for example Berkely Lower Extremily Exeskeleton, for battlefields, that augments the soldiers strength and endurance, permitting them to carry heavy loads during long distances. It works based on two control laws used during the walking cycle: position control for stance leg and sensitivity amplification control for the swing leg).

  The humans wearing these exoskeletons need to control the robotic device and not the other way around. The exoskeleton needs to be capable of following human locomotion, performing the task easily without restricting their natural movements and assuring safety while in contact with the human. Due to the obtained computational time of our IAOC algorithm, for the human tasks studied in this thesis, we can think of future works consisting in developing fast methods for estimating the human behavior by understanding and analyzing online the human movement during physical interaction with the exoskeleton. The online analysis can be done via the approximately or bounded error inverse optimal control and the obtained cost functions can be used to generate input torques for the exoskeleton that ensure natural motions for the one wearing the exoskeleton.

- All the examples of human motion were analyzed in an open loop optimization process. We can consider analyzing the experimental data in a feedback closed loop framework. If we want to do this, a new issue will arise, consisting in questioning what input should be taken to the system? In the study of artificial data, the input was considered to be a sinusoidal wave one, but in reality a more complex state estimation model of sensory integration should be used or maybe one should

estimate the input of the system along with the feedback gains. As proposed by [135], the state estimation uses an internal model of the body and sensor dynamics to process sensor information and determine body orientation. In the latter study, three sensor information consisting in joint proprioception, vestibular organs in the inner ear and vision were modeled and it was predicted that the absence of one sensor lead to an unstable posture. Moreover, due to the known fact that body and sensors dynamics changes throughout life, an internal model would have to be continually updated with these changes and one should think of using an adaptive state estimation.

With such a precise model we can think of testing what happens when any sensor is missing. As in [135], where it was observed that the lack of the vestibular sense leads to loss of balance. We can think of solving this by proposing new innovative robotics systems, for example micro-prosthesis or microchips, that can replace the missing sensors and thus helping people in need.

- According to scientific results, when analyzing the gait initialization task, the gait encounters troubles that precedes falls which indicate neurological diseases. Parkinson's disease (PD) is known to be a degeneration of the dopaminergic neurons in the *substantia nigra pars compacta* of the midbrain that projects to the basal ganglia. The combination between medication and deep brain simulation have revealed inefficient for the gait symptoms in PD. Therefore, tools are needed in order to understand the brain functions in real life situations and to predict warnings of postural events. In order to have an understanding of what is happening in PD, we need to have an idea about the implication of basal ganglia activity in the complex motor coordination. Oscillatory activity in the basal ganglia is relevant to movement disorders, so falls and blockage of gait rarely emerge in clinical or laboratory conditions and cannot be adequately estimated and studied. Because today it is not possible to record brain activity in embedded situations, first we need to obtain a proper basal ganglia model and to use our understanding of the problem to propose devices suitable for clinical use and that the PD patients can use themselves. From a robotics researcher's point of view, this problem may be solved as follows: first, a proper model of basal ganglia needs to be found and also we need to have a good understanding on how the human motor control works. The second step consists in proposing an artificial basal ganglia such as robotic microchips (X DARPA and Google are planning to develop a microchip prosthesis which can be implanted on the human brain in order to erase some memories that

can harm and invoke dependance, bad influences, depression etc.) that can be implanted to the patient brain in order to predict and solve the problems encountered by a PD patient.

The idea of proposing artificial parts of human body that are somehow malfunctioning is not new: for example [136] proposed to develop an autonomous artificial pancreas by using an inverse neural optimal control for trajectory tracking, to regulate glucose level for type 1 diabetes mellitus patients. The proposed inverse optimal control law calculates the insulin delivery rate, which prevents hyperglycemia and hypoglycemia levels. In this study a virtual patient is implemented on a PC host being interconnected with a FPGA controller. The proposed FPGA controller based hardware architecture of a neural inverse optimal control can be used to develop an autonomous artificial pancreas.

Bibliography

[1] N. Sylla, Contribution a l'assistance robotisee du geste au travail : Modelisation, analyse et assistance du geste. PhD thesis, Universite de Montpellier 2, decembre 2014.

[2] V. Bonnet, P. Fraisse, N. Ramdani, J. Lagarde, S. Ramdani, and B.G.Bardy, "A closed loop musculoskeletal model of postural coordination dynamics," in 48th IEEE Conference on Decision and Control, Shanghai., 2009.

[3] Y. Kanamiya, S. Ota, and D. Sato, "Ankle and hip balance control strategies with transitions," in IEEE International Conference on Robotics and Automation, 2010.

[4] N. A. Bernstein, The Co-ordination and regulation of movements. Pergamon Press Ltd., 1967.

[5] A. Hempel, P. J. Goulart, and J. Lygeros, "Inverse parametric optimization with an application to hybrid system control," IEEE Transactions on automatic control, vol. 60, pp. 1064–1069, April 2015.

[6] M. Krstic and P. Tsiotras, "Inverse optimal stabilization of a rigid stpacecraft," IEEE Transactions on Automatic Control, vol. 44, pp. 1042–1049, 1999.

[7] N. D. Ratliff, J. A. Bagnell, and M. A. Zinkevich, "Maximum margin planning," Proceedings of the 23rd ICML, vol. 3, no. 10, 2006.

[8] P. Trautman and A. Krause, "Unfreezing the robot: Navigation in dense, interacting crowds," in Intelligent Robots and Systems (IROS), 2010 IEEE/RSJ International Conference on, pp. 797–803, Oct 2010.

[9] A. Ajami, J.-P. Gauthier, T. Maillot, and U. Serres, "How humans fly," ESAIM: Control, Optimisation and Calculus of Variations, vol. 19, pp. 1030–1054, 2013.

[10] T. Maillot, U. Serres, J.-P. Gauthier, and A. Ajami, "How pilots fly: An inverse optimal control problem approach," in Decision and Control (CDC), 2013 IEEE 52nd Annual Conference on, pp. 1792–1797, Dec 2013.

[11] K. Mombaur, A. Truong, and J.-P. Laumond, "From human to humanoid locomotionan inverse optimal control approach," Autonomous Robots, vol. 28, pp. 369–383, 2010.

[12] F. Jean, P. Mason, and F. Chittaro, "Geometric modeling of the movement based on an inverse optimal control approach," in Decision and Control (CDC), 2013 IEEE 52nd Annual Conference on, pp. 1816–1821, Dec 2013.

[13] F. Chittaro, F. Jean, and P. Mason, "On the inverse optimal control problems of the human locomotion: stability and robustness of the minimizers," Journal of Mathematical Sciences 195, vol. 3, pp. 269 – 287, 2013.

[14] A. V. Papadopoulos, L. Bascetta, and G. Ferretti, "Generation of human walking paths," Auton Robot, Jun 2015.

[15] M. C. Priess, R. Conway, J. Choi, J. P. Jr, and C. Radcliffe, "Solutions to the inverse lqr problem with application to biological systems analysis," IEEE Transactions on control systems technology, vol. 23 (2), pp. 770–777, 2015.

[16] T. Park and S. Levine., "Inverse optimal control for humanoid locomotion," in Robotics Science and Systems Workshop on Inverse Optimal Control & Robotic Learning from Demonstration, 2013.

[17] J. Mainprice, R. Hayne, and D. Berenson, "Predicting human reaching motion in colaborative tasks using inverse optimal control and iterative re-planning," in IEEE International Conference on Robotics and Automation, Washington State Convention Center, Seattle, Washington, May 26th - 30th, 2015.

[18] A. Byravan, M. Monfort, B. D. Ziebart, B. Boots, and D. Fox, "Layered hybrid inverse optimal control for learning robot manipulation from demonstration," in NIPS Workshop on Autonomous Learning Robots,, 2014.

[19] M. Monfort, A. Liu, and B. D. Ziebart, "Intent prediction and trajectory forecasting via predictive inverse linear-quadratic regulation," in AAAI Conference on Artificial Intelligence, 2015.

[20] J. G. Trafton, L. M. Hiatt, A. M. Harrison, F. Tamborello, S. S. Khemlani, and A. C. Schultz, "Act-r/e: An embodied cognitive architecture for human robot interaction," Journal of Human-Robot Interaction, vol. 2, pp. 30–55, 01/2013 2013.

[21] K. Strabala, M. K. Lee, A. Dragan, J. Forlizzi, S. Srinivasa, M. Cakmak, and V. Micelli, "Towards seamless human-robot handovers," Journal of Human-Robot Interaction, 2013.

[22] H. Kidokoro, T. Kanda, D. Brscic, and M. Shiomi, "Will i bother here? - a robot anticipating its influence on pedestrian walking comfort," in Human-Robot Interaction (HRI), 2013 8th ACM/IEEE International Conference on, pp. 259–266, March 2013.

[23] S. Elvira-Ceja and E. Sanchez, "Discrete-time inverse optimal control for stochastic nonlinear systems trajectory tracking," in Decision and Control (CDC), 2013 IEEE 52nd Annual Conference on, pp. 2483–2487, Dec 2013.

[24] B. D. Ziebart, A. Dey, and J. A. D. Bagnell, "Probabilistic pointing target prediction via inverse optimal control," in International Conference on Intelligent User Interfaces (IUI 2012), no. CMU-RI-TR-, February 2012.

[25] B. D. Ziebart, A. L. Maas, J. A. Bagnell, and A. K. Dey, "Human behavior modeling with maximum entropy inverse optimal control," in Human Behavior Modeling, Papers from the 2009 AAAI Spring Symposium, Technical Report SS-09-04, Stanford, California, USA, March 23-25, 2009, p. 92, 2009.

[26] X. Chen and B. Ziebart, "Predictive inverse optimal control for linear quadratic gaussian systems," in Proceedings of the 18th International Conference on Artifician Intelligence and Statistics (AISTATS), San Diego,CA, USA.), 2015.

[27] A. Y. Ng and S. Russell, "Algorithms for inverse reinforcement learning," in in Proc. 17th International Conf. on Machine Learning, pp. 663–670, Morgan Kaufmann, 2000.

[28] K. Dvijotham and E. Todorov, "Inverse Optimal Control with Linearly-Solvable MDPs.," in ICML, pp. 335–342, 2010.

[29] M. Bloem and N. Bambos, "Infinite time horizon maximum causal entropy inverse reinforcement learning," in Decision and Control (CDC), 2014 IEEE 53rd Annual Conference on, pp. 4911–4916, Dec 2014.

[30] A. Surana, "Unsupervised inverse reinforcement learning with noisy data," in Decision and Control (CDC), 2014 IEEE 53rd Annual Conference on, pp. 4938–4945, Dec 2014.

[31] N. D. Ratliff, B. D. Ziebart, K. M. Peterson, J. A. Bagnell, M. Hebert, A. K. Dey, and S. S. Srinivasa, "Inverse optimal heuristic control for imitation learning," in Proceedings of the Twelfth International Conference on Artificial Intelligence and Statistics, AISTATS 2009, Clearwater Beach, Florida, USA, April 16-18, 2009, pp. 424–431, 2009.

[32] L. Rodriguez-Guerrero, O. Santos, and S. Mondie, "Inverse optimality for a class of nonlinear time delay systems: A constructive approach," in Decision and Control (CDC), 2014 IEEE 53rd Annual Conference on, pp. 1972–1977, Dec 2014.

[33] W. Li, E. Todorov, and D. Liu, "Inverse optimality design for biological movement systems," in Proceedings of the 18th International Federation of Automatic Control World Congress, pp. 9662–9667, 2011.

[34] D.Burton and P.Toint, "On an instance of the inverse shortest path problem," Mathematical Programming, vol. 53, pp. 45–61, 1992.

[35] K. Waugh, B. D. Ziebart, and J. A. Bagnell, "Computational rationalization: The inverse equilibrium problem," in Proceedings of the 28th International Conference on Machine Learning ,Bellevue,WA,USA, 2011.

[36] P. Abbeel, A. Coates, and A. Y. Ng, "Autonomous helicopter aerobatics through apprenticeship learning," Int. J. Rob. Res., vol. 29, pp. 1608–1639, Nov. 2010.

[37] P. Abbeel and A. Y. Ng, "Apprenticeship learning via inverse reinforcement learning," in Proceedings of the Twenty-first International Conference on Machine Learning, ICML '04, (New York, NY, USA), pp. 1–, ACM, 2004.

[38] E. Pauwels, D. Henrion, and J.-B. Lasserre, "Inverse optimal control with polynomial optimization," in Decision and Control (CDC), 2014 IEEE 53rd Annual Conference on, pp. 5581–5586, Dec 2014.

[39] E. Pauwels, D. Henrion, and J.-B. Lasserre, "Inverse optimal control with polynomial optimization," arXiv:1403.5180 [math.OC] 20 Mar, 2014.

[40] J.-B. Lasserre, "Inverse polynomial optimization," tech. rep., Rapport LAAS no 11140. 25 pages. ¡hal-00577168v2¿, 2011.

[41] B. Berret, E. Chiovetto, F. Nori, and T. Pozzo, "Evidence for composite cost functions in arm movement planning: An inverse optimal control approach," PLoS Comput Biol, p. 1002183, 2011.

[42] B. Berret, E. Chiovetto, F. Nori, and T. Pozzo, "Manifold reaching paradigm: how do we handle target redundancy?," J Neurophysiol, vol. 106, pp. 2086–2102, 2011.

[43] N. Sylla, V. Bonnet, G. Venture, N. Armande, and P. Fraisse, "Assessing neuromuscular mechanisms in human-exoskeleton interaction," in Engineering in Medicine and Biology Society (EMBC), 2014 36th Annual International Conference of the IEEE, pp. 1210–1213, Aug 2014.

[44] N. Sylla, V. Bonnet, G. Venture, N. Armande, and P. Fraisse, "Human arm optimal motion analysis in industrial screwing task," in Biomedical Robotics and Biomechatronics (2014 5th IEEE RAS EMBS International Conference on, pp. 964–969, Aug 2014.

[45] M. Ulbrich, M. Leibold, and S. Albrecht, "A bilevel optimization approach to obtain optimal cost functions for human arm movements," NACO, vol. 2, p. 105127, Mar 2012.

[46] S. Albrecht, C. Passenberg, M. Sobotka, A. Peer, M. Buss, and M. Ulbrich, "Optimization criteria for human trajectory formation in dynamic virtual environments," Lecture Notes in Computer Science, p. 257262, 2010.

[47] S. Albrecht, K. Ramirez-Amaro, F. Ruiz-Ugalde, D. Weikersdorfer, M. Leibold, M. Ulbrich, and M. Beetz, "Imitating human reaching motions using physically inspired optimization principles," 2011 11th IEEE-RAS International Conference on Humanoid Robots, Oct 2011.

[48] A. Sebastian, "Modeling and analysis of human navigation with crossing interferer using inverse optimal control," 7th Vienna International Conference on Mathematical Modelling, Feb 2012.

[49] A. Keshavarz, Y. Wang, and S. Boyd, "Imputing a convex objective function," in Intelligent Control (ISIC), 2011 IEEE International Symposium on, pp. 613–619, Sept 2011.

[50] A.-S. Puydupin-Jamin, M. Johnson, and T. Bretl, "A convex approach to inverse optimal control and its application to modeling human locomotion," in Robotics and Automation (ICRA), 2012 IEEE International Conference on, pp. 531–536, May 2012.

[51] M. Johnson, N. Aghasadeghi, and T. Bretl, "Inverse optimal control for deterministic continuous-time nonlinear systems," in Decision and Control (CDC), 2013 IEEE 52nd Annual Conference on, pp. 2906–2913, Dec 2013.

[52] N. Aghasadeghi, A. Long, and T. Bretl, "Inverse optimal control for a hybrid dynamical system with impacts," in Robotics and Automation (ICRA), 2012 IEEE International Conference on, pp. 4962–4967, May 2012.

[53] A. M. Panchea and N. Ramdani, "Towards solving inverse optimal control in a bounded-error framework," in The Proceedings of the 2015 American Control Conference, Chicago, IL, USA on July 1-3, 2015.

[54] M. Gilson and P. V. den Hof, "On the relation between a bias-eliminated least-square and an iv estimator in closed-loop identification," Automatica, vol. 37, pp. 1593–1600, 2001.

[55] N. Aghasadeghi and T. Bretl, "Inverse optimal control for differentially flat systems with application to locomotion modeling," in Robotics and Automation (ICRA), 2014 IEEE International Conference on, pp. 6018–6025, May 2014.

[56] A. Herdt, H. Diedam, P.-B. Wieber, D. Dimitrov, K. Mombaur, and M. Diehl, "Online Walking Motion Generation with Automatic Foot Step Placement," Advanced Robotics, vol. 24, no. 5-6, pp. 719–737, 2010.

[57] S. Kajita, M. Morisawa, K. Harada, K. Kaneko, F. Kanehiro, K. Fujiwara, and H. Hirukawa, "Biped walking pattern generator allowing auxiliary ZMP control," in Intelligent Robots and Systems, 2006 IEEE/RSJ International Conference on, (Beijing,), pp. 2993–2999, Oct. 2006.

[58] S. Boyd and L. Vandenberghe, Convex optimization. Cambridge University Press, 2004.

[59] T. Flash and N. Hogans, "The coordination of arm movements: An experimentally confirmed mathematical model," Journal of neuroscience, vol. 5, pp. 1688–1703, 1985.

[60] Y. Wada, Y. Kaneko, E. Nakano, R. Osu, and M. Kawato, "Quantitative examinations for multi joint arm trajectory planningusing a robust calculation algorithm of the minimum commanded torque change trajectory," Neural Networks, vol. 14, p. 381393, May 2001.

[61] S. Ben Itzhak and A. Karniel, "Minimum acceleration criterion with constraints implies bang-bang control as an underlying principle for optimal trajectories of arm reaching movements," Neural Computation, vol. 20, p. 779812, Mar 2008.

[62] W. L. Nelson, "Physical principles for economies of skilled movements," Biological Cybernetics, vol. 46, p. 135147, Feb 1983.

[63] Y. Uno, M. Kawato, and R. Suzuki, "Formation and control of optimum trajectory in human multijoint arm movement: minimum torque-change model," Biological Cybernetics, vol. 61, pp. 89–101, 1989.

[64] A. Biess, M. Nagurka, and T. Flash, "Simulating discrete and rhythmic multi-joint human arm movements by optimization of nonlinear performance indices," Biological Cybernetics, vol. 95, p. 3153, May 2006.

[65] A. Biess, D. G. Liebermann, and T. Flash, "A computational model for redundant human three-dimensional pointing movements: Integration of independent spatial and temporal motor plans simplifies movement dynamics," Journal of Neuroscience, vol. 27, p. 1304513064, Nov 2007.

[66] R. M. Alexander, "A minimum energy cost hypothesis for human arm trajectories," Biological Cybernetics, vol. 76, p. 97105, Feb 1997.

[67] J. Nishii and T. Murakami, "Energetic optimality of arm trajectory," in In Proc of Int Conf on Biomechanics of Man, pp. 30–33, 2002.

[68] B. Berret, C. Darlot, F. Jean, T. Pozzo, C. Papaxanthis, and J. P. Gauthier, "The inactivation principle: Mathematical solutions minimizing the absolute work and biological implications for the planning of arm movements," PLoS Comput Biol, vol. 4, p. e1000194, Oct 2008.

[69] J.-P. Gauthier, B. Berret, and F. Jean, "A biomechanical inactivation principle," Proceedings of the Steklov Institute of Mathematics, vol. 268, pp. 93–116, 2010.

[70] J. F. Soechting, C. A. Buneo, U. Herrmann, and M. Flanders, "Moving effortlessly in three dimensions: Does Donders' law apply to arm movement?," Journal of Neuroscience, vol. 15, pp. 6271–6280, 1995.

[71] E. Todorov and M. I. Jordan, "Optimal feedback control as a theory of motor coordination," Nat Neurosci, vol. 5, p. 12261235, Nov 2002.

[72] E. Guigon, P. Baraduc, and M. Desmurget, "Computational motor control: Redundancy and invariance," Journal of Neurophysiology, vol. 97, p. 331347, Jan 2007.

[73] W. Khalil and E. Dombre, Modeling, Identification and Control of Robots (Kogan Page Science Paper Edition). Elsevier Butterworth Heinemann, 2004.

[74] H. Cheng, L. Obergefell, and A. Rizer, "Generator of body data (gebod) , manual.," tech. rep., Systems Research Labs Inc DAYTON OH, Final rept. Apr 91-Mar 94,, 1994.

[75] I. A. Kapandji, Physiologie articulaire Tome 1 membre superieur. Maloine, 1980.

[76] V. Hue, Simulation de mouvement humain sur postes de travail pour le diagnostic et l'aide la conception. PhD thesis, Institute national Polytechnique de Toulouse-INPT, 2008.

[77] L. Marin, B. Bardy, B. Baumberger, M. Fluckiger, and T. Stroffregen, "Interaction between task demands and surface properties in the control of goal-oriented stance," Human Movement Sciences, vol. 18, pp. 31–47, 1999.

[78] B. G. Bardy, O. Ouillier, R. Bootsma, and T. Stoffregen, "Dynamics of human postural transitions," Journal of Experimental Psychology: Human Perception and Performance, vol. 28, pp. 499–514, 2002.

[79] O. Oullier, B. Bardy, T. Stroffregen, and R. Bootsma, "Postural coordination in looking and tracking tasks," Human Movement Sciences, vol. 21, pp. 147–167, 2002.

[80] L. Martin, V. Cahouet, M. Ferry, and F. Fouque, "Optimization model predictions for postural coordination modes," Journal of Biomechanics, vol. 39, pp. 170–176, 2006.

[81] V. Bonnet, S. Ramdani, P. Fraisse, N. Ramdani, J. Lagarde, and B. G. Bardy, "A structurally optimal control model for predicting and analyzing human postural coordination," Journal of Biomechanics, vol. 44, pp. 2123–2128, 2011.

[82] L. Nashner and G. McCollum, "The organization of postural movements: a formal basis ansd experimental synthesis," Behavioral and Brain Sciences, vol. 26, pp. 135–172, 1985.

[83] B. Stephens, "Integral control of humanoid balance," in Intelligent Robots and Systems, 2007. IROS 2007. IEEE/RSJ International Conference on, pp. 4020–4027, 29 2007-Nov. 2.

[84] V. Bonnet, P. Fraisse, N. Ramdani, J. Lagarde, S. Ramdani, and B.G.Bardy, "A robotic closed-loop scheme to model human postural coordination," in IEEE/RSJ International Conference on Intelligent Robots and Systems, St Louis, MO, USA, pp. 2525–2530, 2009.

[85] K. Yamane and J. Hodgins, "Simultaneous tracking and balancing of humanoid robots for imitating human motion capture data," Intelligent robots and systems, pp. 2510 – 2517, 2009.

[86] C. Liu and C. G. Atkeson, "Standing balance control using a trajectory library," IEEE/RSJ International Conference on Intelligent Robots and Systems, pp. 3031 – 3036, 2009.

[87] B. G. Bardy, L. Marin, T. Stoffregen, and R. Bootsma, "Postural coordination modes considered as emergent phenomena," Journal of Experimental Psychology: Human Perception and Performance, vol. 25, pp. 1284–1301, 1999.

[88] B. Bardy, L. Marin, T. Stoffregen, and R. Bootsma, "Postural coordination modes considered as emergent phenomena," Exp. Psychol. Hum. Percept. Perform., vol. 25, pp. 1284–1301, 1999.

[89] M. Ferry, Formation de la trajectoire pour des taches supra-posturales: modélisation et experimentation. PhD thesis, Univ. Joseph Fourrier, Genoble I, 2004.

[90] C.F.Runge, C. Shupert, F. Horak, and F. Zajac, "Ankle and hip postural strategies defined by joint torques," Gait and Posture, vol. 10, pp. 161–170, 1999.

[91] B. Bardy, O. Ouillier, R. Bootsma, and T. Stoffregen, "Dynamics of human postural transitions," ExP. Psychol. Hum. Percept. Perform., vol. 28, pp. 499–514, 2002.

[92] D. Winter, A. Patla, S. Rietdyk, and M. Ishac, "Ankle muscle stiffness in the control of balance during quiet standing," Journal of Neurophysiol, vol. 85, pp. 1211–1221, 2001.

[93] R. J. Peterka, "Sensorimotor integration in human postural control," Journal of Neurophysiology, vol. 88, pp. 1097–1118, 2002.

[94] P. Micheau, A. Kron, and P. Bourassa, "Evolution of the lambda model for human postural control during ankle strategy," Journal of Biol Cybern, vol. 89, pp. 227 – 236, 2003.

[95] R. Creath, T. Kiemel, F. Horak, R. Peterka, and J. Jeka, "A unified view of quiet and perturbed stance: simultaneous co-existing excitable modes.," NeurNeuroscience Letters, 377(2), 2005.

[96] V. Bonnet, J. Lagarde, P. Fraisse, N. Ramdani, S. Ramdani, P. Poignet, and B. Bardy, "Modeling of the human postural coordination to improve the humanoids control of balance," in IEEE International Conference on Humanoid Robots, Humanoids 2007, Pittsburg, PA, USA, 2007.

[97] S. Park, F. B. Horak, and A. D. Kuo, "Postural feedback responses scale with biomechanical constraints in human standing," Experimental Brain Research, vol. 154, pp. 417–427, 2004.

[98] A. V. Alexandrov, A. A. Frolov, F. B. Horak, P. Carlson-Kuhta, and S. Park, "Feedback equilibrium control during human standing," Biological Cybernetics, vol. 93, no. 5, pp. 309–322, 2005.

[99] S. Kim, C. Atkeson, and S.Park, "Perturbation-dependent selection of postural feedback gain and its scaling," Journal of Biomechanics, 2012.

[100] A. M. Panchea, N. Ramdani, P. Fraisse, and S. Park, "A gain-scheduling approach to model human simultaneous visual tracking and balancing," 2013 IEEE/RSJ International Conference on Intelligent Robots and Systems, Nov 2013.

[101] Kozak, On the Control of Balance During the Performance of a Forward Reach: Effects of Age, Biomechanical and Psychological Factors. PhD thesis, MI: University of Michigan, 1999.

[102] V. Cahouet, L. Martin, and D. Amarantini, "Static optimal estimation of joint accelerations for inverse dynamics problem solution," Journal of Biomechanics, vol. 35, pp. 1507–1513, 2002.

[103] Y. Pai and J. Patton, "Center of mass velocity-position predictions for balance control," Journal of Biomechanics, vol. 30, pp. 347–354, 1997.

[104] B. J. Stephens, "State estimation foe force-controlled humanoid balance using simple models in the presence of modeling error," IEEE International Conference on Robotics and Automation, pp. 3994 – 3999, 2011.

[105] J.-Y. Kim, C. G. Atkeson, J. K. Hodgins, D. C. Bentivegna, and S. J. Cho, "Online gain switching algorithm for joint position control of a hydraulic humanoid robot," IEEE-RAS International Conference on Humanoid Robots, pp. 13 – 18, 2007.

[106] A. Kuo and F. Zajac, "A biomechanical analysis of muscle strength as a limiting factor in standing posture," Journal of Biomechanics, vol. 26, pp. 137–150, 1993.

[107] S. Park, F. Horak, and A. Kuo, "Postural feedback responses scale with biomechanical constraints in human standing," Exp. Brain. Res., vol. 154, pp. 417–427, 2004.

[108] C. D. Marsden, "Parkinsons disease.," Journal of Neurology, Neurosurgery & Psychiatry, vol. 57, p. 672681, Jun 1994.

[109] T. Owings, T. Pavol, and M. Grabiner, "Mechanisms of failed recovery following postural perturbations on a motorized treadmill mimic those associated with an actual forward trip.," Clinical Biomechanics (Bristol, Avon), 2001.

[110] Z. Aftab, Simulation dynamique de perte d'equilibre: Application aux passagers debout de transport en commun. PhD thesis, L'Universite Claude Bernard, Lyon 1, 2012.

[111] Y. Pai, B. Maki, K. Iqbal, W. Mcllroy, and S. Perry, "Thresholds for step initiation induced by support-surface translation: a dynamic center-of-mass model provides much better prediction than a static model.," Journal of Biomechanics, 2000.

[112] M. L. Mille, M. W. Rogers, K. Martinez, L. Hedman, M. Johnson, and R. Fitzpatrick, "Thresholds for inducing protective stepping responses to external perturbations of human standing.," J Neurophysiol, 90(2):666-674., 2003.

[113] S. Kajita and K. Tani, "Study of dynamic biped locomotion on rugged terrain-derivation and application of the linear inverted pendulum mode.," in IEEE Proceedings International In Conference on Robotics and Automation, 1991.

[114] T. Komura, H. Leung, S. Kudoh, and J. Kuffner, "A feedback controller for biped humanoids that can counteract large perturbations during gait.," in IEEE International Conference on Robotics and Automation (ICRA)., 2005.

[115] H. Geyer, A. Seyfarth, and R. Blickhan, "Complient leg behaviour explains basic dynamics of walking and running.," in In Proceedings of the Royal Society B., 2006.

[116] C. H. Jung and S. Park, "Compliant bipedal model with the center of pressure excursion associated with oscillatory behavior of the center of mass reproduces the human gait dynamics.," Journal of Biomechanics., 2013.

[117] S. Kim and S. Park, "Leg stiffness increases with speed to modulate gait frequency propulsion energy.," Journal of Biomechanics, 44:1253-1258., 2011.

[118] H. Hong, S. Kim, C. Kim, S. Lee, and S. Park, "Spring-like gait mechanics observed during walking in both young and older adults.," Journal of Biomechanics, 46:77-82., 2013.

[119] M. Nakamura, M. Mori, and J. Nishii, "Trajectory planning for a leg swing during human walking," in Systems, Man and Cybernetics, 2004 IEEE International Conference on, vol. 1, pp. 784–790 vol.1, 2004.

[120] Z. Aftab, T. Robert, and P.-B. Wieber, "Predicting multiple step placements for human balance recovery tasks," Journal of Biomechanics, 2012.

[121] S. Kajita, F. Kanehiro, K. Kaneko, K. Fujiwara, K. Harada, K. Yokoi, and H. Hirukawa, "Biped walking pattern generation by using preview control of zero-moment point," in IEEE International Conference on Robotics and Automation, vol. 2, pp. 1620 – 1626, september 2003.

[122] S. Kajita, M. Morisawa, K. Miura, S. Nakaoka, K. Harada, K. Kaneko, F. Kanehiro, and K. Yokoi, "Biped walking stabilization based on linear inverted pendulum tracking," in Intelligent Robots and Systems (IROS), 2010 IEEE/RSJ International Conference on, pp. 4489–4496, Oct 2010.

[123] Z. Aftab, T. Robert, and P.-B. Wieber, "Simulating the effect of upper-body inertia on human balance recovery," Computer Methods in Biomechanics and Biomedical Engineering, 2012.

[124] Z. Aftab, T. Robert, and P.-B. Wieber, "Ankle, hip and stepping strategies for humanoid balance recovery with a single model predictive control scheme," in 12th IEEE-RAS International Conference on Humanoid Robots, 2012.

[125] A. Hof, M. Gazendam, and W. Sinke, "The condition for dynamic stability," Journal of biomechanics, 38(2005).

[126] A. Herdt, N. Perrin, and P.-B. Wieber, "Walking without thinking about it," in Intelligent Robots and Systems (IROS), 2010 IEEE/RSJ International Conference on, pp. 190–195, Oct 2010.

[127] H. Diedam, D. Dimitrov, P.-B. Wieber, K. Mombaur, and M. Diehl, "Online walking gait generation with adaptive foot positioning through linear model predictive control," in Intelligent Robots and Systems, 2008. IROS 2008. IEEE/RSJ International Conference on, pp. 1121–1126, Sept 2008.

[128] S. Kajita, F. Kanehiro, K. Kaneko, K. Fujiwara, K. Harada, K. Yokoi, and H. Hirukawa, "Resolved momentum control: Humanoid motion planning based on the linear and angular momentum," in Intl. Conference on Intelligent Robots and Systems, 2003.

[129] S. Kajita, O. Matsumoto, and M. Saigo, "Real-time 3d walking pattern generation for a biped robot with telescopic legs," in Robotics and Automation, 2001. Proceedings 2001 ICRA. IEEE International Conference on, vol. 3, pp. 2299 – 2306, 2001.

[130] L. Jaulin, M. Kieffer, O. Didrit, and E. Walter, Applied Interval Analysis: with examples in parameter and state estimation, robust control and robotics. London: Springer-Verlag, 2001.

[131] T. Raïssi, N. Ramdani, and Y. Candau, "Set membership state and parameter estimation for systems described by nonlinear differential equations," Automatica, vol. 40(10), pp. 1771–1777, 2004.

[132] T. Raïssi, N. Ramdani, and Y. Candau, "Set membership parameter estimation in the frequency domain," International Journal of Control, Automation, and Systems, vol. 7, no. 5, pp. 824–834, 2009.

[133] I. Braems, N. Ramdani, M. Kieffer, L. Jaulin, E. Walter, and Y. Candau, "Guaranteed characterization of thermal conductivity and diffusivity in presence of model uncertainty," Inverse Problems in Science and Engineering, vol. 15, no. 8, pp. 895–910, 2007.

[134] N. Aghasadeghi, H. Zhao, L. J. Hargrove, A. D. Ames, E. J. Perreault, and T. Bretl, "Learning impedance controller parameters for lower-limb prostheses," 2013 IEEE/RSJ International Conference on Intelligent Robots and Systems, Nov 2013.

[135] A. D. Kuo, "An optimal state estimation model of sensory integration in human postural balance," Journal of Neural Engineering, vol. 2, pp. S235–S249, 2005.

[136] J. C. Romero-Aragon, E. N. Sanchez, and A. Y. Alanis, "Glucose level regulation for diabetes mellitus type 1 patients using FPGA neural inverse optimal control," 2014 IEEE Symposium on Computational Intelligence in Control and Automation (CICA), Dec 2014.

Adina M. PANCHEA

Contrôle optimal inverse de systèmes de mouvements biologiques redondants.

Résumé : Cette thèse aborde les problèmes inverses de contrôle optimal (IOCP) pour trouver les fonctions de coûts pour lesquelles les mouvements humains sont optimaux. En supposant que les observations de mouvements humains sont parfaites, alors que le processus de commande du moteur humain est imparfait, nous proposons un algorithme de commande approximative optimale. En appliquant notre algorithme pour les observations de mouvement humaines collectées: mouvement du bras humain au cours d'une tâche de vissage industrielle, une tâche de suivi visuel d'une cible et une tâche d'initialisation de la marche, nous avons effectué une analyse en boucle ouverte. Pour les trois cas, notre algorithme a trouvé les fonctions de coût qui correspondent mieux ces données, tout en satisfaisant approximativement les Karush-Kuhn-Tucker (KKT) conditions d'optimalité. Notre algorithme offre un beau temps de calcul pour tous les cas, fournir une opportunité pour son utilisation dans les applications en ligne. Pour la tâche de suivi visuel d'une cible, nous avons étudié une modélisation en boucle fermée avec deux boucles de rétroaction PD. Avec des données artificielles, nous avons obtenu des résultats cohérents en termes de tendances des gains et les critères trouvent par notre algorithme pour la tâche de suivi visuel d'une cible. Dans la seconde partie de notre travail, nous avons proposé une nouvelle approche pour résoudre l'IOCP, dans un cadre d'erreur bornée. Dans cette approche, nous supposons que le processus de contrôle moteur humain est parfait tandis que les observations ont des erreurs et des incertitudes d'agir sur eux, étant imparfaite. Les erreurs sont délimitées avec des limites connues, sinon inconnu. Notre approche trouve l'ensemble convexe de de fonction de coût réalisables avec la certitude qu'il comprend la vraie solution. Nous numériquement garanties en utilisant des outils d'analyse d'intervalle.

Mots clés : Contrôle optimal inverse, optimisation et de contrôle optimal, biomimétique, la cinématique, le mouvement et la planification de parcours, suivi visuel, Direct / Inverse Dynamics formulation, Motion Control, systèmes redondants, Dynamics

Inverse optimal control for redundant systems of biological motion.

Summary : This thesis addresses inverse optimal control problems (IOCP) to find the cost functions for which the human motions are optimal. Assuming that the human motion observations are perfect, while the human motor control process is imperfect, we propose an approximately optimal control algorithm. By applying our algorithm to the human motion observations collected for: the human arm trajectories during an industrial screwing task, a postural coordination in a visual tracking task and a walking gait initialization task, we performed an open loop analysis. For the three cases, our algorithm returned the cost functions which better fit these data, while approximately satisfying the Karush-Kuhn-Tucker (KKT) optimality conditions. Our algorithm offers a nice computational time for all cases, providing an opportunity for its use in online applications. For the visual tracking task, we investigated a closed loop modeling with two PD feedback loops. With artificial data, we obtained consistent results in terms of feedback gains' trends and criteria exhibited by our algorithm for the visual tracking task. In the second part of our work, we proposed a new approach to solving the IOCP, in a bounded error framework. In this approach, we assume that the human motor control process is perfect while the observations have errors and uncertainties acting on them, being imperfect. The errors are bounded with known bounds, otherwise unknown. Our approach finds the convex hull of the set of feasible cost function with a certainty that it includes the true solution. We numerically guaranteed this using interval analysis tools.

Keywords : Inverse optimal control, Optimization and Optimal control, Biomimetic, Kinematics, Motion and Path Planning, Visual Tracking, Direct/Inverse Dynamics Formulation, Motion control, Redundant systems, Dynamics

Centre Val de Loire UNIVERSITÉ Spirit of the Loire Valley

PRISME EA 4229

Université d'Orléans

8 rue Leonard de Vinci, 45072 Orléans

UNIVERSITE D'ORLEANS